**Mechanics and Materials Center**
**TEXAS A&M UNIVERSITY**
**College Station, Texas**

# ANALYSIS OF THE EFFECT OF MATRIX DEGRADATION ON FATIGUE BEHAVIOR OF A GRAPHITE/EPOXY LAMINATE

BY

ROBERT THOMAS ARENBURG



AIR FORCE OFFICE OF SCIENTIFIC RESEARCH
OFFICE OF AEROSPACE RESEARCH
UNITED STATES AIR FORCE
CONTRACT NO. F49620-78-C-0034



MM 3724-82-2

MAY 1982

# ANALYSIS OF THE EFFECT OF MATRIX DEGRADATION ON FATIGUE BEHAVIOR OF A GRAPHITE/EPOXY LAMINATE

A Thesis

by

ROBERT THOMAS ARENBURG

Submitted to the Graduate College of
Texas A&M University
in partial fulfillment of the requirement for the degree of

MASTER OF SCIENCE

May 1982

Major Subject: Civil Engineering

# ANALYSIS OF THE EFFECT OF MATRIX DEGRADATION ON FATIGUE BEHAVIOR OF A GRAPHITE/EPOXY LAMINATE

A Thesis

by

ROBERT THOMAS ARENBURG

Approved as to style and content by:

| | |
|---|---|
| (Chairman of Committee) | (Member) |
| (Member) | (Member) |
| (Member) | (Head of Department |

May 1982

# ABSTRACT

Analysis of the Effect of Matrix Degradation on Fatigue Behavior of a Graphite/Epoxy Laminate. (May 1982)

Robert Thomas Arenburg, B.C.E.T., Southern Technical Institute

Chairman of Advisory Committee: Dr. R. A. Schapery

An analytical study of the effect of fatigue on a $[\pm 45/90_2]_s$ graphite/epoxy laminate is conducted considering two levels of damage. The first one is microscopic damage, which is viewed as a matrix softening mechanism that is accounted for by the use of micromechanics. The second level of damage is delamination. An evaluation of lamination theory versus a finite element elasticity solution which accounts for free edge stresses is made first. Lamination theory is found to be inadequate due to its inability to account for large amounts of shear deformation as the matrix degrades. Experimental data are used to evaluate the matrix degradation as a function of fatigue cycles, and then a parametric study of the strain energy release rate as a function of delamination size at various degrees of matrix degradation is conducted. For a constant maximum stress fatigue test, the matrix degradation leads to an increase in strain energy which is predicted to eventually cause rapid delamination. Reasonably good agreement between theory and experimental data on the $[\pm 45/90_2]_s$ laminate is demonstrated.

# ACKNOWLEDGEMENTS

I would like to thank Dr. W.E. Haisler, Dr. M. Henriksen, and especially Dr. R.A. Schapery, for their continual support and advice throughout the duration of this study. I would like to thank the entire staff of the Mechanics and Materials Center for their advice, programming assistance, drafting, and typing. I would like to extend my best wishes to my fellow M.S. students for their friendship which made the course of study at A&M all the more a pleasure.

Thanks are also extended to Tim Morse for his assistance in the preparation of the final manuscript. Special thanks go to my parents for their continual support throughout college and to Diana for her love and assurance.

This investigation was performed under Contract F49620-78-C-0034 from the Air Force Office of Scientific Research. This support is gratefully acknowledged.

# TABLE OF CONTENTS

TABLE OF CONTENTS

(Continued)

# LIST OF TABLES

# LIST OF FIGURES

LIST OF FIGURES

(Continued)

# LIST OF FIGURES

(Continued)

LIST OF FIGURES

(Continued

# LIST OF TERMS

$A$ - total laminate cross-section

$A_{CLT}$ - fraction of laminate cross-section in which CLT solution was obtained

$A_{FEM}$ - fraction of laminate cross-section in which FEM solution was obtained

$a$ - delamination size

$a_c$ - critical delamination size

$a_o$ - initial delamination size

$a_{11}$ - first term of extensional compliance matrix

$b$ - half-width of laminate

$b'$ - width of FEM mesh near free edge

$C_{ij}$ - modulus matrix

CLT - classical lamination theory

$E$ - laminate stiffness

$E_{APPARENT}$ - apparent laminate stiffness

$E_{CLT}$ - laminate stiffness obtained from CLT solution

$E_{ELAST}$ - elasticity solution for axial laminate stiffness

$E_{FEM}$ - laminate stiffness obtained from FEM solution

$E^m_{initial}$ - initial matrix modulus

$E_{LAM}$ - laminate stiffness for a fully bonded laminate

$E_{REF}$ - laminate stiffness obtained from the elasticity solution for the initial matrix modulus

$E^*$ - laminate stiffness for a fully delaminated laminate

$E_1, E_2, E_3$ - Young's modulus for the 1, 2, and 3 directions, respectively.

## LIST OF TERMS

(Continued)

| | |
|---|---|
| FEM | - finite element method |
| G | - energy release rate |
| $G_I, G_{II}, G_{III}$ | - mode I, II, and III energy release rates |
| $G_c$ | - critical energy release rate |
| $G_{12}, G_{23}$ | - shear modulus for 1-2 and 2-3 planes, respectively |
| h | - ply thickness |
| k | - bulk modulus |
| $k_{23}$ | - plane strain bulk modulus |
| L | - laminate length |
| $S_{ij}$ | - compliance matrix |
| t | - laminate thickness |
| UTS | - ultimate tensile strength |
| $\alpha_i$ | - vector of coefficients of thermal expansion |
| $\varepsilon_i$ | - vector of strain components |
| $\overline{\varepsilon}$ | - mean strain |
| $\sigma_i$ | - vector of stress components |
| $\overline{\sigma}$ | - mean stress |

# I. INTRODUCTION

Fiber reinforced composite materials are known for their good fatigue characteristics. Helicopter rotor blade technology has recognized this fact, and today most current rotor blade designs have adopted the use of composite materials. The study conducted considers the influence of two fatigue mechanisms: matrix degradation and free edge delaminations, and their influence on deformation and failure behavior.

Consider a matrix dominated, graphite/epoxy laminate, which is fatigued under constant maximum stress conditions. The mean strain response as a function of fatigue cycles has been characterized as predominately linear if plotted on log-log scales. Near failure the mean strain departs from its previous linear path and increases very rapidly to failure. It is speculated that the laminate response to the fatigue loading can be explained as follows.

The initial linear response is a result of an accumulation of matrix "damage." The reason for the damage to be associated with the matrix can be explained by the considerably higher stiffness and strength of the graphite fibers compared to the matrix. When considering a matrix dominated laminate, i.e., a laminate without fibers oriented in the direction of the load introduction, the fibers can be viewed as rigid inclusions and thus act as stress concentrators or stress risers. Due to the stress riser effect of the fibers and their higher strength, the matrix is the first phase damaged by the

---

This thesis follows the style of the Journal of Composite Materials

fatigue loading. An important form of damage induced by the rigid inclusion effect would be a fiber-matrix disbond.

Polymers with a highly nonuniform crosslink density could provide "soft spots," weak regions causing strain concentrations. The soft spots could provide initiation sites for microcracking. Other zones of damage could be composed of microscopic voids and cracks. In general, the term "damage" will be used in reference to microscopic events which result in reduced global laminate stiffness.

The next phase might be the interaction of the matrix damage, characterized by microscopic flaws, with macroscopic delaminations. Once the delamination has penetrated most of the specimen width, failure should occur very rapidly due to the degraded matrix strength.

The prime concern of this thesis is to account for the observed fatigue behavior through an analytical study of the effects of matrix degradation and free edge delaminations.

## Present Status

Frequently the fracture damage in fibrous composite laminates involving matrix cracks can be characterized by two damage modes. The first mode consists of multiple transverse cracks which occur in plies with fibers oriented perpendicular or nearly perpendicular to the applied load. The second mode consists of inter-ply delaminations which usually start near the free edge of the laminate.

Experimental studies have shown there exists a threshold stress state below which neither transverse cracks nor edge delaminations occur. Bader et al. [1] showed that the strain required for initia-

tion of transverse cracks in a $[0_n/90_m]_s$ graphite/epoxy laminate increased as the thickness of the 90° plies decreased. The outside 0° plies of the laminate performed as an arresting barrier for the transverse cracks. Also noted was a state of crack saturation which was characterized by a typical crack spacing. These results confirm the idea of ply interaction in the transverse cracking process. The results of Bader et al. confirm the earlier trends noted in a micromechanical analysis by Aveston and Kelly [2].

Free edge delamination has been attributed to locally high edge stresses, in which the magnitude and direction of the stresses are dependent on the ply stacking sequence. Rodine and Eisenmann [3] showed for a $[\pm 45_n/0_n/90_n]_s$ graphite/epoxy laminate that the onset of edge delamination occurred at a lower stress level for thicker laminates. They used a statistical argument that a thicker laminate had potentially more flaws to initiate the delamination.

We believe the observed thickness effect on the threshold stress for edge delamination and transverse cracking may be explained from an energy argument. The strain energy contained within a laminate plays an important role in the initiation and behavior of cracks and from this the ply thickness becomes an important parameter. Since the strain energy is dependent upon the ply interaction, and this can be altered by the kinematics of a crack, the study of the energy state of a laminate should provide a criterion for crack growth.

Rybicki et al. [4] used linear fracture mechanics in characterizing free edge delamination. The critical strain energy release rate was used as a criterion for unstable crack growth. In their analysis,

free edge flaws were assumed to initiate the delamination. The finite element method in conjunction with a virtual crack closure method [5] was used to calculate the energy release rate. The energy release rate was found to be constant during stable crack growth, and was based upon extensional strain and delamination size provided by uniaxial tensile tests. From these results it was verified that linear elastic fracture mechanics could be applied to fiber reinforced composites and the strain energy release rate could be a suitable parameter.

Wang and Crossman et. al. [6, 7] continued the energy approach, recognizing its ability to account for the structural interaction of plies. They considered both transverse cracking and edge delamination in uniaxial tensile specimens. Energy release rate, G, as a function of crack length due to a unit load was introduced. This function was used to describe the energy available for crack growth. The finite element method was used to evaluate the function; from this the threshold stresses for edge delamination and transverse cracking were calculated for a constant critical G, which yielded the ply thickness dependence of the threshold stress for transverse cracking and edge delamination. Correlation of their method with experimental data of a $[\pm 25/90_n]_s$ (n = 1,2,3) graphite/epoxy laminate showed good agreement.

O'Brien [8] developed a simple energy approach to analyze delamination onset and growth. His analysis used classical lamination theory to evaluate the strain energy release rate based upon a simple rule-of-mixtures expression for the laminate stiffness. In studying a $[\pm 30/\pm 30/90/\overline{90}_s]_s$ laminate, O'Brien did not try to model both trans-

verse cracking in the 90° plies and interlaminar delaminations explicitly. Instead, he considered an idealized delamination, as shown in Figure 1. The modeled delamination, Figure 1(b), consists of two planar delaminations at the -30/90 interfaces. The reason for using the two delaminations in the model is to account for two mechanisms. The first mechanism is the delamination shifting from one -30/90 interface to the other through existing transverse cracks in the 90° plies. This shifting is believed to reduce the bending-extension coupling effect which would occur if the delamination was planar at only one of the -30/90 ply interfaces. Hence, the two symmetric delaminations were used to reduce the bending-extension coupling effect. The second mechanism is the effect of the transverse cracks in the 90° plies. The transverse cracks reduce the axial stiffness of the laminate; this effect was small and was considered "lumped" into the use of the two symmetric delaminations.

Micromechanics has been used to model the limiting strength of composites by reducing the matrix modulus while retaining the original modulus of the reinforcing fibers [9, 10]. In Reference [9], the static failure stress of a short glass-fiber reinforced polyester composite was modeled by reducing the matrix modulus to zero. This produced results in close agreement with experimental data. In Reference [10], the large amounts of strain which occurred during fatigue testing was partially accounted for by reducing the matrix modulus to zero. The micromechanics model accounted for the mean strain response very well until the strain increased rapidly close to failure. The departure of the mean strain from the micromechanics

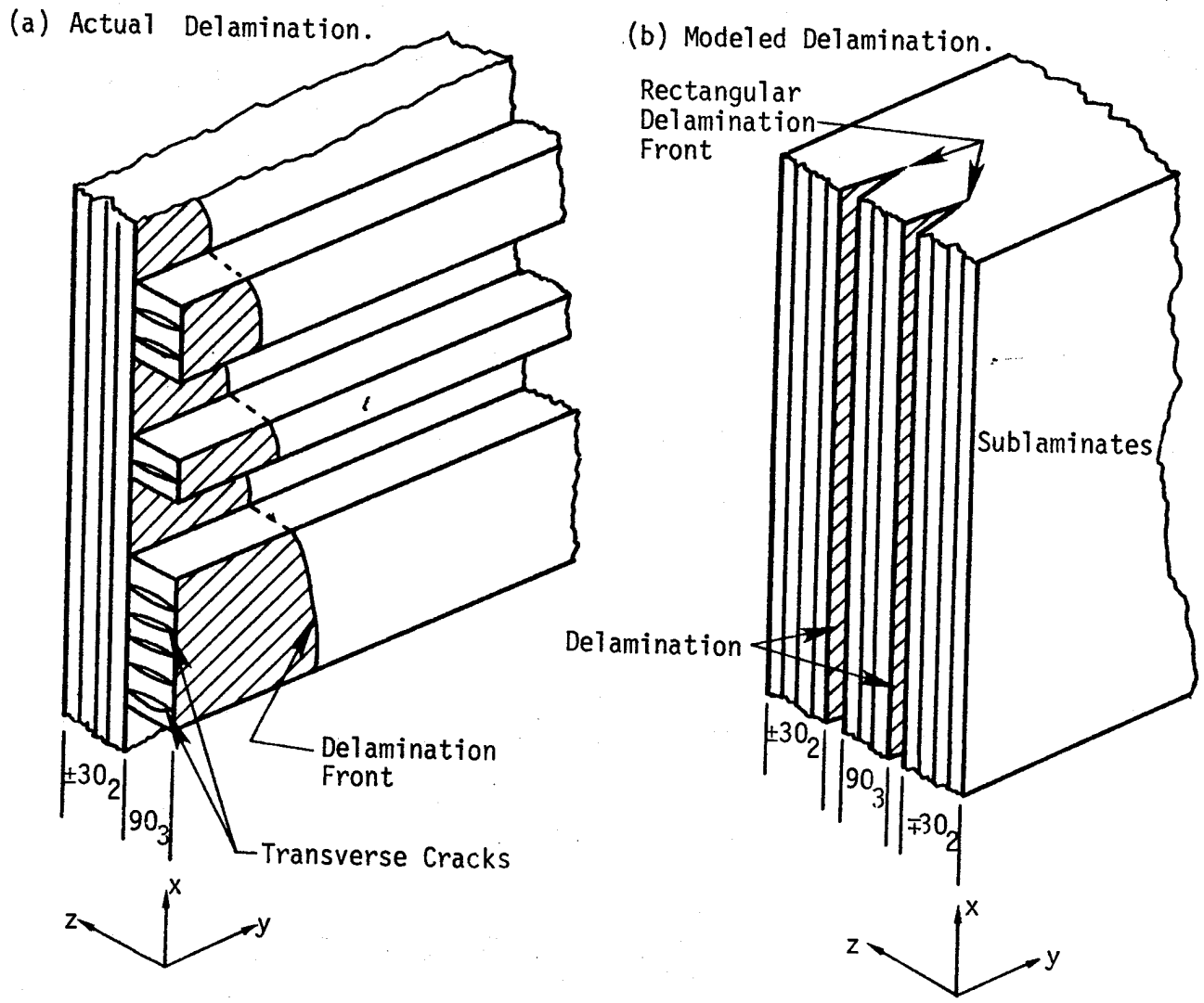


Figure 1 . Idealized model of observed damage.

model was speculated to be due to other failure mechanisms such as delamination.

## Method of Analysis

In this study, an in-depth examination of the damage state of fatigued composite laminates will be performed. Since in Reference [10] it was shown that not all of the strain observed could be accounted for by reducing the matrix modulus in a micromechanics model, it is felt that a more detailed study of the same $[\pm 45/90_2]_2$ graphite/epoxy laminate is required.

The first phase of this study involves an elasticity solution for the composite. The finite element method will be employed for this due to the complexity of the problem. A state of "uniform axial extension" as described by Reference [11] will be assumed. This is the same as the "generalized plane strain state" used in Reference [12].

The micromechanics equations for fibrous composites presented in [13] will be used to obtain the effective lamina moduli as functions of the constituent properties and the fiber volume fraction. The matrix modulus will be reduced uniformly throughout the laminate in order to account for fatigue induced matrix damage. It has been suggested [14] that the matrix modulus reduction could be a function of the local average octahedral shear stress in the matrix. A future study of this should be made to account for stress gradients.

The second phase of the study will involve a fracture mechanics analysis of the laminate with reduced matrix modulus, as it is doubtful

that the modulus reduction alone can account for the entire fatigue behavior of the composite. Also, the analysis method of O'Brien [8] will be used as a comparison with the finite element based analysis.

The search for a locally available finite element program to perform the required stress and fracture analyses was quickly abandoned since the available programs lacked anisotropic material behavior and fracture analysis. A simple two-dimensional, plane stress/plane strain program with an eight node isoparametric element listed in Reference [15] was chosen for development. For crack analysis, the virtual crack closure method as described in Reference [5] is used. This method is particularly attractive, since a special crack tip element is not required.

The experimental data used for correlation is from the extensive characterization of AS/3501-6 graphite/epoxy performed by Dr. T. Ho of Vought Corporation, Dallas, Texas [10,16,17].

# II. MICROMECHANICS

Micromechanics provides the means by which the homogeneous constituent properties of a composite are related to the macroscopically observed properties. This section will provide the means by which the matrix modulus can be related to the laminate deformation behavior. The author makes no attempt to cover the vast amount of material in the field of micromechanics other than to document the pertinent items used in this investigation. Readers are referred to References [18,19, and 20] for additional information on the subject of micromechanics. The article by Chamis and Sendeckyj [18] is an excellent overview of many analytic micromechanics theories. Hashin presents an extensive treatment of the subject in Reference [19]. More recent work in micromechanics has begun to rely upon numerical methods to model inelastic behavior; a brief history of these are presented in Reference [20].

## The Constitutive Relationship

The constitutive relationship for a linearly elastic body including thermal effects can be expressed in contracted notation as:

$$\sigma_i = C_{ij} (\varepsilon_j - \alpha_j \Delta T) \qquad (i,j = 1,6) \qquad (1)$$

or inverted as

$$\varepsilon_i = S_{ij} \sigma_j + \alpha_i \Delta T \qquad (i,j = 1,6) \qquad (2)$$

In the above expressions the repeated j index is summed and i is a

free index. Both indices range from 1 to 6. The quantities $\sigma_i$, $\varepsilon_i$ and $\alpha_i$ are the stress, strain and coefficient of thermal expansion matrices, respectively. These are defined as:

$$\{\sigma\}^T = (\sigma_{xx}, \sigma_{yy}, \sigma_{zz}, \sigma_{yz}, \sigma_{zx}, \sigma_{xy}) \tag{3}$$

$$\{\varepsilon\}^T = (\varepsilon_{xx}, \varepsilon_{yy}, \varepsilon_{zz}, \varepsilon_{yz}, \varepsilon_{zx}, \varepsilon_{xy}) \tag{4}$$

$$\{\alpha\}^T = (\alpha_{xx}, \alpha_{yy}, \alpha_{zz}, 0, 0, 0) \tag{5}$$

The term $\Delta T$ is the change in temperature from a stress free reference temperature. The remaining terms, $C_{ij}$ and $S_{ij}$, are the modulus matrix and compliance matrix components, respectively. These will be defined next.

Consider a unidirectional fiber reinforced laminate as shown in Figure 2. Notice, for fibers which are parallel to axis 1 and randomly positioned, axis 1 is an axis of isotropy. Hence, the laminate is transversely isotropic and requires only five independent constants in the stress-strain relationship [21].

The modulus matrix in the principal material coordinates shown in Figure 2 is:

$$[C_{ij}] = \begin{bmatrix} C_{11} & C_{12} & C_{12} & 0 & 0 & 0 \\ C_{12} & C_{22} & C_{23} & 0 & 0 & 0 \\ C_{12} & C_{23} & C_{22} & 0 & 0 & 0 \\ 0 & 0 & 0 & C_{44} & 0 & 0 \\ 0 & 0 & 0 & 0 & C_{66} & 0 \\ 0 & 0 & 0 & 0 & 0 & C_{66} \end{bmatrix} \tag{6}$$

where $C_{44} = 1/2(C_{22} - C_{23})$

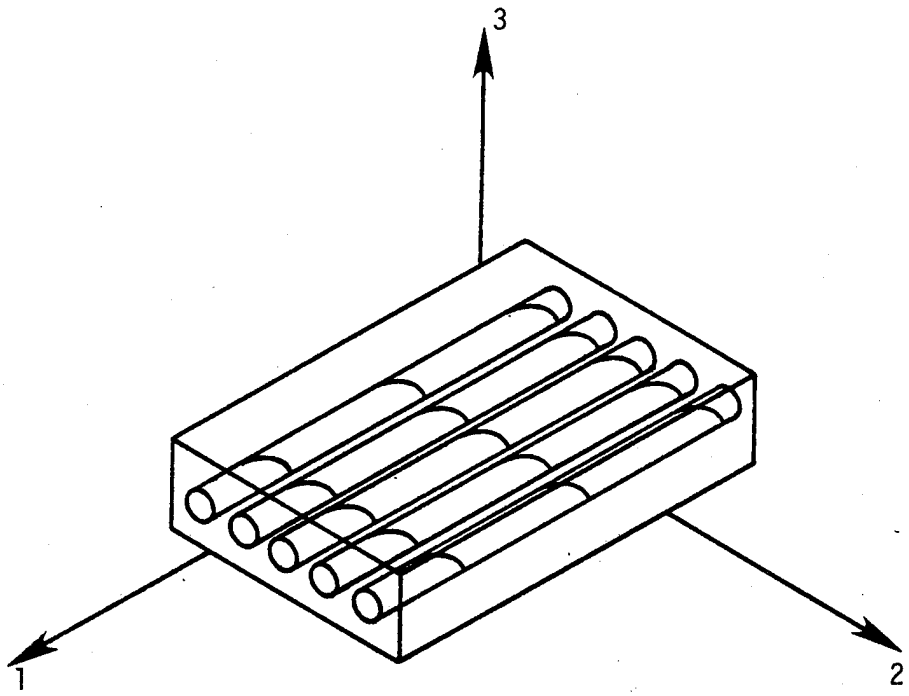


Figure 2 . Principal material coordinates, (1,2,3) used to define the engineering constants.

Alternatively, we can express the compliance matrix in terms of the engineering constants:

$$S_{ij} = \begin{bmatrix} 1/E_1 & -\nu_{21}/E_2 & -\nu_{21}/E_2 & 0 & 0 & 0 \\ -\nu_{12}/E_1 & 1/E_2 & -\nu_{32}/E_2 & 0 & 0 & 0 \\ -\nu_{12}/E_1 & -\nu_{23}/E_2 & 1/E_2 & 0 & 0 & 0 \\ 0 & 0 & 0 & 1/G_{23} & 0 & 0 \\ 0 & 0 & 0 & 0 & 1/G_{12} & 0 \\ 0 & 0 & 0 & 0 & 0 & 1/G_{12} \end{bmatrix} \quad (7)$$

The compliance matrix as shown in (7) consists of eight constants. To retain the five independent constants, the following relationships are required:

$$\frac{\nu_{12}}{E_1} = \frac{\nu_{21}}{E_2} \quad (8)$$

$$\nu_{23} = \nu_{32} \quad (9)$$

$$G_{23} = \frac{E_2}{2(1 + \nu_{23})} \quad (10)$$

Since the compliance matrix is the inverse of the modulus matrix, we can express the modulus matrix in terms of the engineering constants [22, 23]:

$$C_{11} = \frac{(1 - \nu_{23})E_1}{1 - \nu_{23} - 2\nu_{12}\nu_{21}} \quad (11)$$

$$C_{12} = \frac{\nu_{12}E_2}{1 - \nu_{23} - 2\nu_{12}\nu_{21}} \quad (12)$$

$$C_{22} = k + G_{23} \quad (13)$$

$$C_{23} = k - G_{23} \tag{14}$$

$$C_{44} = G_{23} \tag{15}$$

$$C_{66_1} = G_{12} \tag{16}$$

$$k = \frac{E_2}{2(1 - \nu_{23} - 2\nu_{12}\nu_{21})} \tag{17}$$

$$G_{23} = \frac{E_2}{2(1 + \nu_{23})} \tag{18}$$

In Equation (17), k is the bulk modulus for plane strain.

## The Micromechanics Equations

The micromechanics theory to be used is based upon an idealized geometry which leads to modified rule-of-mixtures Equations [13]. The method assumes a concentric cylinder model, Figure 3 , in which the fiber phase is embedded in matrix material. This is surrounded by an infinite homogeneous medium indistinguishable from the composite. The fiber is considered continuous and perfectly aligned. Both fiber and matrix phases are assumed homogeneous. For an isotropic matrix material and a transversely isotropic fiber, the composite engineering properties are:

$$E_1 = E_1^f v^f + E^m v^m \tag{19}$$

$$\nu_{12} = \nu_{12}^f v^f + \nu^m v^m \tag{20}$$

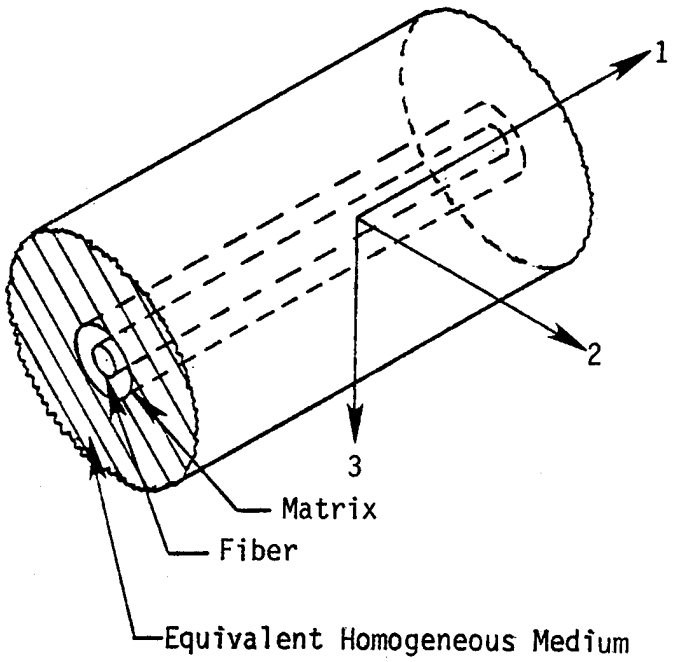


Figure 3 . Concentric cylinder model.

$$G_{12} = \frac{v^f + \eta_s v^m}{\frac{v^f}{G_{12}^f} + \frac{\eta_s v^m}{G^m}} \tag{21}$$

where $\eta_s = 1/2\left(1 + \frac{G^m}{G_{12}^f}\right)$ (22)

$$G^m = \frac{E^m}{2(1 + \nu^m)} \tag{23}$$

$$G_{23} = \frac{v^f + \eta_G v^m}{\frac{v^f}{G_{23}^f} + \frac{\eta_G v^m}{G^m}} \tag{24}$$

where $\eta_G = \frac{3 - 4\nu^m + \frac{G^m}{G_{23}^f}}{4(1 - \nu^m)}$ (25)

$$k_{23} = \frac{v^f + \eta_k v^m}{\frac{v^f}{k_{23}^f} + \frac{\eta_k v^m}{k^m}} \tag{26}$$

where $k^m = \frac{E^m}{2(1 - 2\nu^m)(1 + \nu^m)}$ (27)

$$k_{23}^f = \frac{E_{22}^f}{2(1 - \nu_{23}^f - 2\nu_{12}^f \nu_{21}^f)} \tag{28}$$

$$\eta_k = \frac{1 + \frac{G^m}{k_{23}^f}}{2\ (1 - \nu^m)} \tag{29}$$

$$E_2 = \frac{4k_{23}G_{23}}{k_{23} + \mu G_{23}} \tag{30}$$

$$\nu_{23} = \frac{k_{23} - \mu G_{23}}{k_{23} + \mu G_{23}} \tag{31}$$

$$\text{where } \mu = 1 + \frac{4k_{23}\nu_{12}^2}{E_1} \tag{32}$$

and the coefficients of thermal expansion are

$$\alpha_1 = \frac{1}{E_1}\left[\alpha_1^f E_1^f v^f + \alpha^m E^m v^m\right] \tag{33}$$

$$\alpha_2 = (\alpha_2^f + \alpha_1^f \nu_{12}^f)v^f + (1 + \nu^m)\alpha^m v^m - \nu_{12}\alpha_1 \tag{34}$$

In the above equations, the superscripts f and m are fiber and matrix properties and v is the volume fraction.

Constituent Material Properties

As presented in the last section, the laminate will be composed of transversely isotropic fibers in an isotropic matrix. For the generalized plane strain finite element modeling to be done, a full set of three-dimensional engineering properties is required.

Since this investigation was planned as an analytical study, the author necessarily relied upon existing experimental work. Initially, the extensive experimental characterization, including static, viscoelastic, and fatigue testing at various evnironments of the AS/3501-6 graphite/epoxy system performed by Renton and Ho [10,16,17] seemed adequate. But the characterization of consituent properties was limited in two areas. First, the fibers were assumed to be isotropic and second, only evaluation of the in plane material properties were considered. These shortcomings leave this characterization inadequate for

this investigation.

The required constituent material properties to be considered in this investigation are presented in Table 1 and were obtained from Reference [20].

Laminate properties are presented in Table 2. Experimentally determined laminate properties were obtained from Monib and Adams [24] and Renton and Ho [16]. Monib and Adams reported $\alpha_1 = 0.88 \times 10^{-6}/°C$. Upon investigation, this value was found to be unreasonably high and was replaced with $\alpha_1 = 0.15 \times 10^{-6}/°C$ from Reference [25]. The last column of Table 2 are the material properties determined by micromechanics using the constituent properties from Table 1.

Due to the very low predicted values for the major Poisson's ratio, $\nu_{12}$, obtained by the micromechanics, a more detailed expression was considered to improve the current rule-of-mixtures expression. From Hashin [22], the following expression for $\nu_{12}$ was considered:

$$\nu_{12} = \bar{\nu}_{12} + \nu^*_{12} \tag{35}$$

$$\bar{\nu}_{12} = \nu^f_{12} v^f + \nu^m v^m \tag{36}$$

$$\nu^*_{12} = \frac{(\nu^f_{12} - \nu^m)\left(\frac{1}{k^m_{23}} - \frac{1}{k^f_{23}}\right) v^f v^m}{\frac{v^m}{k^f_{23}} + \frac{v^f}{k^m_{23}} + \frac{1}{G^m}} \tag{37}$$

where $k^f_{23}$, $k^m_{23}$ are the plane strain bulk moduli defined in equations (27) and (28). In Equation (35) the term $\bar{\nu}_{12}$ is the rule-of-mixtures expression previously used. The second term, $\nu^*_{12}$, is an

Table 1. Constituent Material Properties From Reference [20], for Room Temperature, Dry Conditions.

| | Hercules AS-Graphite Fiber | Hercules 3501-6 Epoxy Matrix |
|---|---|---|
| $E_1$(GPa) | 220. | 4.27 |
| $E_2$(GPa) | 13.9 | 4.27 |
| $G_{12}$(GPa) | 34.5 | 1.58 |
| $G_{23}$(GPa) | 5.5 | 1.58 |
| $\nu_{12}$ | 0.2 | 0.34 |
| $\nu_{23}$ | 0.25 | 0.34 |
| $\alpha_1(10^{-6}/°C)$ | -0.36 | 40.0 |
| $\alpha_2(10^{-6}/°C)$ | 18.0 | 40.0 |

Table 2. Comparison of Laminate Properties.

| | Experimental, References [24,25] | Experimental, Reference [16] | Micromechanics Properties** |
|---|---|---|---|
| $E_1$(GPa) | 129.3 | 130.7 | 139.1 |
| $E_2$(GPa) | 10.7 | 6.19 | 8.58 |
| $G_{12}$(GPa) | 6.65 | 6.50 | 5.84 |
| $G_{23}$(GPa) | 3.54 | | 3.16 |
| $\nu_{12}$ | 0.31 | 0.35 | 0.25 |
| $\nu_{23}$ | 0.49 | | 0.36 |
| $\alpha_1(10^{-6}/°C)$ | 0.15* | | .11 |
| $\alpha_2(10^{-6}/°C)$ | 30.6 | | 31.23 |
| $V^f$(%) | | 62.0 | 62.0 |

*the only material property from Reference [25]
** using constituent properties from Table 1.

interaction term which accounts for secondary effects. Note that $\nu_{12}^*$ becomes negative when $\nu^m > \nu_{12}^f$ and $k_{23}^f > k_{23}^m$ which is the case for the constituent materials in Table 1; in fact, $\nu_{12} = -.0037$. Since $\nu_{12}^*$ is small and negative, the rule-of-mixtures expression originally used will be considered sufficient to predict $\nu_{12}$.

At this point, experimental work seems necessary to resolve the question of validity of the micromechanics and the constituent material properties. Since the present study is primarily concerned with the development of an analytical model, and considerable time is required to perform the required experimental work, the micromechanics shall be assumed valid. The material properties have been adjusted to those shown in Table 3. A new comparison of the predicted material properties from micromechanics to experimental values is shown in Table 4. The predicted material properties are in close agreement with the experimental values of References [24,25]. The selection of the constituent material properties was done by trial and error. No specific criterion was used in selecting the constituent material properties with the exception of $G_{23}$ of the fiber. The transverse shear modulus, $G_{23}$, of the laminate was found to be very insensitive to $G_{23}$ of the fiber; therefore, $G_{23}$ of the fiber was assumed to be 60 GPa, an amount reported by Reference [16] as an upper limit.

Table 3. Revised Constituent Material Properties.

| | Hercules AS Graphite Fiber | Hercules 3501-6 Epoxy Matrix |
|---|---|---|
| $E_1$(GPa) | 206.0 | 4.6 |
| $E_2$(GPa) | 18.0 | 4.6 |
| $G_{12}$(GPa) | 60.0 | 1.65 |
| $G_{23}$(GPa) | 6.77 | 1.65 |
| $\nu_{12}$ | 0.265 | 0.39 |
| $\nu_{23}$ | 0.33 | 0.39 |
| $\alpha_1(10^6/°C)$ | 0.39 | 40.0 |
| $\alpha_2(10^6/°C)$ | 20.0 | 40.0 |

Table 4. Comparison of Laminate Properties With Revised Constituent Material Properties.

| | Experimental, References [24,25] | Experimental, Reference | Micromechanics Properties* |
|---|---|---|---|
| $E_1$(GPa) | 129.3 | 130.7 | 129.5 |
| $E_2$(GPa) | 10.7 | 6.19 | 10.4 |
| $G_{12}$(GPa) | 6.65 | 6.50 | 6.35 |
| $G_{23}$(GPa) | 3.54 | | 3.53 |
| $\nu_{12}$ | 0.31 | 0.35 | 0.31 |
| $\nu_{23}$ | 0.49 | | 0.47 |
| $\alpha_1(10^6/°C)$ | 0.15** | | 0.16 |
| $\alpha_2(10^6/°C)$ | 30.6 | | 33.4 |
| $V^f$(%) | | 62.0 | 62.0 |

* using constituent properties from Table 3.
**the only material property from Reference [25].

# III. STRAIN ENERGY RELEASE RATE

The use of strain energy release rate as a fracture growth criterion for cracks in brittle elastic materials is one of long standing. In 1921, Griffith [26] noted that when a crack was introduced to a stressed elastic plate, an energy balance must be maintained between the decrease in the elastic strain energy and the increase in the surface energy resulting from growth of the crack. Griffith's crack growth criterion for fixed grips can be stated as

$$\frac{dU}{da} = \frac{dW}{da} \tag{38}$$

where U is the elastic strain energy, W is the energy required for crack growth, and a is the crack length. The term $\frac{dU}{da}$ is usually called the strain energy release rate, G. The strain energy release rate is a measure of the driving force the body contains to extend a crack. The term $\frac{dW}{da}$ is the energy consumed during crack growth. This is sometimes called the crack resistance, R. The units associated with G and R are energy per unit of crack surface.

Irwin [27] considered an infinite plate with fixed ends containing a crack size a. If forces are applied to the crack edge, sufficient to close the crack over an infinitesimal distance (see Figure 4) work will be done. If this process is reversed, then work will be released from the plate. This work per unit of cracked area is another definition of strain energy release rate.

Referring once again to Figure 4, let $\vec{\Delta u}$ be a vector representing

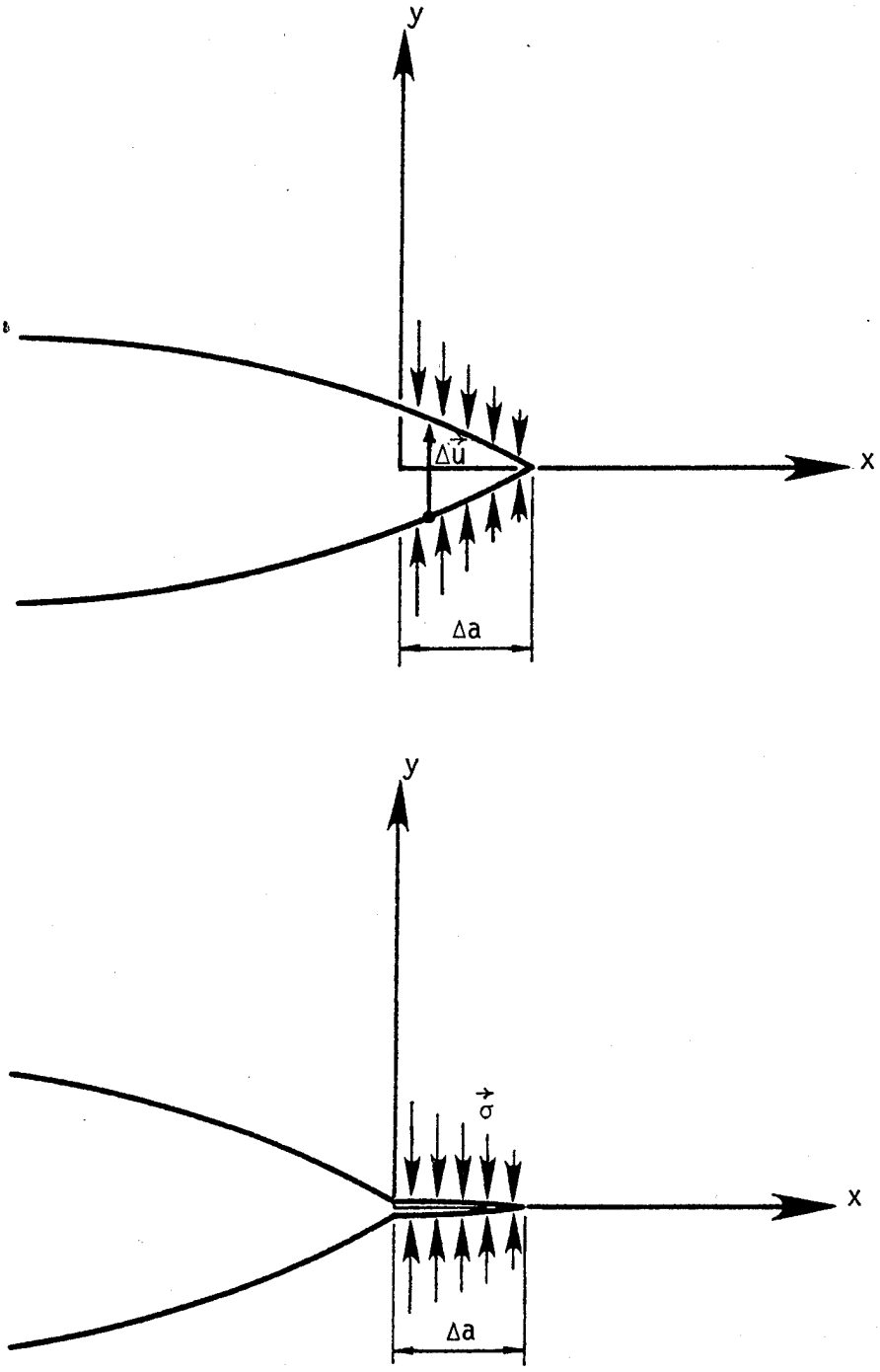


Figure 4 . Schematic of crack closure.

the relative normal and sliding displacements between the crack faces. Let $\vec{\sigma}$ be a vector defining the normal and shear force components per unit area which are required to close the crack. Then Irwin's crack closure integral can be expressed as :

$$G = \lim_{\Delta a \to o} \frac{1}{2\Delta a} \int_0^{\Delta a} \vec{\sigma} \cdot \Delta \vec{u} \, da \tag{39}$$

By writing the inner product in component form, the strain energy release rate can be expressed as :

$$G = G_I + G_{II} + G_{III} \tag{40}$$

where :

$$G_I = \lim_{\Delta a \to o} \frac{1}{2\Delta a} \int_0^{\Delta a} \sigma_y \, \Delta w \, da \tag{41}$$

$$G_{II} = \lim_{\Delta a \to o} \frac{1}{2\Delta a} \int_0^{\Delta a} \sigma_{yz} \, \Delta v \, da \tag{42}$$

$$G_{III} = \lim_{\Delta a \to o} \frac{1}{2\Delta a} \int_0^{\Delta a} \sigma_{xz} \, \Delta u \, da \tag{43}$$

The components $G_I$, $G_{II}$, and $G_{III}$, also referred to as mode I, mode II, and mode III strain energy release rates, are illustrated in Figure 5. These correspond to the crack opening, sliding, and tearing modes, respectively.

Finite Element Evaluation of Crack Closure Integral

Rybicki and Kanninen [5] presented a very simple method of evaluating the Irwin's crack closure integral (39). This technique greatly

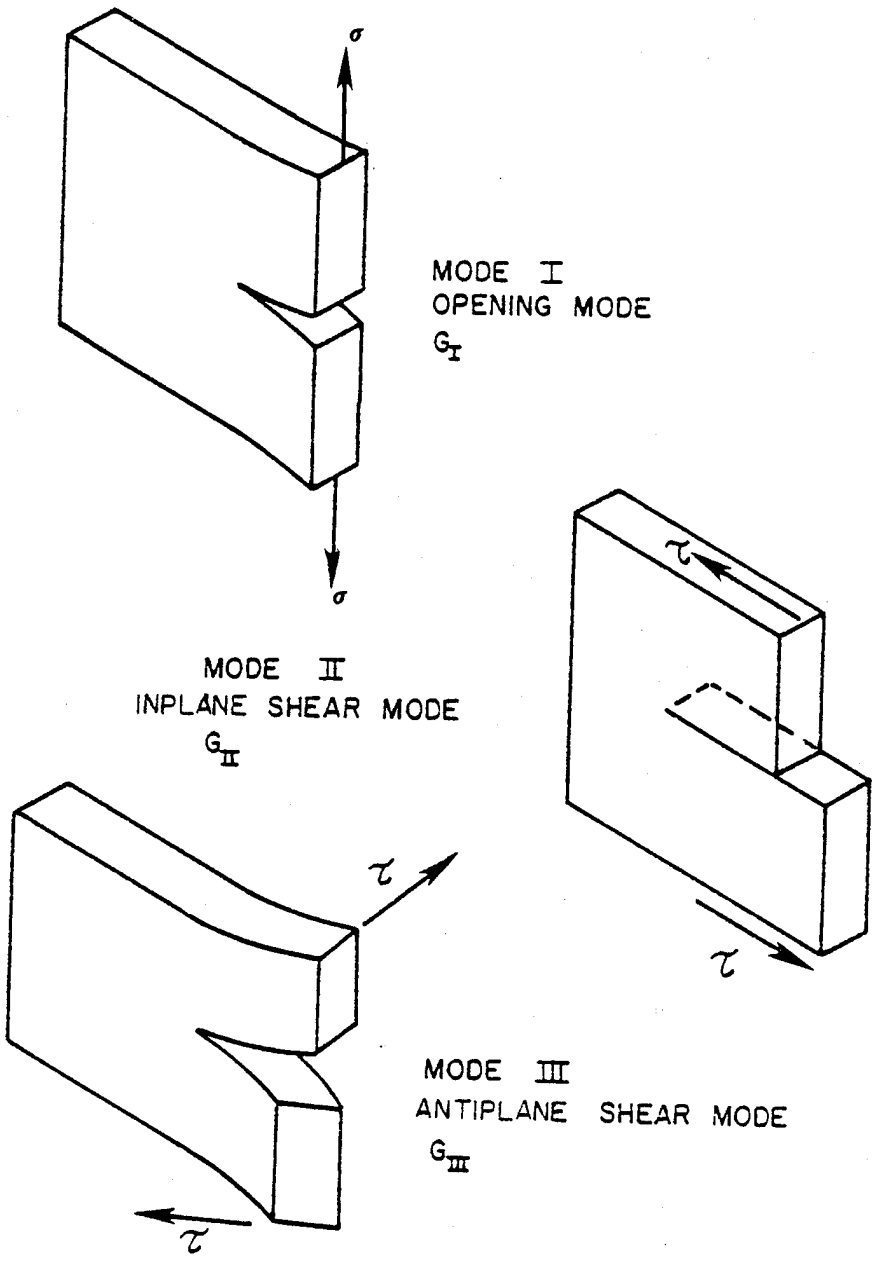


Figure 5 . Standardized crack extension modes.

simplifies the energy release rate computation because knowledge of the singular stress field near the crack tip is not required.

Referring to Figure 6 (a), first the nodal forces are evaluated at nodes b and c for a crack of size a. Then nodes b and c are released and the crack is allowed to extend an amount $\Delta a$ as in Figure 6 (b). After the crack extension the relative displacements between nodes b' and e' and between c' and f' are measured. The energy release rate can now be expressed as the work required to close the crack an amount $\Delta a$ or simply:

$$G_I = \frac{1}{2\Delta a} [F_{zb}(w_{b'} - w_{e'}) + F_{zc}(w_{c'} - w_{f'})] \tag{44}$$

$$G_{II} = \frac{1}{2\Delta a} [F_{yb}(v_{b'} - v_{e'}) + F_{yc}(v_{c'} - v_{f'})] \tag{45}$$

$$G_{III} = \frac{1}{2\Delta a} [F_{xb}(u_{b'} - u_{e'}) + F_{xc}(u_{c'} - u_{f'})] \tag{46}$$

where, for example, $F_{zb}$ is the nodal force in the z direction at node b. Observe that nodal forces at node b are composed of contributions from both elements 1 and 2. One expression from which the nodal forces can be evaluated for the linear case is:

$$R^e_i = K^e_{ij}\ q^e_j - Q^e_i \qquad i, j = 1, \text{NDOFE} \tag{47}$$

where:

$R^e_i$ = nodal force of element

$K^e_{ij}$ = element stiffness matrix

$q^e_j$ = element nodal displacements

$Q^e_i$ = applied elemental nodal forces

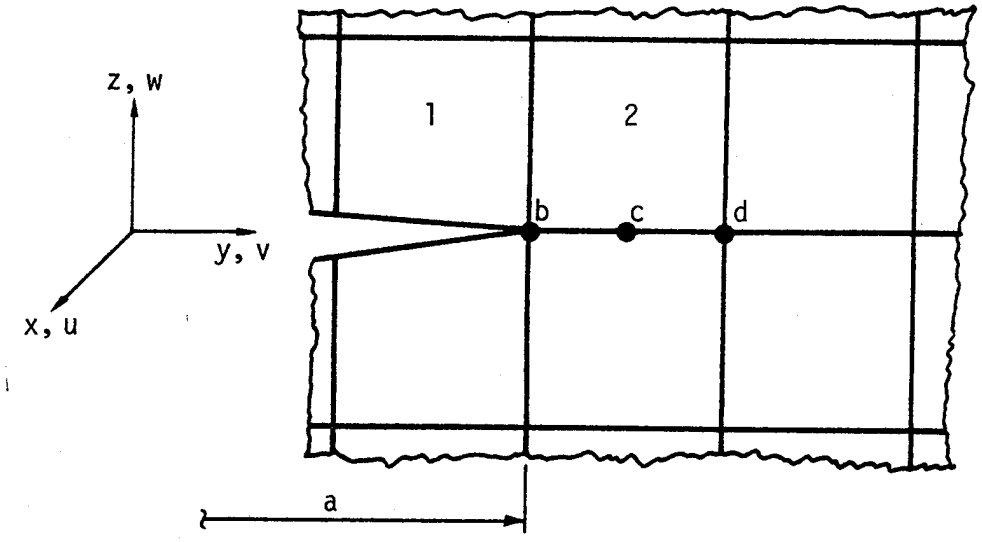


(a) Before Extension

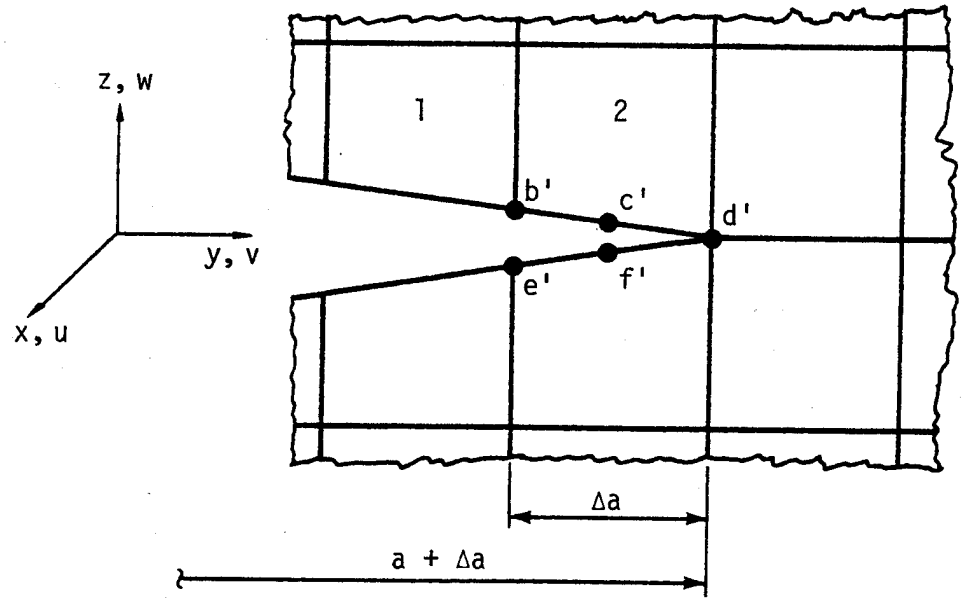


(b) After Extension

Figure 6. Crack closure, energy release calculation technique.

NDOFE = number of degrees of freedom per element.

Delamination Analysis Based Upon Classical Lamination Theory

In this section a method of delamination analysis will be presented based upon classical lamination theory (CLT). This method was first used by O'Brien [8] for the case of a constant axial strain or "fixed-grip" condition. The following analysis will be for the case of constant axial stress.

The first step is to develop the rule of mixtures expression for the change in the axial stiffness which is common to both load cases. From CLT the axial stiffness of a laminate, Figure 7(a), can be expressed as:

$$E_{LAM} = \frac{1}{a_{11} t} \tag{48}$$

where $a_{11}$ is the first element of the extensional compliance matrix and t is the total laminate thickness. Now consider one or more planar delaminations to extend across the laminate. These delaminations have completely severed the laminate into separate sublaminates. The sublaminates are assumed to be gripped in such a manner as to allow identical axial strains in all the sublaminates, but the transverse strain is free to do as it will. The axial stiffness after the full delamination, Figure 7(b), can be expressed as:

$$E^* = \frac{1}{t} \sum_{i=1}^{n} E_i t_i \tag{49}$$

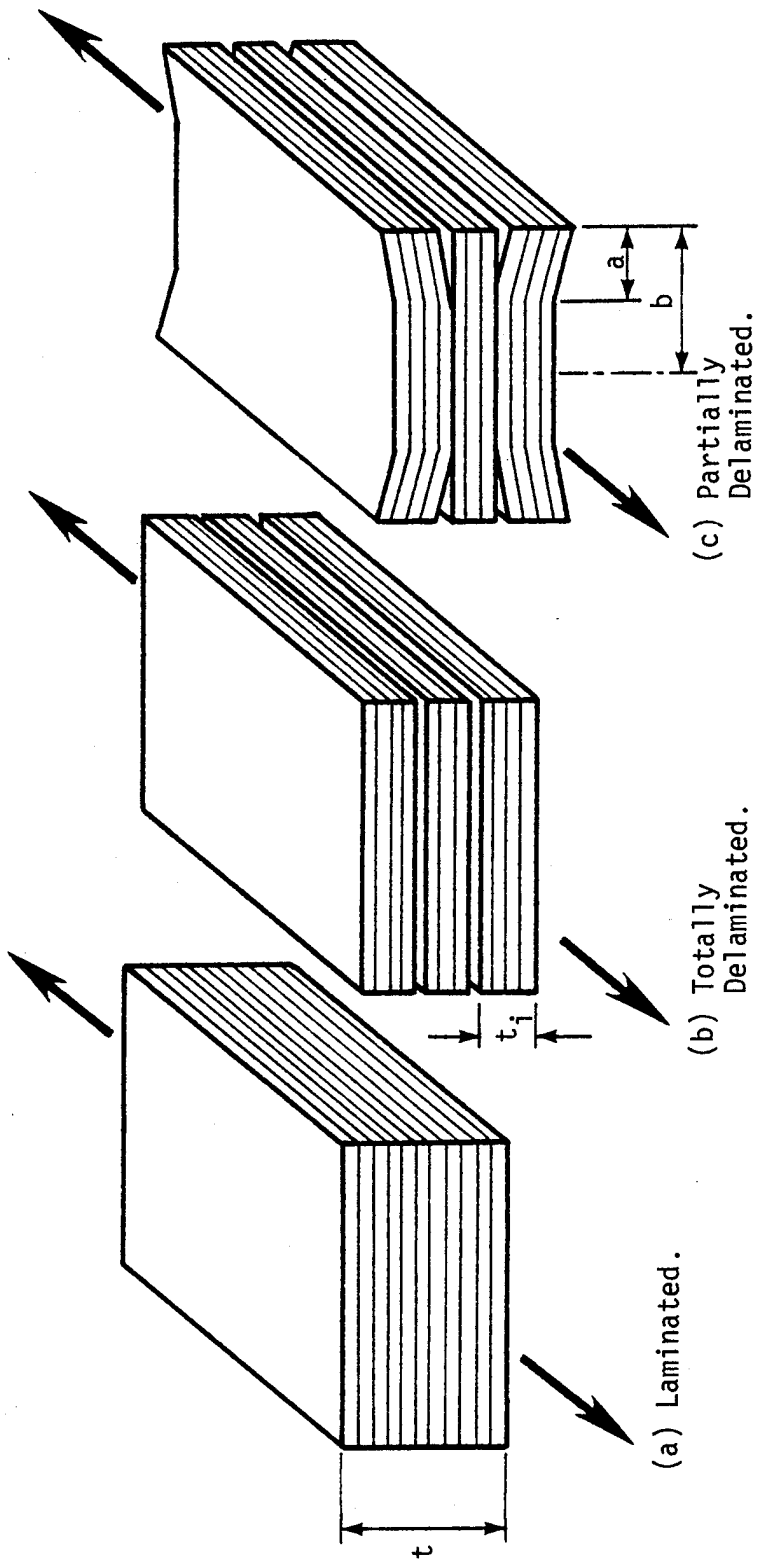


Figure 7 . Rule-of-mixtures analysis for stiffness loss.

where $E_i$ = the axial stiffness of the ith sublaminate formed

$t_i$ = the thickness of the ith sublaminate formed

$t$ = the total laminate thickness

$n$ = the number of sublaminates formed.

Since the axial stiffness of the sublaminate is:

$$E_i = \frac{1}{(a_{11})_i t_i} \tag{50}$$

then E* is simply:

$$E^* = \frac{1}{t} \sum_{i=1}^{n} \frac{1}{(a_{11})_i} \tag{51}$$

The limiting cases for the axial stiffness have now been established. These are the totally bonded laminate and the totally delaminated laminate. If a linear variation of axial stiffness with respect to the nondimensional delamination size a/b, as in Figure 7(c), is assumed then a rule-of-mixtures expression is derived for the axial stiffness,

$$E = (E^* - E_{LAM}) \frac{a}{b} + E_{LAM} \tag{52}$$

Note that the delamination is considered to extend the entire length of the laminate and delaminations are considered to extend inward from both sides simultaneously.

O'Brien [8] experimentally verified the rule-of-mixtures expression for the axial stiffness for a $[\pm 30/\pm 30/90/\overline{90}]_s$ laminate. But the verification required neglecting the contributions of the bending-extension coupling matrix. Recall that the axial stiffness of a sublaminate can be expressed as:

$$E_i = \frac{1}{(a_{11})_i t_i} \tag{53}$$

where $[a] = [A]^{-1} + [A]^{-1}[B]\,[D^*]\,[B]\,[A]^{-1}$

and $[D^*] = [D] - [B]\,[A]^{-1}[B]$

where [A], [B], and [D] are the extensional, coupling, and bending matrices as defined in reference [28]. Provided the laminate or sublaminate in question is symmetric, $a_{11}$ has no contribution from the [B] matrix since it vanishes for this case. But for the laminate examined by O'Brien delaminations formed at the -30/90 interfaces, and E* was calculated based upon the following three sublaminates: $[\pm 30_2]_T$, $[90_3]_T$ and $[\mp 30_2]_T$. Two of the sublaminates: $[\pm 30_2]$ and $[\overline{\mp} 30_2]$ are nonsymmetric, hence the coupling matrix [B] is not zero. O'Brien neglected the effect of the [B] matrix to obtain the best match to experimental results. The reason for neglecting the [B] matrix is due to the fact that instead of two planar delaminations which were assumed in the model, there was one delamination which jumps back and forth from one -30/90 interface to the other as in Figure 1(a). The delaminations were believed to grow in this manner to reduce the effect of the bending-extension coupling that would have been present in a planar delamination. At this point, it cannot be concluded that the effect of the [B] matrix in general can be neglected without further investigation of other laminate configurations.

The strain energy release rate, G, for a planar flaw of area, A, can be expressed as [8],

$$G = \frac{\partial W}{\partial A} - \frac{\partial U}{\partial A} \tag{54}$$

where W is the potential energy of the applied tractions and U is the elastic strain energy. For a laminate under uniaxial stress $\sigma$(in which $\sigma$ = axial force/area) the strain energy is:

$$U = \frac{\sigma^2 V}{2E} \tag{55}$$

where axial stiffness E, equation (52), is a function of flaw area and V is the volume of the body. Differentiating the strain energy, one gets:

$$\frac{\partial U}{\partial A} = \frac{-\sigma^2 V}{2E^2} \frac{dE}{dA} \tag{56}$$

Assuming a laminate with two planar delaminations as in Figure 8, the quantities V, A, and dA can be expressed as:

$$V = 2bt \tag{57}$$

$$A = 2La \tag{58}$$

$$dA = 2L(da) \tag{59}$$

and using the rule-of-mixtures expression for the modulus of elasticity, then:

$$\frac{dU}{dA} = \frac{\sigma^2 t(E_{LAM}-E^*)}{2E^2} \tag{60}$$

The potential energy, W, for a linear elastic body can be expressed as:

$$W = 2U \tag{61}$$

thus,

$$\frac{\partial W}{\partial A} = 2 \frac{\partial U}{\partial A} \tag{62}$$

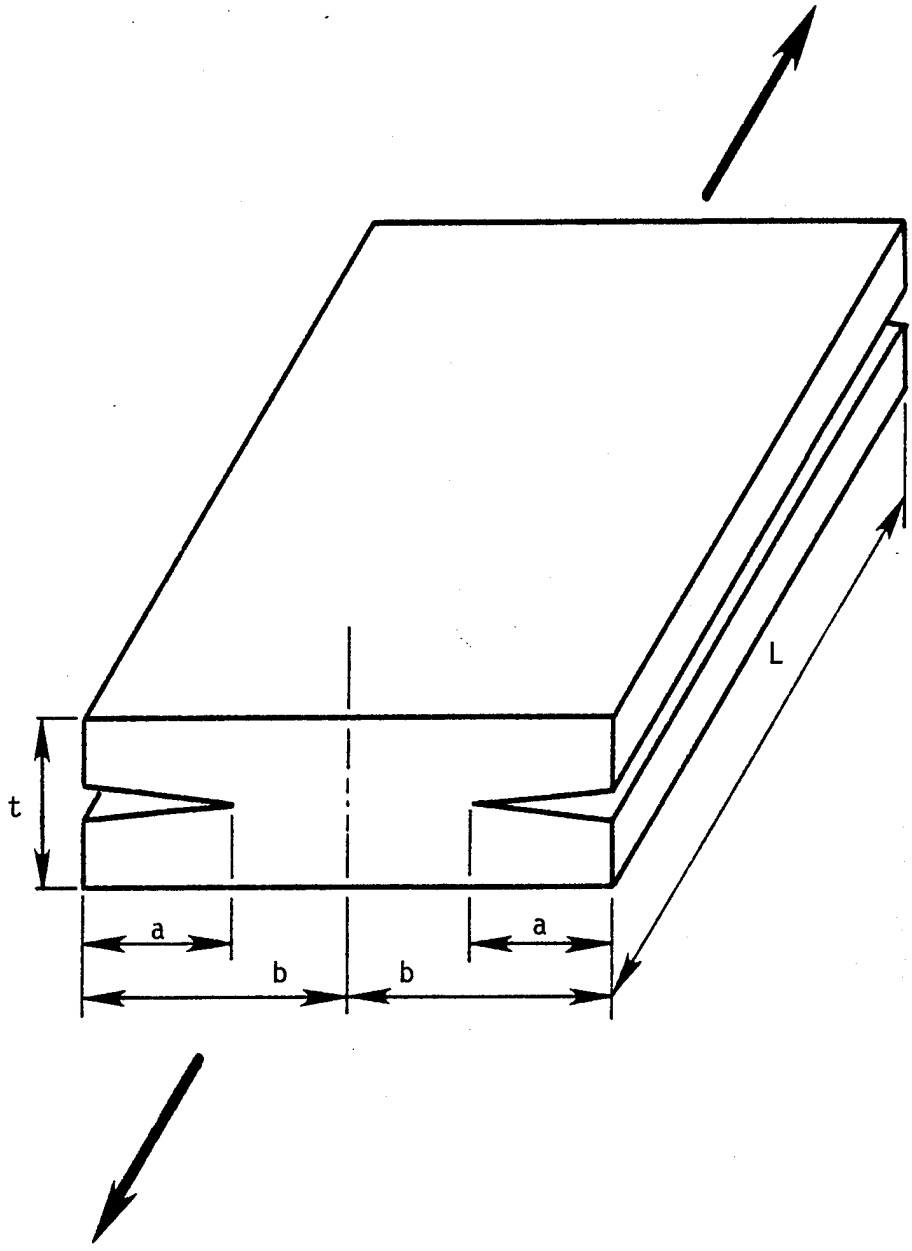


Figure 8 . Configuration of delamination.

From equations (54), (60), and (62) we obtain,

$$G = \frac{\sigma^2 t(E_{LAM} - E^*)}{2[(E^*-E_{LAM})\frac{a}{b} + E_{LAM}]^2} \tag{63}$$

Note that the strain energy release rate becomes infinite as $E^*$ goes to zero and $\frac{a}{b}$ goes to one.

# IV. APPLICATIONS

In this chapter, several problems will be considered using the analytical tools developed in the previous chapters. An extensive discussion of the finite element method used in this chapter is contained in Appendix A. First, an investigation of the axial laminate stiffness as a function of a reduction in the matrix modulus is conducted. Once this is obtained, the matrix degradation as a function of fatigue cycles is established. The chapter is then closed with a parametric study of the effect of matrix degradation on the available strain energy release rate for a delamination at the -45/90 ply interface. Throughout this entire chapter, only a $[\pm 45/90_2]_s$ laminate will be analyzed. Residual stresses induced by moisture and thermal effects have been neglected.

## Laminate Stiffness as a Function of Matrix Modulus

In this section, the axial laminate stiffness as a function of matrix modulus for a $[\pm 45/90_2]_s$ test specimen will be investigated. The main point of this will be to assess the accuracy of classical lamination theory (CLT) versus a finite element method (FEM) which accounts for free edge effects. For this study, the micromechanics theory previously outlined was used with the constituent properties from Table 3. The test specimen geometry used for the laminate was from Reference [10], this information being contained in Appendix B.

Recall from the previous section, from CLT the axial stiffness for the laminate can be expressed as:

$$E_{LAM} = \frac{1}{a_{11}t} \tag{64}$$

where $a_{11}$ is the first term in the extensional compliance matrix and t is the laminate thickness. For the FEM solution, the axial laminate stiffness can be calculated as:

$$E_{LAM} = \frac{\sigma_{AVG}}{\varepsilon_o} \tag{65}$$

$$\text{where } \sigma_{AVG} = \frac{1}{A} \int \int \sigma_{xx} \, dydz. \tag{66}$$

The term $\sigma_{AVG}$ can easily be identified as the average axial stress and $\varepsilon_o$ is the axial strain.

Since the free edge stresses are local to the free edge, only a portion of the entire width of the laminate was modelled using the finite element method. The width of the laminate selected to be modelled was determined by the distance required from the free edge for the stresses to converge to the CLT solution. Hence, the elasticity solution was obtained by a combination of the FEM solution near the free edge and the CLT solution for the interior of the laminate. Because of this, the expression for the axial laminate stiffness had to be modified. It is a simple matter to show that the axial stiffness for the elasticity solution is a rule-of-mixtures expression obtained from the two solutions, if one considers two parallel bars which are deformed uniformly. The rule-of-mixtures expression can be stated as:

$$E_{LAM} = E_{CLT} A_{CLT} + E_{FEM} A_{FEM} \tag{67}$$

where $E_{CLT}$ and $E_{FEM}$ are the axial stiffnesses from the CLT and the FEM solutions, respectively, and $A_{CLT}$ and $A_{FEM}$ are the fractions of the cross-sectional area for the respective solutions. The elasticity solution is depicted in Figure 9. Due to symmetry, only one-quarter

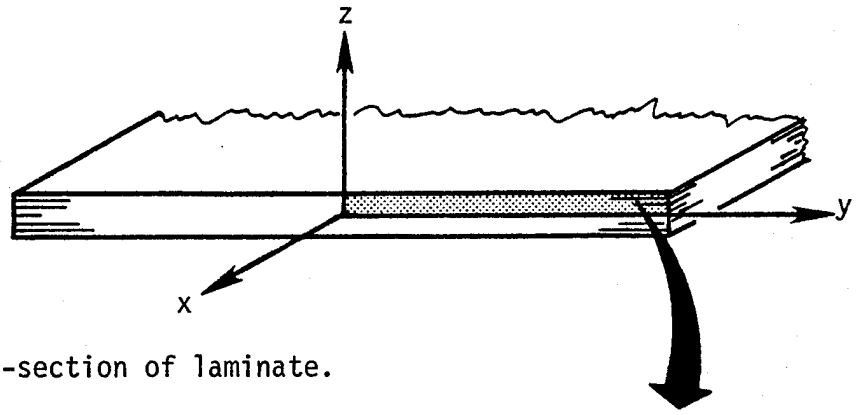


(a) Cross-section of laminate.

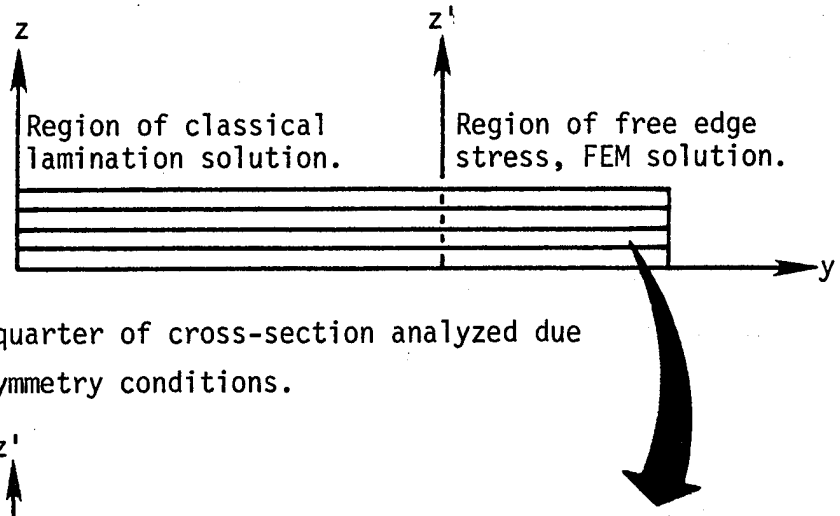


(b) One-quarter of cross-section analyzed due to symmetry conditions.

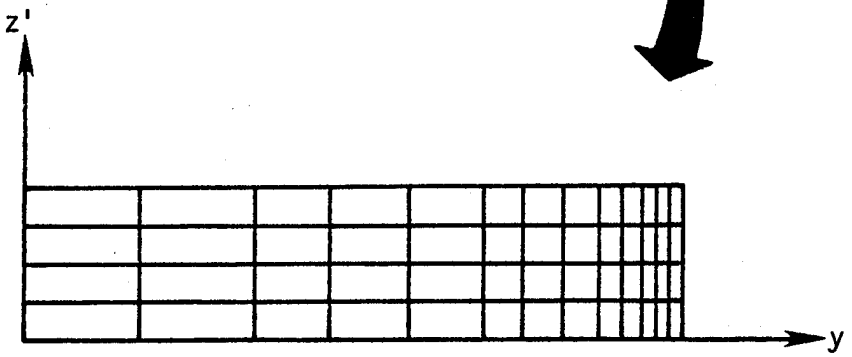


(c) Only free edge region requires finite element modelling.

Figure 9. Schematic of elasticity solution.

of the laminate required modelling and of that quarter, only the portion to the right of the z'axis required finite element modeling.

The axial stiffness was evaluated for six values of the matrix modulus, from the initial matrix modulus of 4.6 GPa, down to a value of 0.0723 GPa. This wide range of values for the matrix modulus required using two different meshes for the finite element model. The first mesh, see Figure 10, was selected to model one-third of the laminate half-width and maintain a maximum element aspect ratio of 10:1. This mesh was adequate for the initial matrix modulus and 63% of the initial matrix modulus, but for 25% of the initial matrix modulus, the stresses along the z' axis did not converge to the CLT solution; hence, the region of free edge effects was not modelled sufficiently. To correct this, two-thirds of the laminate half-width was modelled. Due to program limitations, additional elements were not available, so the first mesh was simply expanded. The second mesh is shown in Figure 11. In expanding the mesh, the aspect ratio increased proportionately to 20:1. The second mesh was used to compute the axial stiffness for matrix modulus values from 25% to 1.6% of the initial matrix modulus. Both meshes contained 120 elements and 1158 degrees of freedom.

Presented in Figure 12 is the axial laminate stiffness as a function of matrix modulus. In evaluating the laminate stiffness, only the matrix modulus was allowed to vary while all other constituent material properties were held constant. On the x-axis, the matrix modulus was normalized by $E^m_{initial}$, which was the initial matrix modulus from Table 3. On the y-axis, the laminate stiffness was normalized by $E_{REF}$, which was defined as the laminate stiffness obtained from the

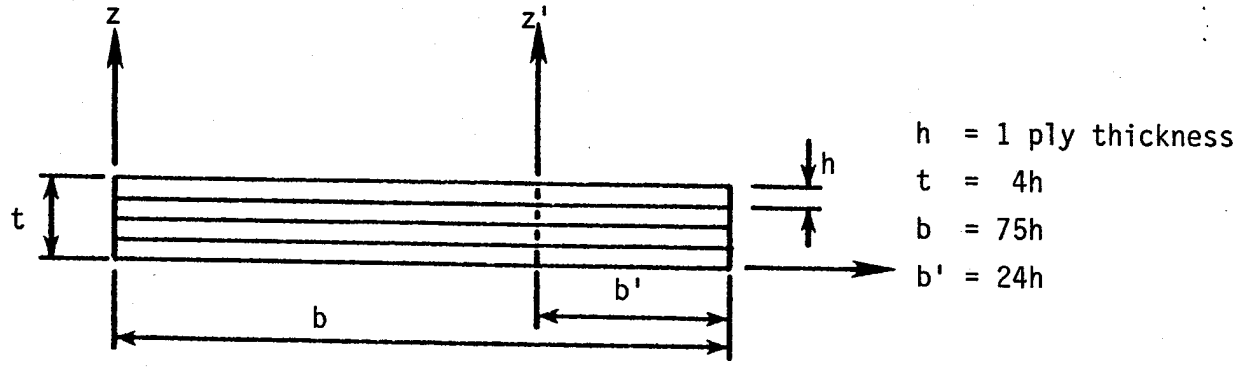


(a) One-quarter of laminate cross-section.

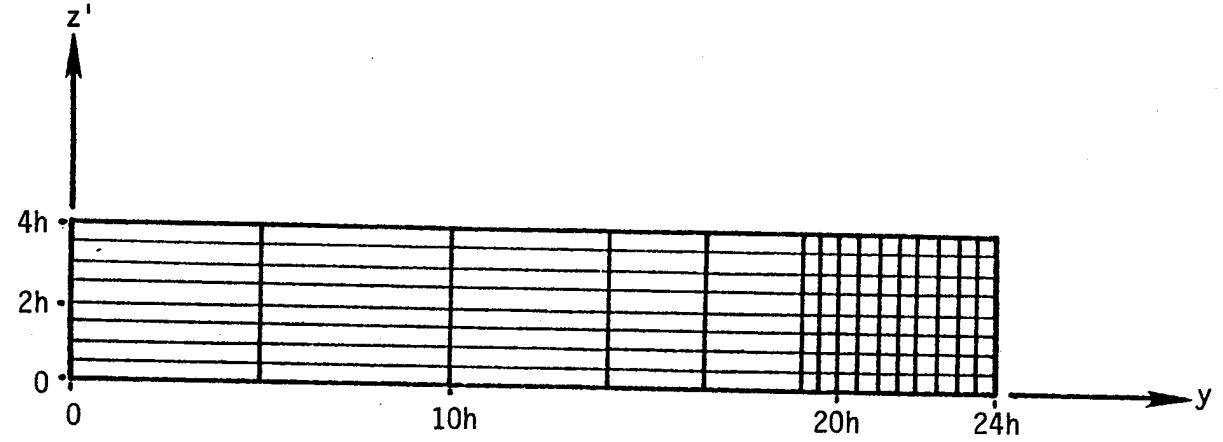


(b) Finite element mesh at free edge.

Figure 10. Finite element line mesh.

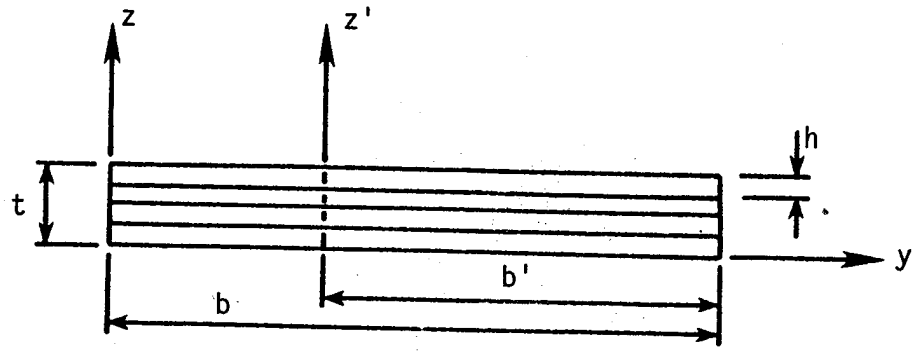


h = 1 ply thickness
t = 4 h
b = 75h
b' = 50h

(a) One-quarter of laminate cross-section.

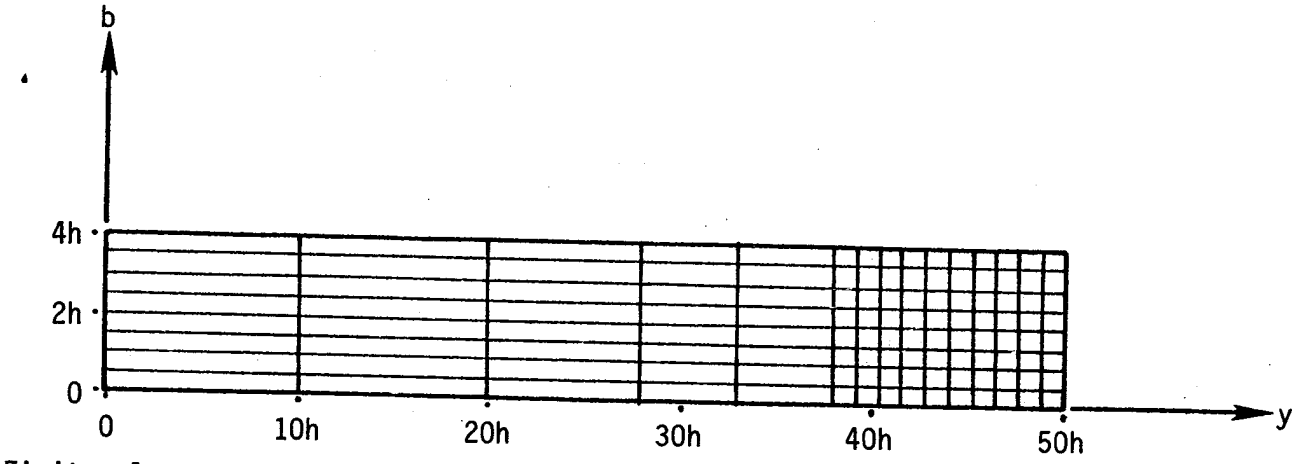


(b) Finite element mesh at free edge.

Figure 11. Finite element coarse mesh.

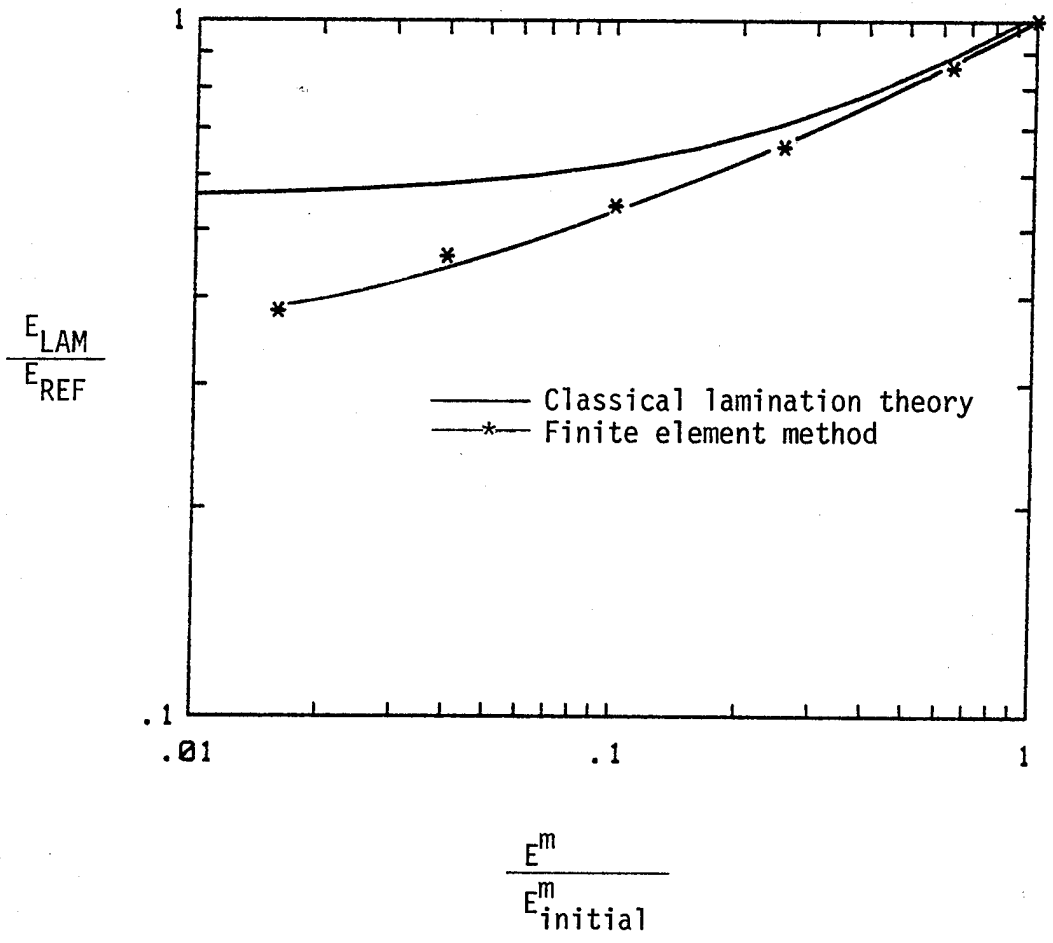


Figure 12. Axial laminate stiffness as a function of matrix modulus.

elasticity solution when $E^m/E^m_{initial} = 1.0$. The value of $E_{REF}$ was found to be 23.02 GPa. It should be noted that $E_{REF}$ will be used throughout the rest of this work in presenting the results in a nondimensional form. From Figure 12, the CLT solution is shown to be stiffer than the FEM solution and for smaller values of the matrix modulus the discrepancy becomes quite considerable. This discrepancy is due to the fact that as the matrix modulus goes to zero, CLT yields a finite value of 12.7 GPa for the laminate stiffness while the finite element stiffness appears to vanish.

Presented in Figure 13 is the error in the laminate stiffness as a function of matrix modulus when calculated by CLT. The x-axis is the normalized matrix modulus as used previously. For the y-axis, $E_{CLT}$ and $E_{ELAST}$ are the axial laminate stiffnesses obtained by CLT and the elasticity solution, respectively. It can be seen for the initial value of the matrix modulus that the difference is a modest 2.4%, but for the normalized values of the matrix modulus of 0.1 and 0.016, the difference increased to 14.7% and 48.0%, respectively.

The reason for this extreme discrepancy in the CLT solution is that the shear modulus of the laminate tends to maintain a value on the same order of magnitude as the matrix modulus. Hence, as the matrix modulus goes to zero, so does the shear moduli. This resulting decrease in the shear modulus allows for considerable shear deformation which tends to warp the laminate cross-section. Due to the fundamental Kirchhoff-Love hypothesis of CLT, it is unable to model the necessary shear deformation encountered with the very small shear modulus, and this accounts for the erroneously stiff solutions predicted by

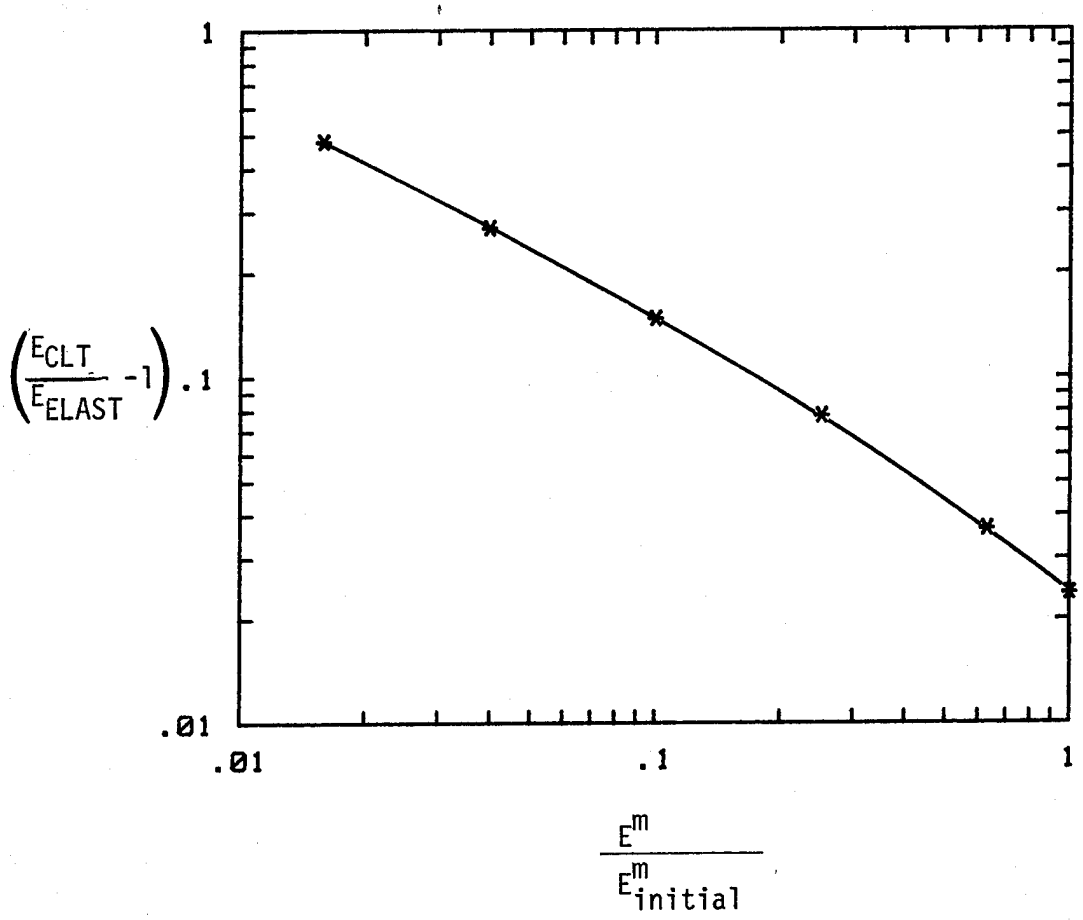


Figure 13. Classical lamination theory error in axial stiffness.

CLT. It should be noted that the FEM used in analyzing the laminate contained sufficient freedom to model the shear warping.

Matrix Degradation as a Function of Fatigue Cycles

In this section, we shall evaluate the matrix modulus as a function of the fatigue cycles. This will be based upon the mean strain fatigue test data from Ho and Schapery [10] which is included in Appendix B. Throughout this section, the laminate will be considered without any delaminations. The study of the effect of delaminations will be conducted in the next section.

Constant stress amplitude fatigue tests were conducted with maximum tensile stresses of 50%, 55%, and 60% of the ultimate tensile stress of the laminate. The ratio of the minimum stress to maximum stress was +0.1. Additional information concerning test conditions are contained in Appendix B.

Presented in Figure 14 is the mean strain response as a function of the number of fatigue cycles for each of the tests. These curves are somewhat idealized due to scatter and the limited amount of test data. A further discussion of the mean strain idealization is contained in Appendix B. The mean strain behavior is characterized by an increasing, predominately linear, response in logarithmic scales. Near failure, the mean strain breaks away from its previous linear path and increases very rapidly to failure.

Throughout the remainder of this work the fatigue tests shall be analyzed as though they were static tests. Simply stated, no dynamic effects will be considered. Also, the effects of the stress amplitude

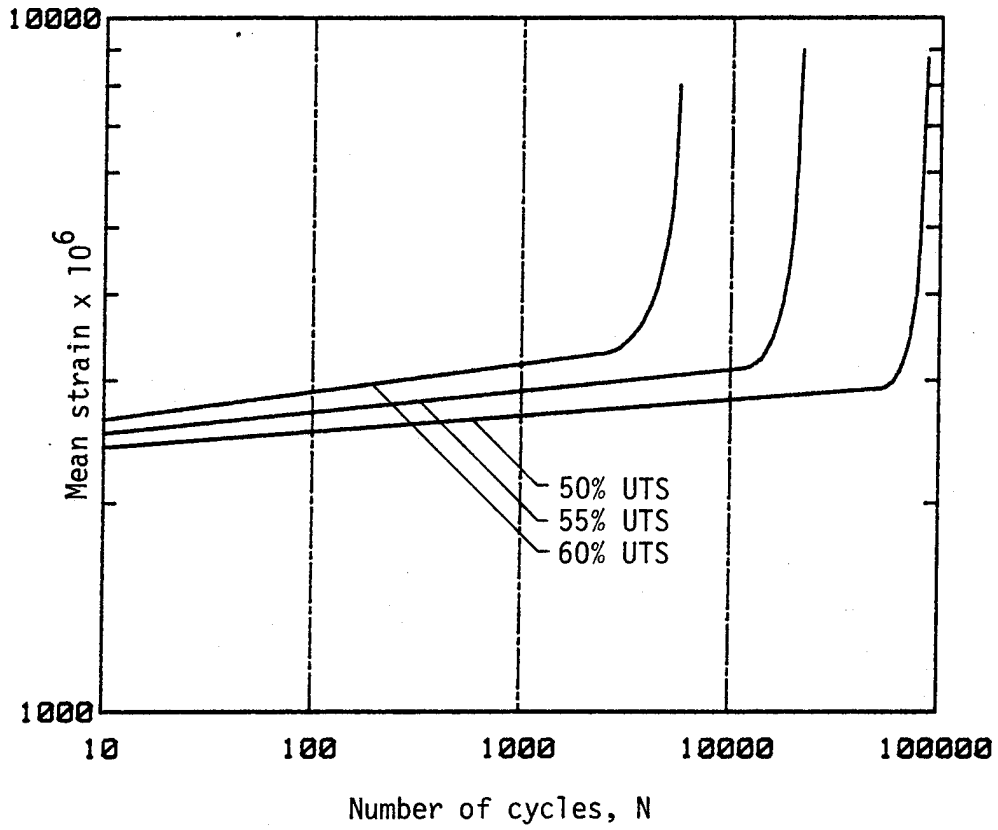


Figure 14. Idealized mean strain curves for a $[\pm 45/90_2]_s$ laminate.

will not be addressed directly. Instead, only the mean stress input and the mean strain response will be addressed. From this very narrow viewpoint, the fatigue tests somewhat resemble creep tests. With this in mind, we shall define the apparent laminate stiffness as:

$$E_{APPARENT} = \frac{\bar{\sigma}}{\bar{\varepsilon}} \tag{68}$$

where $\bar{\sigma}$ is the mean stress and $\bar{\varepsilon}$ is the mean strain. The apparent laminate stiffness for the three fatigue tests is shown in Figure 15. The apparent stiffness was normalized by the term $E_{REF}$, which is the initial laminate stiffness previously defined. From this figure it is easy to see that in all of the tests, the stiffnesses degraded to approximately 75% of their original stiffness by the tenth cycle, which is quite interesting. One possible explanation for the 30% reduction in the axial stiffness is the initial matrix damage as a result of the residual thermal stresses incurred during the cool down from the laminate cure temperature.

The relationship of matrix modulus to fatigue cycles was difficult to obtain due to the lack of explicit functions. This resulted in determining the desired function graphically. First, the elasticity solution for the laminate stiffness as a function of matrix modulus from Figure 12 was inverted to yield the matrix modulus as a function of laminate stiffness. Then, the apparent laminate stiffness as a function of the fatigue cycles from Figure 15 were substituted in for the laminate stiffness in the previous function which then yielded the matrix modulus as a function of the fatigue cycles. The procedure is depicted in Figure 16. The matrix modulus as a function of the

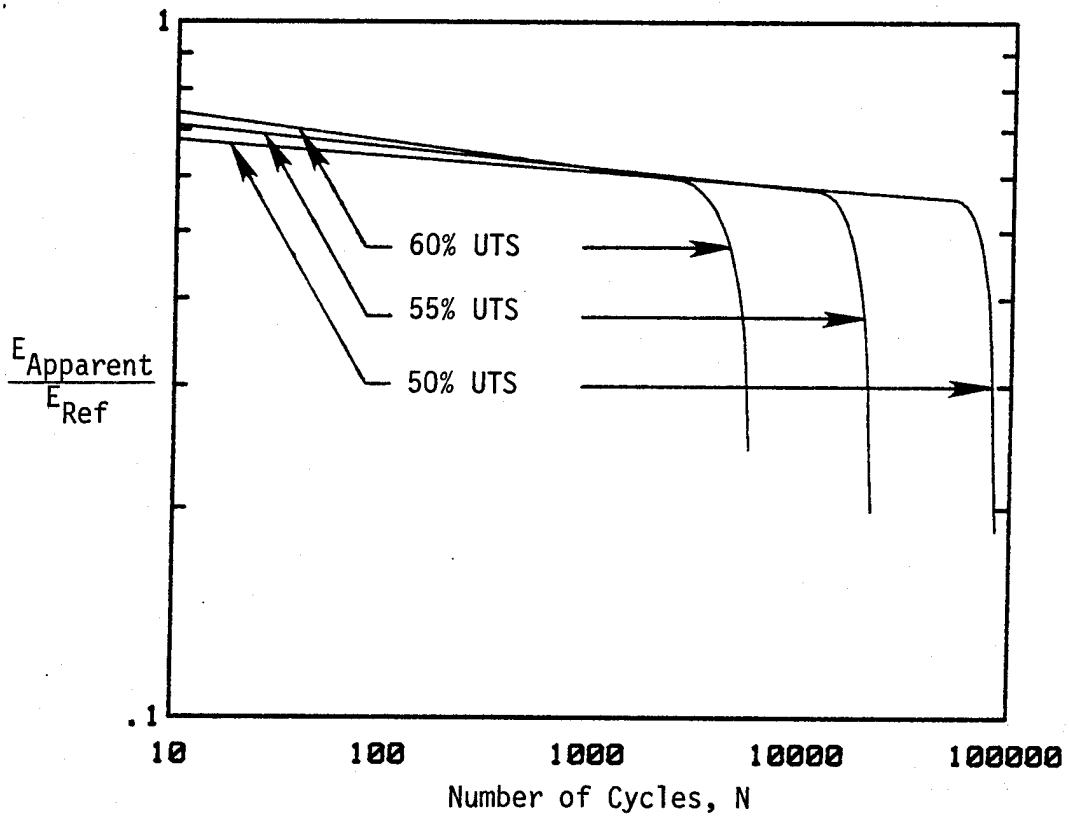


Figure 15. The apparent laminate stiffness as a function of fatigue cycles.

ANALYTICAL

GRAPHICAL

(a) $E_{Lam} = E_{Lam}(E^m)$

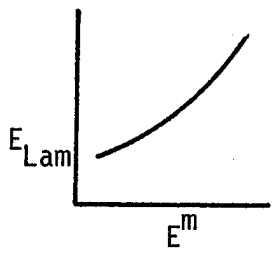


Inverting (a) yields,

(b) $E^m = E^m(E_{Lam})$

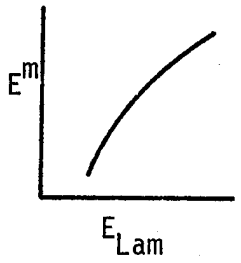


(c) $E_{Apparent} = E_{Apparent}(N)$

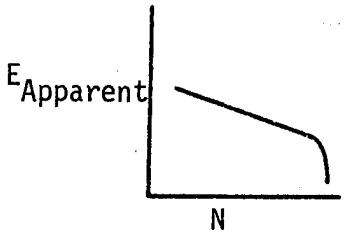


Substituting (c) into (b), with $E_{APPARENT} = E_{LAM}$, yields,

(d) $E^m = E^m(E_{Apparent}(N))$

or

$E^m = E^m(N)$

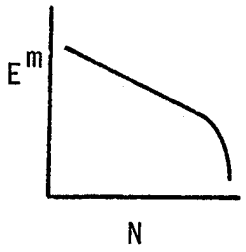


Figure 16. Analytical versus graphical method for obtaining matrix modulus as a function of fatigue cycles.

number of fatigue cycles is presented in Figure 17. Since the curves are represented by only four points, considerable detail is lost. This is particularly unfortunate, since the data points at the matrix modulus, ratio values of .25 and .1 bracket the location where the mean strain began its sharp upward turn which would appear to be a critical point of concern. For this reason, matrix modulus values of .25 and .1, in addition to 1.0, will be considered for a parametric study of interply delamination in the next section.

Strain Energy Release Rate as a Function of Matrix Degradation

In this section, a parametric study of the effect of matrix softening upon the strain energy release rate as a function of delamination length is made. Only three values of the matrix modulus are studied, because of the considerable amount of computational time involved in the finite element analysis. The three values of matrix modulus ratio, $E^m/E^m_{initial}$, studied are 1, 0.25, and 0.1. Matrix modulus ratios of 0.25 and 0.1 bracket the location of the breakaway point on the mean strain versus fatigue cycle curves. Further discussion of this point is contained in the previous section.

The selection of the most energetically favorable location for the free edge delamination was done using O'Brien's method of analysis. The analysis indicated that more energy was available for delamination at the -45/90 interface than at any other point. This conclusion is supported by the study of Law [29]. In a similar laminate, a $[\pm 25, 90_2]_s$ stacking sequence, Law used the finite element method to predict

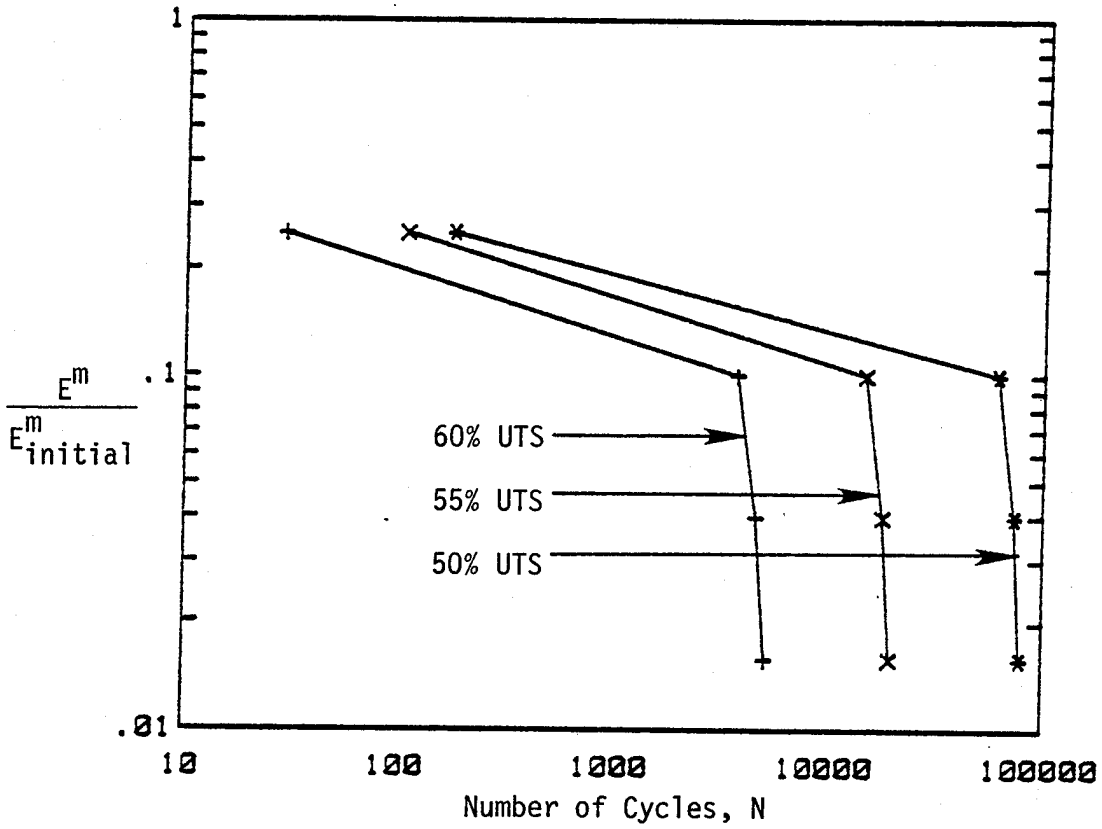


Figure 17. Matrix modulus as a function of fatigue cycles.

delamination at the -25/90 interface. This interface corresponds to the -45/90 interface of the laminate considered in this study. Hence, all the subsequent delamination analysis was conducted at the 45/90 ply interface; examination of $[\pm 45/90_2]_s$ test specimens seems to support this assumption.

The finite element modeling was performed with the same meshes as were used to evaluate the axial stiffness. For the matrix modulus ratio of one, the strain energy release rate was calculated for a series of nine crack extensions for both meshes. The strain energy release rate, calculated by the crack closure technique, displayed considerable insensitivity to the mesh coarseness. The difference in the coarse mesh prediction compared to the fine mesh varied from 5% at one ply thickness from the free edge to 2% at four ply thicknesses. It was decided to use the coarse mech of Figure 11 for all the analysis. For the same number of crack extensions, the energy release rate could be evaluated for a length of 10 ply thicknesses from the free edge versus only 4 ply thicknesses with the finer mesh at a sacrifice of about 5% error in the accuracy near the free edge.

The first load case was a fixed grip condition. The energy release rates as a function of the delamination for each of the values of $E^m/E^m_{initial}$ are presented in Figures 18, 19, and 20. The length of delamination, a, is normalized by the ply thickness, h, throughout the remainder of this study. The strain energy release rate, G, is normalized by the maximum value of the total strain release rate for a particular value of the matrix modulus ratio. These figures were included to illustrate the relative contributions of the individual components

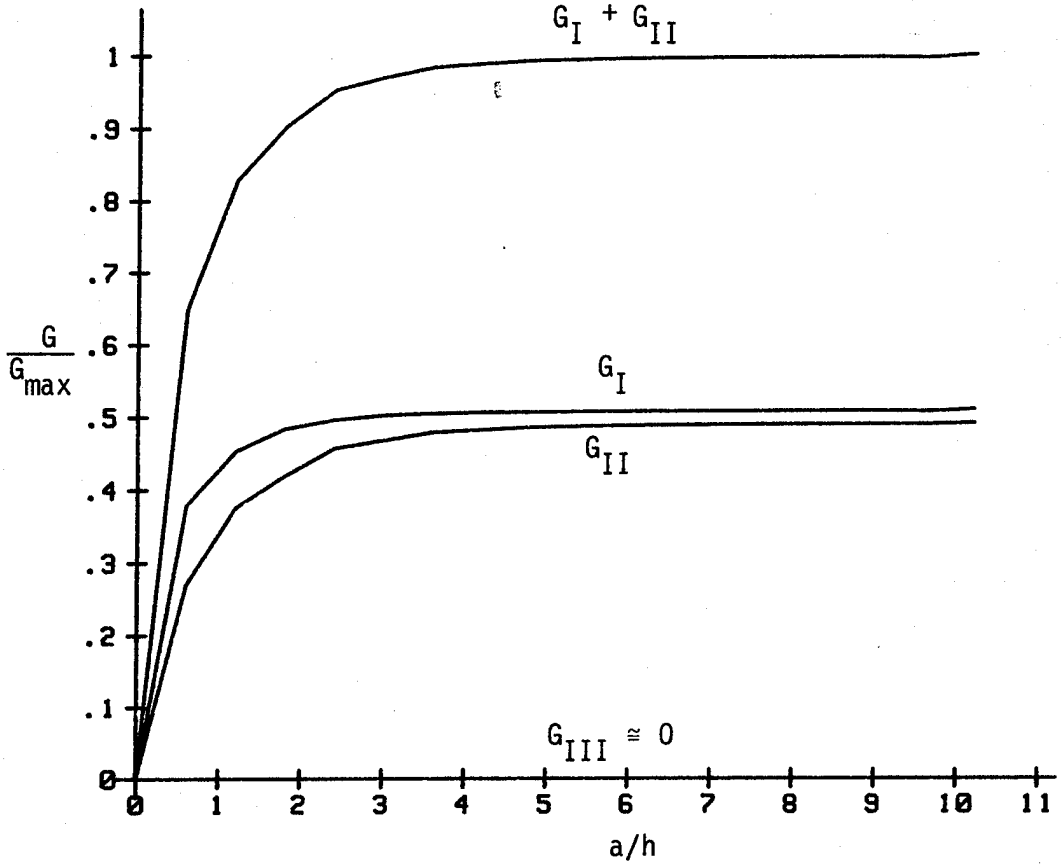


Figure 18. Components of strain energy release rate for $E^m/E^m_{initial} = 1.0$.

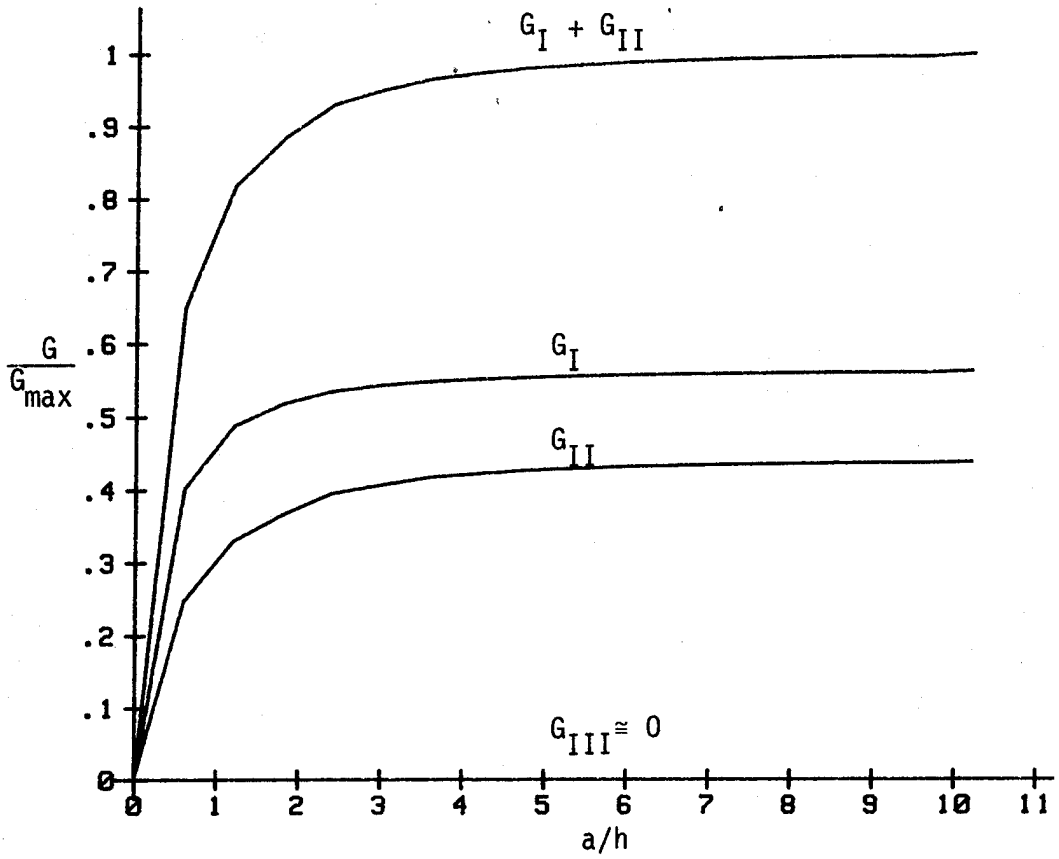


Figure 19. Components of strain energy release rate for $E^m/E^m_{initial} = 0.25$.

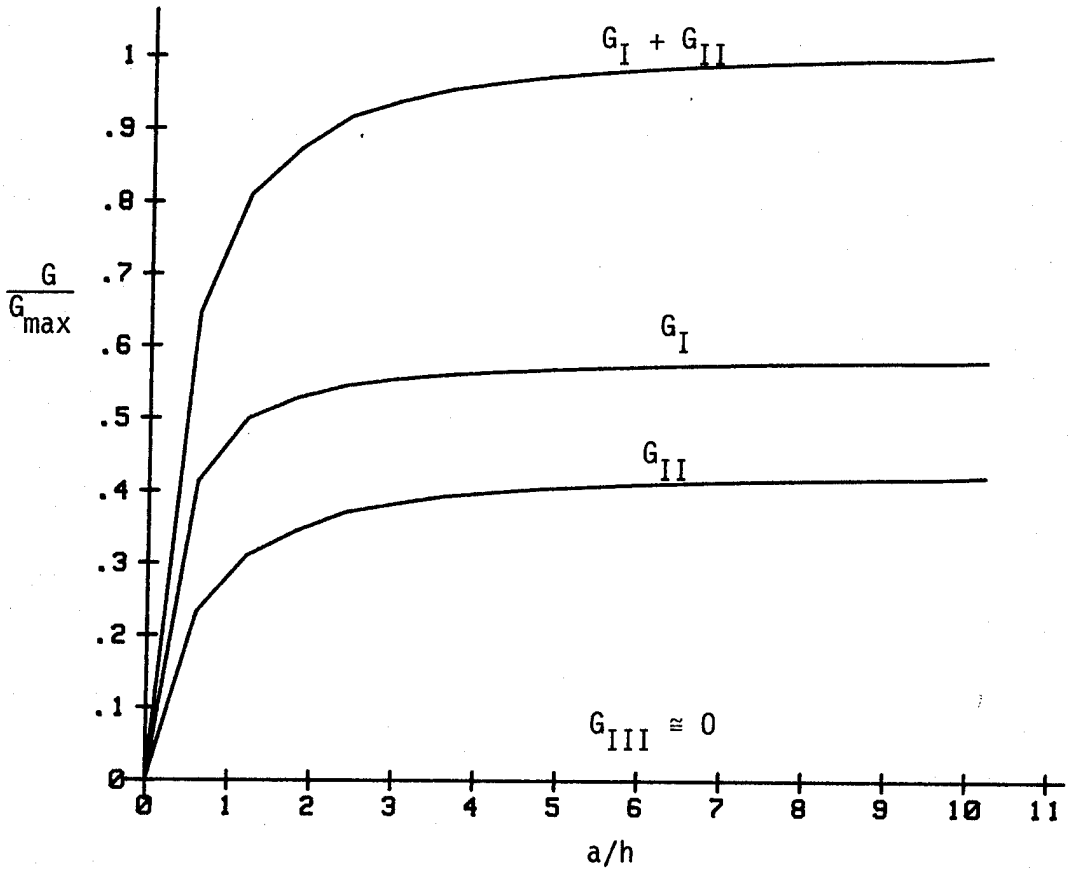


Figure 20. Components of strain energy release rate for $E^m/E^m_{initial} = 0.1$.

of the strain energy release rate. The mode III strain energy, $G_{III}$, was typically one to two orders or magnitude less than the other strain energy release rate components and has been neglected. The mode II energy release rate is observed to decrease as the matrix modulus decreases. This trend is due to the corresponding decrease in the shear moduli which restricts the ability of the laminate to store energy in this mode. Hence, less energy is available to be released in mode II. This is summarized by Figure 21.

The total strain energy release rate, G, as a function of the normalized delamination length is shown in Figure 22. The total strain energy release rate was normalized by the applied strain, $\varepsilon_o$, the total laminate thickness, t, and the reference laminate stiffness, $E_{REF}$. The strain energy release rate obtained by the finite element method, shown by the solid curves, appears to converge to the values obtained from O'Brien's method, shown by the dashed lines.

The expression for the energy release rate under a fixed grip condition for O'Brien's method can be easily obtained from equation (63). Recall that the expression in equation (63) is for G under a specified stress loading condition and that the  term in the denominator is the laminate stiffness; viz:

$$G = \frac{\sigma^2 t(E_{LAM}-E^*)}{2\,E^2} \tag{69}$$

Simply substituting $\varepsilon_o^2$ into the above equation for $\sigma^2/E^2$ will yield the fixed grip expression for G, hence:

$$G = \frac{\varepsilon_o^2 t}{2}\,(E_{LAM}-E^*) \tag{70}$$

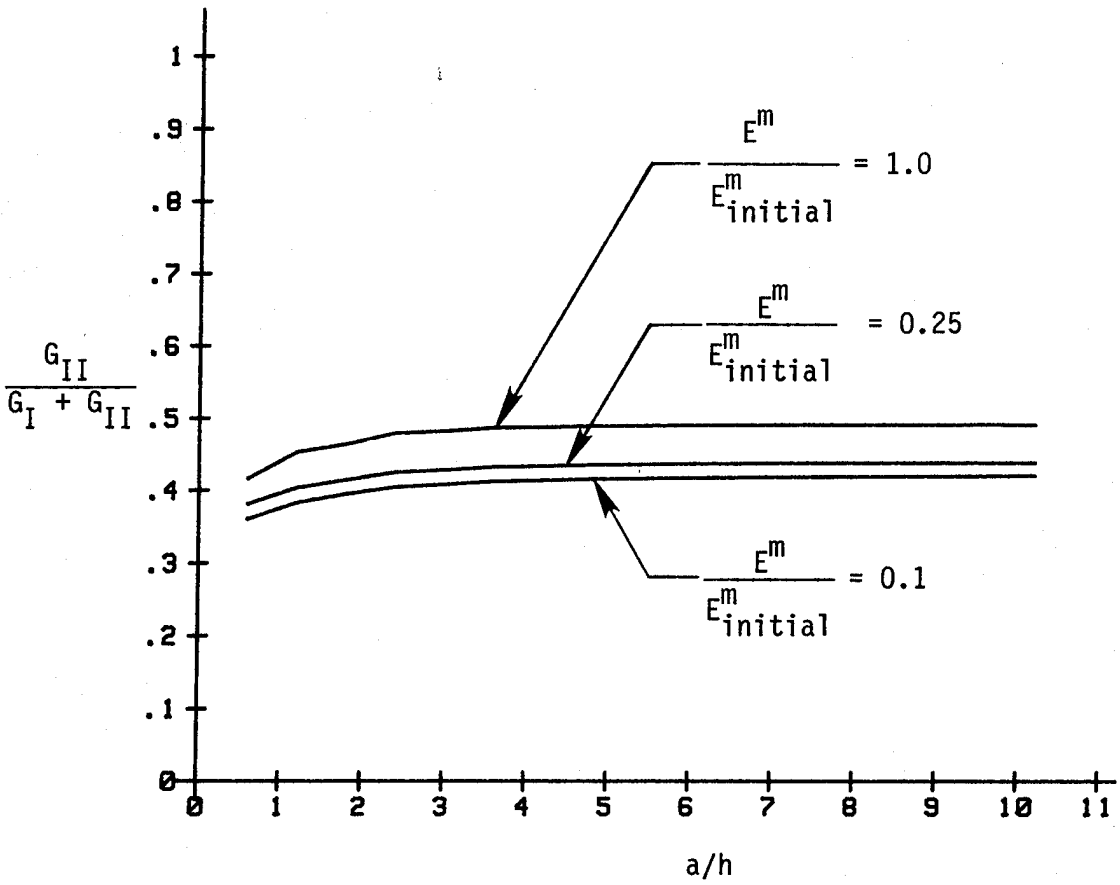


Figure 21. Mode II fraction of total energy release rate as a function of crack length.

From the previous expression, it can be seen that O'Brien's method for the fixed grip condition is independent of the delamination length. What is quite remarkable is the accuracy of this expression for values of the matrix modulus ratio of 0.1, whereas classical lamination theory predicted a 14.7% error in the laminate stiffness. This apparent discrepancy can be accounted for because the energy release rate is actually proportional to the term $E_{LAM}$-E* which is related to dE/da. This seems to imply that the linear variation of the laminate stiffness as a function of delamination size is valid, and as shown by Figure 23, the lamination theory can accurately predict dE/da. For the fixed grip loading case, this will allow the use of the finite element method to evaluate the strain energy release rate in the vicinity of the free edge and O'Brien's lamination theory to evaluate the strain energy in the interior of the laminate.

Now consider the implications of Figure 22 with respect to the fracture behavior of the laminate. Since a fixed grip (specified strain) was applied, this figure could represent a constant strain amplitude fatigue test. For this type of a fatigue test, the mean strain input would be constant and mean stress response would be decreasing. The mean stress-strain behavior would somewhat resemble a viscoelastic relaxation test. At this point we shall assume that the energy required for delamination is constant, and shall be denoted as $G_c$, the critical energy release rate.

Referring to Figure 22, at the beginning of the fatigue test the available energy for delamination is shown by the curve corresponding to $E^m/E^m_{initial} = 1.0$. As fatiguing continues, the matrix becomes

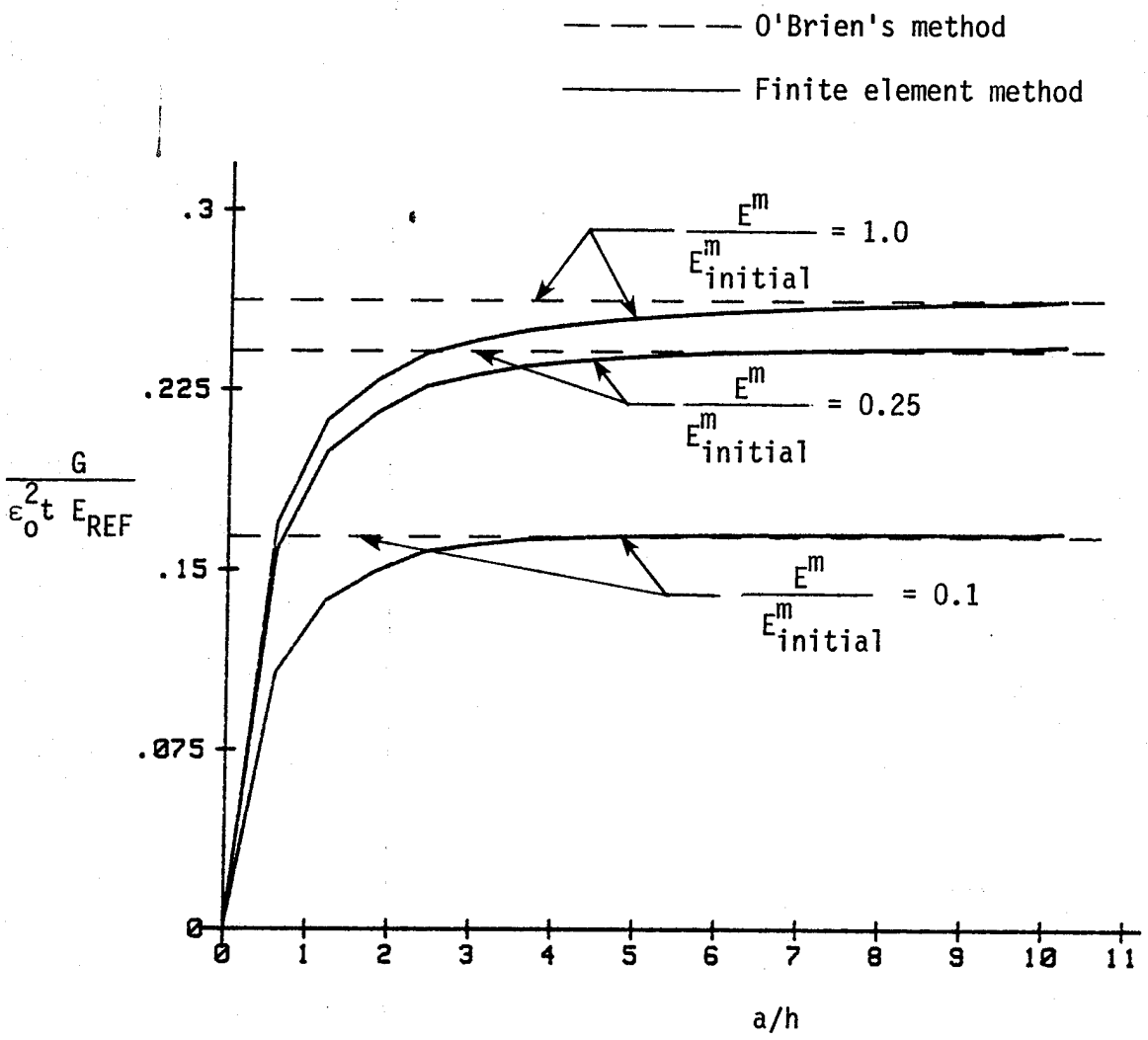


Figure 22. Total strain energy release rate as a function of delamination length under a fixed grip condition.

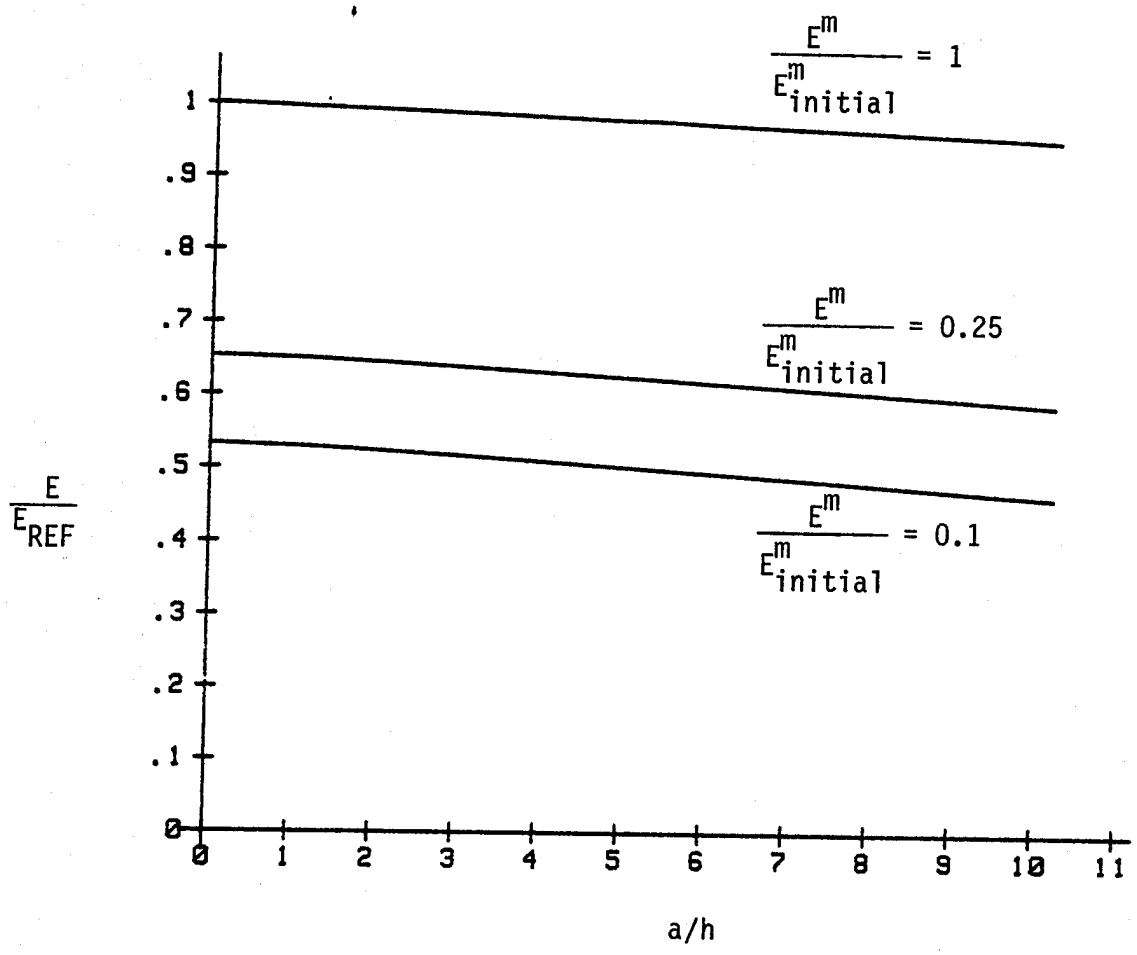


Figure 23. Axial laminate stiffness evaluated by the finite element method.

damaged, resulting in a decrease in the apparent matrix modulus. In the figure, it should be noted that as the matrix modulus decreases, the available strain energy release rate also decreases. Hence, a critical period for constant strain amplitude fatigue would be early in the test when the available strain energy release rate is largest.

Since the strain energy release rate as a function of delamination size is an increasing function and does not exhibit any minimum points, a delamination will grow when the Griffith criterion, $G = G_c$, is satisfied. Referring to Figure 24, the intersection point of the critical strain energy release rate, $G_c$, and the available strain energy curve shall be defined as $a_c$, the critical delamination size. During the initial phase of the fatigue test, an initial flaw in the laminate which was smaller than $a_c$ would remain stable and not grow. Initial flaws which are equal to or larger than $a_c$ would grow due to the excess energy available and since there appears to be no minimum point in the available energy the growth will be unstable. Once unstable delamination has begun, the delamination will cover the entire specimen width and specimen failure would likely result.

A constant stress loading condition is considered next. Once again, the finite element solution and the classical lamination theory based method of O'Brien is compared. O'Brien's method has been presented in a previous section. At this point, a description of how the fixed grip solution obtained from the finite element method was converted to a constant stress condition will be discussed.

Since linear elastic fracture mechanics has been employed, the strain energy release rate is proportional to the square of the applied

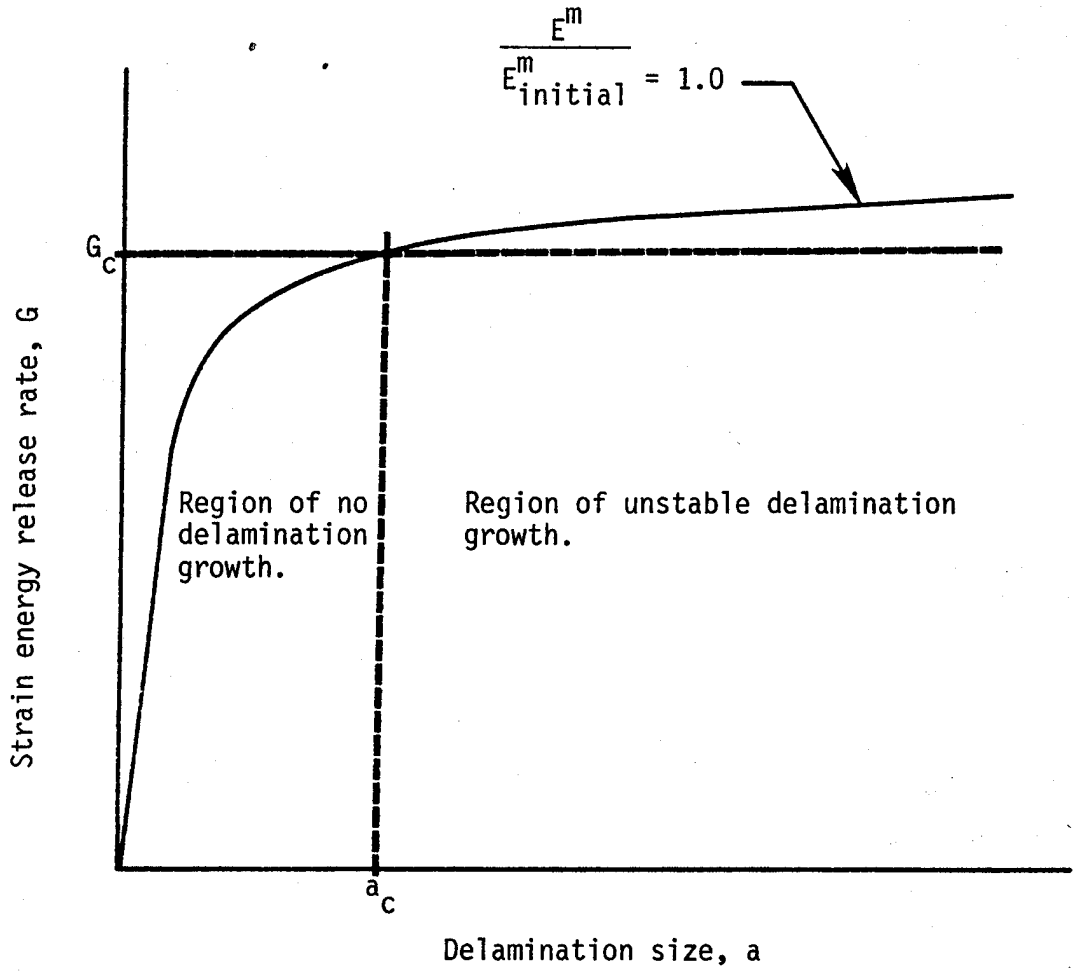


Figure 24. Delamination growth criterion.

strain. This factor is employed to scale the constant strain values of the strain energy release rate. When the laminate is loaded initially the delamination size is zero and the stress can be expressed as:

$$\sigma_o = E_{initial}\ \varepsilon_o \tag{71}$$

When a delamination of size a is introduced, the laminate stiffness decreases to a value of E, and to maintain a constant stress of $\sigma_o$, the strain must be increased such that:

$$\varepsilon = \frac{E_{initial}}{E}\ \varepsilon_o \tag{72}$$

In the above expression, the term $E_{initial}/E$ is the amplification factor required to maintain a constant stress condition. Since the laminate stiffness is a function of the delamination size, the correction factor is best defined as the laminate stiffness evaluated at a delamination size of zero divided by the laminate stiffness evaluated at the current delamination size. Hence, to obtain the strain energy release rate for a constant $\sigma_o$, simply multiply the strain energy release rate for a constant $\varepsilon_o$ by the square of the amplification factor defined above.

Presented in Figure 25 is the total strain energy release rate as a function of the normalized delamination length. The strain energy release rate was normalized by the applied stress, $\sigma_o$, the total laminate thickness, and the reference laminate stiffness, $E_{REF}$. The strain energy release rate is observed to increase as the matrix modulus decreases. For the matrix modulus ratio of 1, there is reasonable agreement between O'Brien's method and the finite element

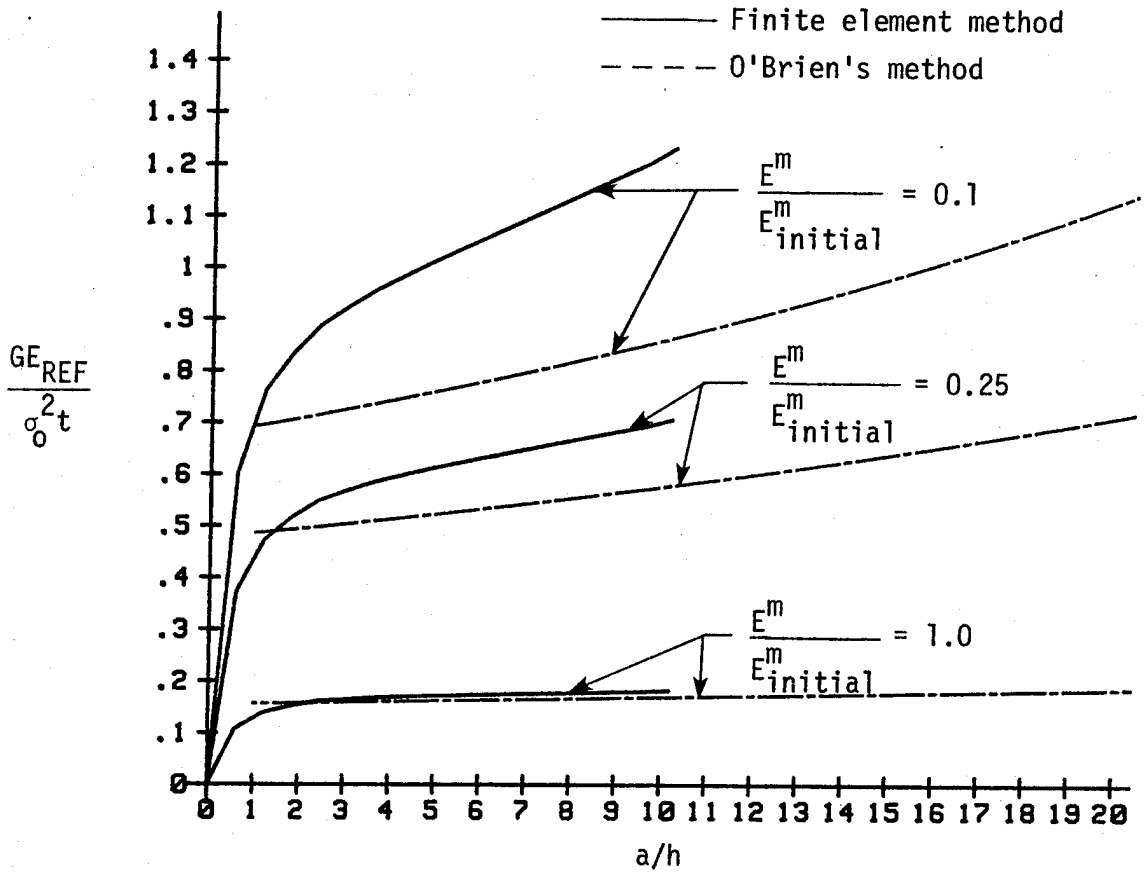


Figure 25. Total normalized strain energy release rate as a function of delamination length/ply thickness for a constant stress condition.

method, but this deteriorates as the matrix modulus decreases. The discrepancy of O'Brien's method is due to the inability of the lamination theory to predict the laminate stiffness. Despite this problem, O'Brien's method is of considerable importance, because it contains all of the essential elements required to describe the energy release rate, and substantial insight can be obtained by the study of it.

Consider a laminate with an initial flaw size of $a_o$ and a critical strain energy release rate of $G_c$. As this laminate is fatigued in a constant maximum stress fatigue test, the matrix modulus degrades, and, as a result, the available energy increases. This process is depicted by points A, B, and C in Figure 26. Point C is a critical point since the energy available is equal to the critical strain energy release rate. At this point, the initial flaw will propagate unstably across the entire sample width since the available energy appears to continue to increase. Once the laminate has fully delaminated, failure will occur very quickly due to the degraded matrix properties.

Now if a critical energy release rate is assumed, we can determine the critical flaw size from Figure 25. Assuming $G_c$ = 175 $N \cdot M/M^2$, the corresponding flaw sizes for the 50%, 55%, and 60% UTS fatigue tests are 2.5h, 1.5h, and 1h respectively, where h is the ply thickness. This range of flaw sizes is reasonable for an edge flaw in the type of composite considered.

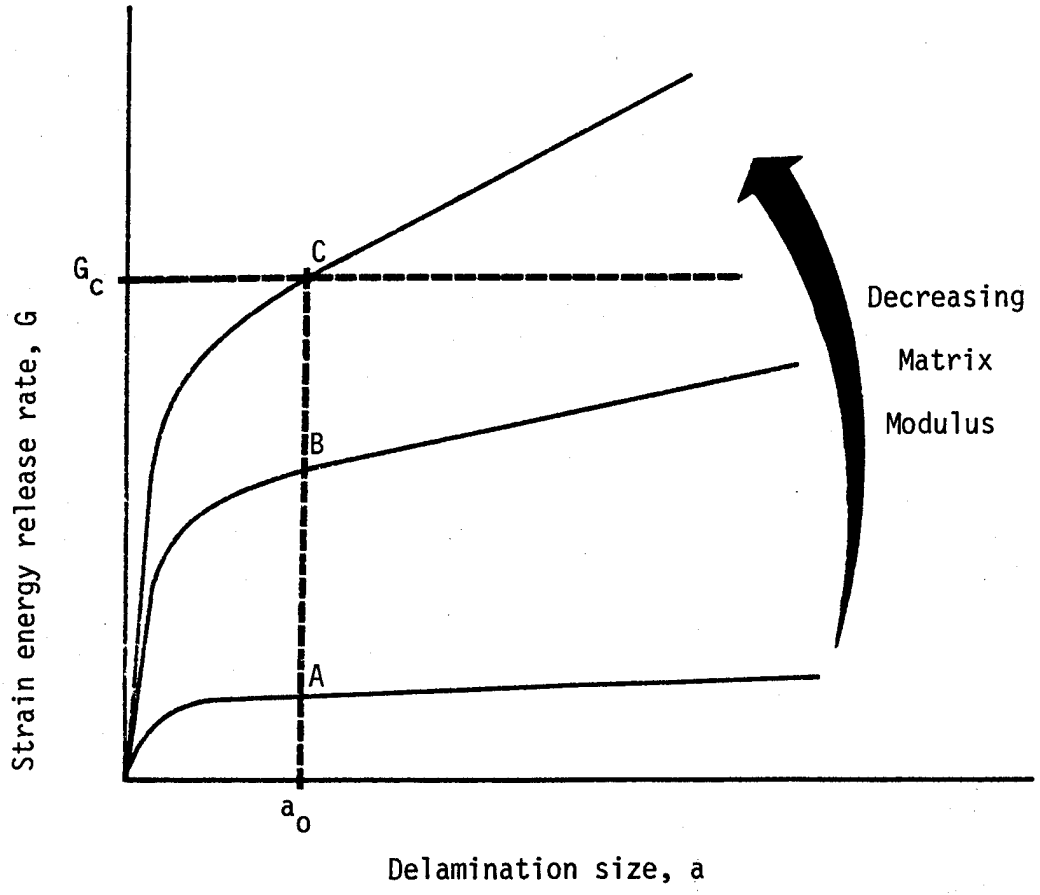


Figure 26. Delamination growth criterion for a constant maximum stress fatigue test.

# VI. CONCLUSIONS

Matrix degradation modelled by a reduced matrix modulus through micromechanics principals shows considerable promise as a means to analyze fatigue behavior. The study conducted was of a preliminary nature in that only mean stress and mean strain fatigue responses were considered, and the influence of stress gradients on matrix damage was neglected. The major purpose of this study was to assemble the necessary analytical tools required to analyze the combined effects of matrix degradation and delamination. Considerable energy was expended in developing a generalized plane strain finite element program capable of analyzing free edge effects and performing fracture analysis. Throughout this study, the accuracy of the finite element method and classical lamination theory was assessed.

In evaluating laminate stiffness, it was found that as the matrix modulus was reduced, considerable shear deformations occurred which lamination theory was unable to model. The shear deformations, which are associated with free edge effects, were found to penetrate a considerable distance in from the free edge. For the smallest value of the matrix modulus considered, the finite element results showed that significant free edge effects extended five laminate thicknesses into the interior of a $[\pm 45/90_2]_s$ laminate.

A parametric study of free edge delaminations as a function of matrix damage was performed for constant maximum strain and constant maximum stress fatigue tests. For the constant maximum strain

fatigue test the available energy for delamination was greatest at the beginning of the test and then was subsequently reduced by the matrix damage. For the constant maximum stress fatigue test, the effect of matrix damage was to increase the energy available for delamination. Once sufficient energy became available, a flaw was shown to propagate unstably across the entire laminate width.

The accuracy of the classical lamination theory based delamination analysis of O'Brien suffered from the inaccurate laminate stiffness predictions due to the influence of the free edge. This problem was amplified due to the small width of the laminate. None the less, considerable insight can be obtained by the use of O'Brien's method, since it contains all of the essential elements which are required to evaluate the strain energy release rate, in a simple closed form solution. The only major limitation of O'Brien's method is it does not provide values for the separate modes of strain energy release rate, $G_I$, $G_{II}$, or $G_{III}$.

# VII. RECOMMENDATIONS FOR FUTURE WORK

In order to develop a more realistic fatigue damage model for fibrous composites, several additional parameters must be included other than those considered in this study. Influence of such factors as the effect of stress gradients, the stress amplitude, cyclic frequency, residual stresses, and environmental effects all deserve attention. The most important consideration in developing an analytical model is maintaining a firm physical foundation.

At this point, considerable experimental work is needed to understand fatigue behavior and the sequence of events which lead to failure. Such a study should try to assess the relative influence of matrix degradation and delamination. Experimental techniques such as dye penetrant enhanced X-radiography could be used to study fatigue delamination growth. The effects of stress gradients could be evaluated by conducting tests of specimen widths in an effort to isolate the free edge effects. It is believed that until a sufficient experimental data base has been established, it will be difficult to established an accurate fatigue damage model.

One last remark to future researchers, "I think you will find that if you plot it on log-log paper it will be linear," from Reference [14].

# REFERENCES


1. Bader, M.G., Bailey, J.E., Curtis, P.T. and Parvizi, A., "The Mechanisms of Initiation and Development of Damage in Multiaxial Fibre-Reinforced Plastic Laminates," Proceedings for 3rd International Symposium on Mechanical Behavior of Materials. Cambridge U.K., Vol. 3, 1979, p. 227.

2. Aveston, J. and Kelly, A., "Theory of Multiple Fracture of Fibrous Composites," J. of Material Science, Vol. 8, 1973, p. 352.

3. Rodini, B.T. and Eisenmann, "An Analytical and Experimental Investigation of Edge Delamination in Composite Laminates," Proceedings of the 4th Conference of Fibrous Composites, San Diego, CA, November, 1978.

4. Rybicki, E.F., Schmuser, D.W., and Fox, J., "An Energy Release Rate Approach for Stable Crack Growth in the Free Edge Delamination Problem," J. Composite Materials, Vol. 11, October, 1977, p. 470.

5. Rybicki, E.F. and Kanninen, M.F., "A Finite Element Calculation of Stress Intensity Factors by a Modified Crack Closure Integral," Eng. Fracture Mechanics, Vol. 9, 1977, p. 931.

6. Wang, A.D. and Crossman, F.W., "Initiation and Growth of Transverse Cracks and Edge Delamination in Composite Laminates: Part 1 An Energy Method," J. Composite Materials, Suppl. Vol., 1980, p. 71.

7. Crossman, F.W., Warren, W.J., Wang, A.D. and Law, G.E., Jr., "Initiation and Growth of Transverse Cracks and Edge Delamination in Composite Laminates: Part 2 Experimental Correlation," J. Composite Materials, Suppl. Vol., 1980, p. 88.

8. O'Brien, T.K., "Characterization of Delamination Onset and Growth in a Composite Laminate," NASA TM-81940, January 1981.

9. Alexander, R.M., Schapery, R.A., Jerina, K.L. and Sanders, B.A., "Fracture Characterization of a Random Fiber Composite Material," Texas A&M University Report No. MM3979-80-4, April, 1980.

10. Ho, T. and Schapery, R. A., "The Effect of Environment on the Mechanical Behavior of AS/3501-6 Graphite/Epoxy Material Phase III," ATC Report No. R-92100/1CR-5, Contract No. N00019-79-C-0580, January 1981.

11. Pipes, R.B. and Pagano, N.J., "Interlaminar Stresses in Composite Laminates Under Uniform Axial Extension," J. Composite Materials, Vol. 4, 1970, p. 538.

12. Wang, A.S.D. and Crossman, F.W., "Some New Results on Edge Effects in Symmetric Composite Laminates," J. Composite Materials, Vol. 11, 1977, p. 92.

13. Tsai, S.W., and Hahn, H.T., "Introduction to Composite Materials," Technomic, Stanford, Conn., 1980.

14. Schapery, R.A., Private communication, Texas A&M University, March 1981.

15. Hinton, E. and Owen, D.R.J., "Finite Element Programming," Academic Press, London, U.K., 1977.

16. Renton, W.J. and Ho, T., "The Effect of Environment on the Mechanical Behavior of AS/3501-6 Graphite/Epoxy Material," ATC Report No. B-92100/8CR-105, Contract No. N00019-77-C-0369, August 1978.

17. Ho, T., "The Effect of Environment on the Mechanical Behavior of AS/3501-6 Graphite/Epoxy Material Phase II," ATC Report No. R-92100/9CR-61, Contract No. N00019-78-C-0599, January, 1980.

18. Chamis, C.C., and Sendeckyj, G.P., "Critique on Theories Predicting Thermoelastic Properties of Fibrous Composites," J. of Composite Materials, July, 1968, pp. 332-358.

19. Hashin, Z., "Theory of Fiber Reinforced Materials" NASA CR-1974, 1972.

20. Crane, D.A. and Adams, D.F., "Finite Element Micromechanical Analysis of a Unidirectional Composite Including Longitudinal Shear Loading," AMMRC TR 81-7, Army Materials and Mechanics Research Center, February 1981.

21. Christensen, R.M., Mechanics of Composite Materials, John Wiley and Sons, New York, 1979.

22. Hashin, Z., "Analysis of Properties of Fiber Composites With Anisotropic Constituents," J. of Applied Mechanics, Vol. 46, Sept. 1979, p. 543.

23. Halpin, J.C. and Kardos, J.L., "The Halpin-Tsai Equations: A Review," Polymer Engineering and Science, May 1976, p. 344.

24. Monib, M.M. and Adams, D.F., "Three-Dimensional Elastoplastic Finite Element Analysis of Laminated Composites," U.S. Army Research Office, Report Number UWME-DR-001-102-1, November 1980.

25. Grimes, G.C. and Adams D.F., "Investigation of Compression Fatigue Properties of Advanced Composites," Northrop Technical Report NDR 79-17, Northrop Corporation, Hawthorn, California, October 1979.

26. Griffith, A.A., "The Phenomena of Rupture and Flow in Solids," Phil. Trans. Roy. Soc. of London, Vol. 221, 1921, p. 163.

27. Irwin, G. R., "Fracture," Handbuch der Physik, Vol. VI, Springer, Berlin, 1958, p. 551.

28. Jones, R.M., Mechanics of Composite Materials, Scripta, Washington, D.C., 1975.

29. Law, G.E., "Fracture Analysis of $(\pm 25/90_n)_s$ Graphite-Epoxy Composites Laminates," Ph.D. Dissertation, Drexel University, Philadelphia, PA, June 1981.

30. Wang, A. S. D. and Crossman, F. W., "Edge Effects on Thermally Induced Stresses in Composite Laminates," J. Composite Materials, Vol. 11, 1977, p. 300.

31. Crossman, F. W. and Wang, A. S. D., "Stress Field Induced by Transient Moisture Sorption in Finite-Width Composite Laminates," J. Composite Materials, Vol. 12, 1978, p.2.

32. Raju, I. S., Whitcomb, J. E., and Goree, J. G., "A New Look at Numerical Analyses of Free-Edge Stresses in Composite Laminates," NASA Technical Paper 1751, 1980.

33. Rice, J. C., "Stresses in an Infinite Strip Containing a Semi-Infinite Crack," J. of Applied Mechanics, March 1967, p. 248.

# APPENDIX A

# FINITE ELEMENT FORMULATION

Consider the linear elastic lamina shown in Figure A1. Each lamina is discretely modeled as a homogeneous orthotropic material. The modulus matrix in the principal material coordinates (1, 2, 3), [21], is

$$\bar{C}_{ij} = \begin{bmatrix} \bar{C}_{11} & \bar{C}_{12} & \bar{C}_{13} & 0 & 0 & 0 \\ \bar{C}_{12} & \bar{C}_{22} & \bar{C}_{23} & 0 & 0 & 0 \\ \bar{C}_{13} & \bar{C}_{23} & \bar{C}_{33} & 0 & 0 & 0 \\ 0 & 0 & 0 & \bar{C}_{44} & 0 & 0 \\ 0 & 0 & 0 & 0 & \bar{C}_{55} & 0 \\ 0 & 0 & 0 & 0 & 0 & \bar{C}_{66} \end{bmatrix} \qquad \text{(A-1)}$$

The modulus matrix will be expressed in terms of engineering constants referenced to the principal material coordinates. The notation and definition of the following engineering constants was adopted from Jones [28]:

$E_1, E_2, E_3$ = Young's moduli in 1, 2, and 3 directions respectively.

$\nu_{ij}$ = Poisson's ratio for transverse strain in the j-direction when stressed in the i-direction.

$G_{23}, G_{31}, G_{12}$ = Shear moduli for 2-3, 3-1, and 1-2 planes respectively.

The modulus matrix can be expressed in terms of the engineering constants as:

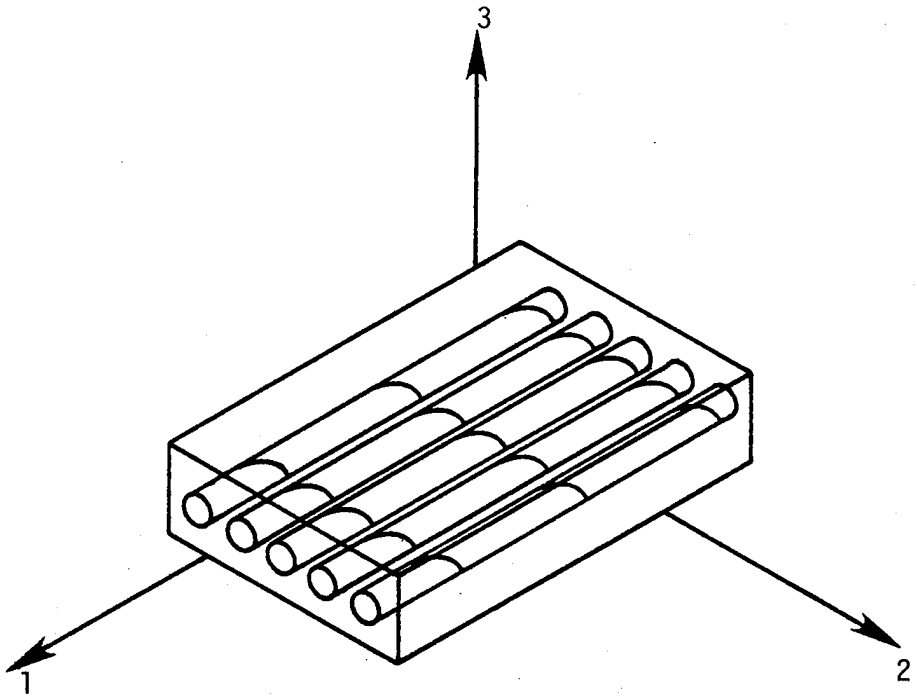


Figure A1. Principal material coordinates, (1,2,3) used to define the engineering constants.

$$\bar{C}_{11} = \frac{1 - \nu_{23}\nu_{32}}{E_2 E_3 \Delta}$$

$$\bar{C}_{12} = \frac{\nu_{21} + \nu_{31}\nu_{23}}{E_2 E_3 \Delta} = \frac{\nu_{12} + \nu_{32}\nu_{13}}{E_1 E_3 \Delta}$$

$$\bar{C}_{13} = \frac{\nu_{31} + \nu_{21}\nu_{32}}{E_2 E_3 \Delta} = \frac{\nu_{13} + \nu_{12}\nu_{23}}{E_1 E_2 \Delta}$$

$$\bar{C}_{22} = \frac{1 - \nu_{13}\nu_{31}}{E_1 E_3 \Delta}$$

$$\bar{C}_{23} = \frac{\nu_{32} + \nu_{12}\nu_{31}}{E_1 E_3 \Delta} = \frac{\nu_{23} + \nu_{21}\nu_{13}}{E_1 E_2 \Delta}$$

$$\bar{C}_{33} = \frac{1 - \nu_{12}\nu_{21}}{E_1 E_2 \Delta}$$

$$\bar{C}_{44} = G_{23}$$

$$\bar{C}_{55} = G_{31}$$

$$\bar{C}_{66} = G_{12}$$

$$\Delta = \frac{1 - \nu_{12}\nu_{21} - \nu_{23}\nu_{32} - \nu_{31}\nu_{13} - 2\nu_{21}\nu_{32}\nu_{13}}{E_1 E_2 E_3}$$

$$\nu_{21} = \frac{\nu_{12} E_2}{E_1}$$

$$\nu_{31} = \frac{\nu_{13} E_3}{E_1}$$

$$\nu_{32} = \frac{\nu_{23} E_3}{E_2}$$

When the lamina is rotated an arbitrary amount about the 3, z axis, Figure A2, the modulus matrix is of a monoclinic material form with respect to the global x, y, z coordinate system. The monoclinic modulus matrix is

$$C_{ij} = \begin{bmatrix} C_{11} & C_{12} & C_{13} & 0 & 0 & C_{16} \\ C_{12} & C_{22} & C_{23} & 0 & 0 & C_{26} \\ C_{13} & C_{23} & C_{33} & 0 & 0 & C_{36} \\ 0 & 0 & 0 & C_{44} & C_{45} & 0 \\ 0 & 0 & 0 & C_{45} & C_{55} & 0 \\ C_{16} & C_{26} & C_{36} & 0 & 0 & C_{66} \end{bmatrix} \qquad \text{(A-2)}$$

The transformation from principal material coordinates to the global x, y, z coordinates by a rotation, $\theta$, about the z axis are [21]:

$$\begin{aligned}
C_{11} &= m^4 C_{11} + 2m^2n^2(C_{12} + 2\overline{C}_{66}) + n^4\overline{C}_{22} \\
C_{12} &= m^2n^2(\overline{C}_{11} + \overline{C}_{22} - 4\overline{C}_{66}) + (m^4 + n^4)\overline{C}_{12} \\
C_{13} &= m^2\overline{C}_{13} + n^2\overline{C}_{23} \\
C_{16} &= mn[m^2\overline{C}_{11} - n^2\overline{C}_{22} - (m^2 - n^2)(\overline{C}_{12} + 2\overline{C}_{66})] \\
C_{22} &= n^4\overline{C}_{11} + 2m^2n^2(\overline{C}_{12} + 2\overline{C}_{66}) + m^4\overline{C}_{22} \\
C_{23} &= n^2\overline{C}_{13} + m^2\overline{C}_{23} \\
C_{26} &= mn[n^2C_{11} - m^2C_{22} + (m^2 - n^2)(C_{12} + 2C_{66})] \\
C_{33} &= \overline{C}_{33} \\
C_{36} &= mn(\overline{C}_{13} - \overline{C}_{23}) \\
C_{44} &= m^2\overline{C}_{44} + n^2\overline{C}_{55} \\
C_{45} &= mn(\overline{C}_{55} - \overline{C}_{44}) \\
C_{55} &= m^2\overline{C}_{55} + n^2\overline{C}_{44}
\end{aligned} \qquad \text{(A-3)}$$

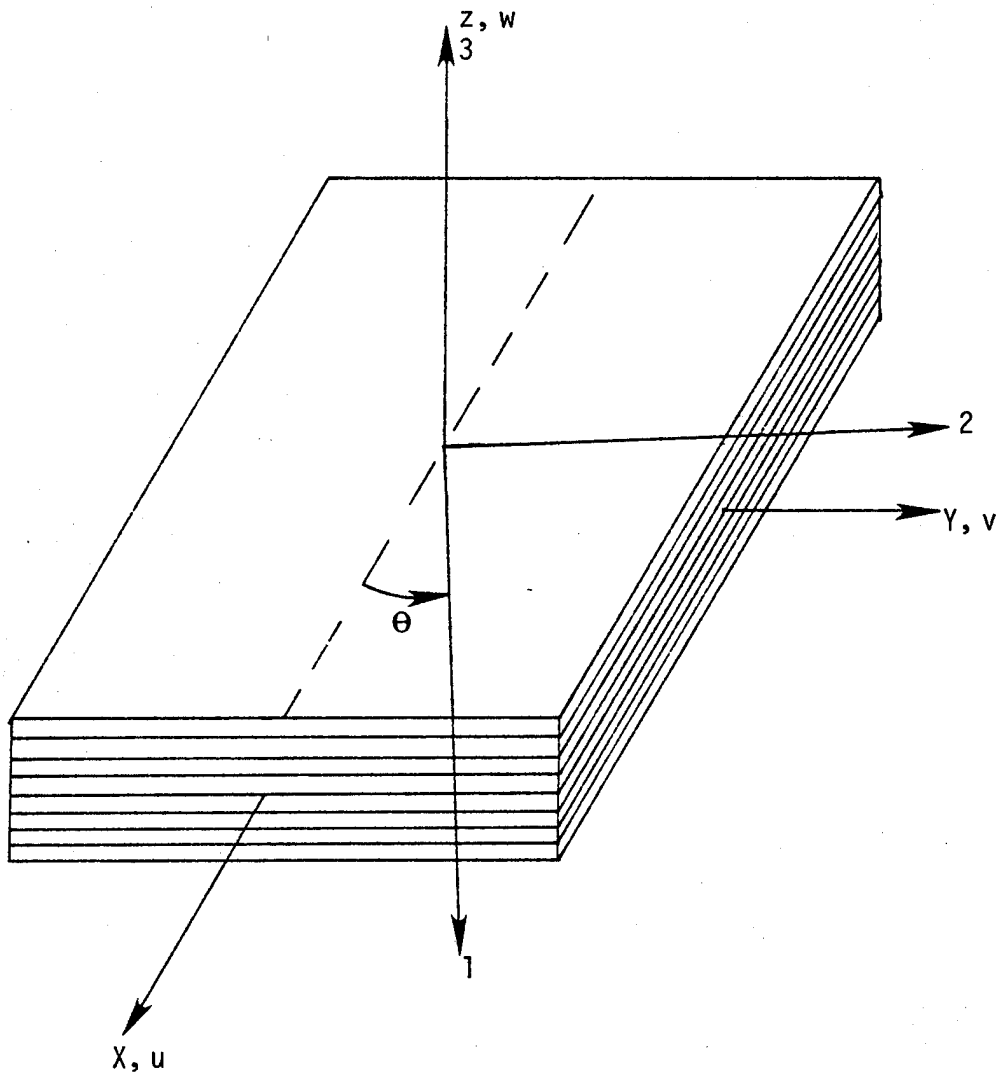


Figure A2. Laminate geometry.

$$C_{66} = m^2n^2(\bar{C}_{11} + \bar{C}_{22} = 2\bar{C}_{12}) + (m^2 - n^2)^2\,\bar{C}_{66} \qquad \text{(A-3)}$$

where $m = \cos\theta$, $n = \sin\theta$.

Note that the above transformation is based upon the right hand rule for positive rotations about the z axis, Figure A2. Note that an opposite convention was used in [22].

The following displacement field is assumed [11],

$u(x, y, z) = \varepsilon_o x + U(y, z)$

$v(x, y, z) = V(y, z)$

$w(x, y, z) = W(y, z)$

Let us determine the class of problems that can be solved. Differentiating the assumed displacments yields the following strains and curvatures.

$$\varepsilon_x = \varepsilon_o$$

$$\varepsilon_y = \frac{\partial V}{\partial y}$$

$$\varepsilon_z = \frac{\partial W}{\partial y}$$

$$\gamma_{xy} = \frac{\partial U}{\partial y}$$

$$\gamma_{zy} = \frac{\partial V}{\partial z} + \frac{\partial W}{\partial y} \qquad \text{(A-4)}$$

$$\gamma_{zx} = \frac{\partial U}{\partial z}$$

$$k_x = \frac{\partial^2 w}{\partial x^2} = 0$$

$$k_{xy} = -\frac{\partial^2 w}{\partial y^2} = -\frac{\partial^2 W}{\partial y^2}$$

$$k_{xy} = -2\frac{\partial^2 w}{\partial x \partial y} = 0$$

From classical lamination theory (CLT), using the notation of Jones [28], the stress and moment resultants can be expressed in terms of

mid plane strains and curvatures as

$$\begin{Bmatrix} N_x \\ N_y \\ N_{xy} \\ M_x \\ M_y \\ M_{xy} \end{Bmatrix} = \begin{bmatrix} A_{11} & A_{12} & A_{16} & B_{11} & B_{12} & B_{16} \\ A_{21} & A_{22} & A_{26} & B_{21} & B_{22} & B_{26} \\ A_{61} & A_{62} & A_{66} & B_{61} & B_{62} & B_{66} \\ B_{11} & B_{12} & B_{16} & D_{11} & D_{12} & D_{16} \\ B_{21} & B_{22} & B_{26} & D_{21} & D_{22} & D_{26} \\ B_{61} & B_{62} & B_{66} & D_{61} & D_{62} & D_{66} \end{bmatrix} \begin{Bmatrix} \varepsilon_x \\ \varepsilon_y \\ \gamma_{xy} \\ k_x \\ k_y \\ k_{xy} \end{Bmatrix} \qquad \text{(A-5)}$$

where

$$N_x, N_y, N_{xy} = \int_{-t/2}^{t/2} (\sigma_x, \sigma_y, \tau_{xy})\, dz$$

$$M_x, M_y, M_{xy} = \int_{-t/2}^{t/2} (\sigma_x, \sigma_y, \tau_{xy})\, z dz$$

$$A_{ij}, B_{ij}, D_{ij} = \int_{-t/2}^{t/2} Q_{ij}(1, z, z^2)\, dz$$

$$Q_{ij} = \begin{bmatrix} S_{11} & S_{12} & S_{16} \\ S_{12} & S_{22} & S_{26} \\ S_{16} & S_{26} & S_{66} \end{bmatrix}^{-1}$$

Substituting in the strains and curvatures from equation (A-4) into equation (A-5) we obtain

$$\begin{Bmatrix} N_x \\ N_y \\ N_{xy} \\ M_x \\ M_y \\ M_{xy} \end{Bmatrix} = \begin{bmatrix} A_{11} & A_{12} & A_{16} & B_{11} & B_{12} & B_{16} \\ A_{21} & A_{22} & A_{26} & B_{21} & B_{22} & B_{26} \\ A_{61} & A_{62} & A_{66} & B_{61} & B_{62} & B_{66} \\ B_{11} & B_{12} & B_{16} & D_{11} & D_{12} & D_{16} \\ B_{21} & B_{22} & B_{26} & D_{21} & D_{22} & D_{26} \\ B_{61} & B_{62} & B_{66} & D_{61} & D_{62} & D_{66} \end{bmatrix} \begin{Bmatrix} \varepsilon_o \\ \frac{\partial X}{\partial y} \\ \frac{\partial U}{\partial y} \\ 0 \\ -\frac{\partial^2 W}{\partial y^2} \\ 0 \end{Bmatrix} \qquad \text{(A-6)}$$

The most important implication of the assumed displacement field is that the normal strain $\varepsilon_x = \varepsilon_o$ and the $k_x$ and $k_{xy}$ curvatures are zero. Notice the effect of the bending-extension coupling matrix and the zero $k_x$ and $k_{xy}$ curvature terms. When any of $B_{1i}$ or $B_{6i}$ $(i = 1,2,6)$ terms are not zero, a normal strain would result in an externally applied $M_x$ or $M_{xy}$ moment resultant to maintain a zero curvature.

In this paper, we will be concerned with symmetric laminates, which do not have bending-extension coupling. If we consider the specific case of a symmetric laminate under uniform axial extension, $\varepsilon_x = \varepsilon_o$, we can take advantage of the following symmetry conditions for the x-y plane

$$\begin{aligned} u(x, y, z) &= u(x, y, -z) \\ v(x, y, z) &= v(x, y, -z) \\ w(x, y, z) &= w(x, y, -z) \end{aligned} \qquad \text{(A-7)}$$

and for the x-z plane

$$\begin{aligned} v(x, y, z) &= -v(x, -y, z) \\ w(x, y, z) &= -w(x, -y, z). \end{aligned} \qquad \text{(A-8)}$$

Because of the above symmetry conditions, a symmetric laminate under uniform axial extension requires only one quarter of the y-z plane to be modeled.

Since a linear elastic material was assumed, the constitutive law can be expressed as

$$\sigma_i = C_{ij}(\varepsilon_j - \alpha_j \Delta T) \qquad i, j = 1, 6 \qquad \text{(A-9)}$$

or

$$\varepsilon_i = S_{ij}\sigma_j + \alpha_i \Delta T \qquad i, j = 1, 6 \qquad \text{(A-10)}$$

where $\sigma_i$ = stress components

$\varepsilon_j$ = strain components

$C_{ij}$ = modulus matrix

$S_{ij}$ = compliance matrix

$\alpha_i$ = coefficients of thermal expansion

$\Delta T$ = temperature change

From equation (A-10) the first equation (i=1) can be rewritten in terms of $\sigma_1$, the axial normal stress component, as

$$\sigma_1 = \frac{1}{S_{11}} [\varepsilon_1 - \Delta T\alpha_1 - S_{12}\sigma_2 - S_{13}\sigma_3 - S_{16}\sigma_6] \qquad \text{(A-11)}$$

noting $\varepsilon_1 = \varepsilon_o$ is the axial strain. Since $\sigma_1$ can be expressed in terms of the axial strain and the other five stress components, then equation (A-9) can be expressed in a reduced form as [12],

$$\hat{\sigma}_i = D_{ij}(\hat{\varepsilon}_j - \hat{\alpha}_j\Delta T) + \sigma_i^* \qquad i, j = 1, 5 \qquad \text{(A-12)}$$

where $\hat{\sigma}_i = \sigma(i + 1)$

$\hat{\varepsilon}_j = \varepsilon(j + 1)$

$\hat{\alpha}_j = \alpha(j + 1)$ $\qquad i, j = 1, 5$

$D_{ij} = C(i + 1)(j + 1)$

$\sigma_i^* = (\varepsilon_o - \alpha_1\Delta T)C_1(j + 1)$

With the reduced constitutive law established as in equation (A-12), the finite element formulation is conventional. Eight-noded, isoparametric, quadrilateral elements were used having conventional quadratic, serendipity shape functions [15] and three degrees of freedom (u, v, and w) per node. The global system of simultaneous

linear algebraic equations is

$$K_{ij}q_j = Q_i^{\Delta T} + Q_i^{\sigma *} \qquad i, j = 1, NDOF \qquad \text{(A-13)}$$

where $K_{ij}$ = global stiffness matrix

$q_j$ = nodal displacement vector

$Q_i^{\Delta T}$ = in-plane thermal load vector

$Q_i^{\sigma *}$ = out-of-plane load vector

NDOF = number of degrees of freedom

The above system of equations is assembled from their elemental constituents which are

$$K_{ij}^e = \int_v B_{mi} D_{mn} B_{nj} dV$$

$$Q_i^{e(\Delta T)} = \int_v B_{mi} D_{mn} \hat{\alpha}_n dV \qquad i, j = 1, 24 \quad m, n = 1, 5 \qquad \text{(A-14)}$$

$$Q_i^{e(\sigma *)} = -\int B_{mi} D_{mn} \sigma_n^* dV$$

where $B_{nj}$ = the nodal displacement strain transformation

$D_{mn}$ = reduced modulus matrix (equation A-12)

$\hat{\alpha}_n$ = reduced coefficient of thermal expansion (equation A-12)

$\sigma_n^*$ = in-plane stresses due to out-of-plane strain and temperature change (equation A-12)

V = the volume of the element

The boundary conditions for the problem in Figure A3 can be easily established by symmetry; these are

$$u(o, z) = 0$$

$$v(o, z) = 0 \qquad \text{(A-15)}$$

$$w(y, o) = 0$$

This allows only one quarter of the laminate to be modeled.

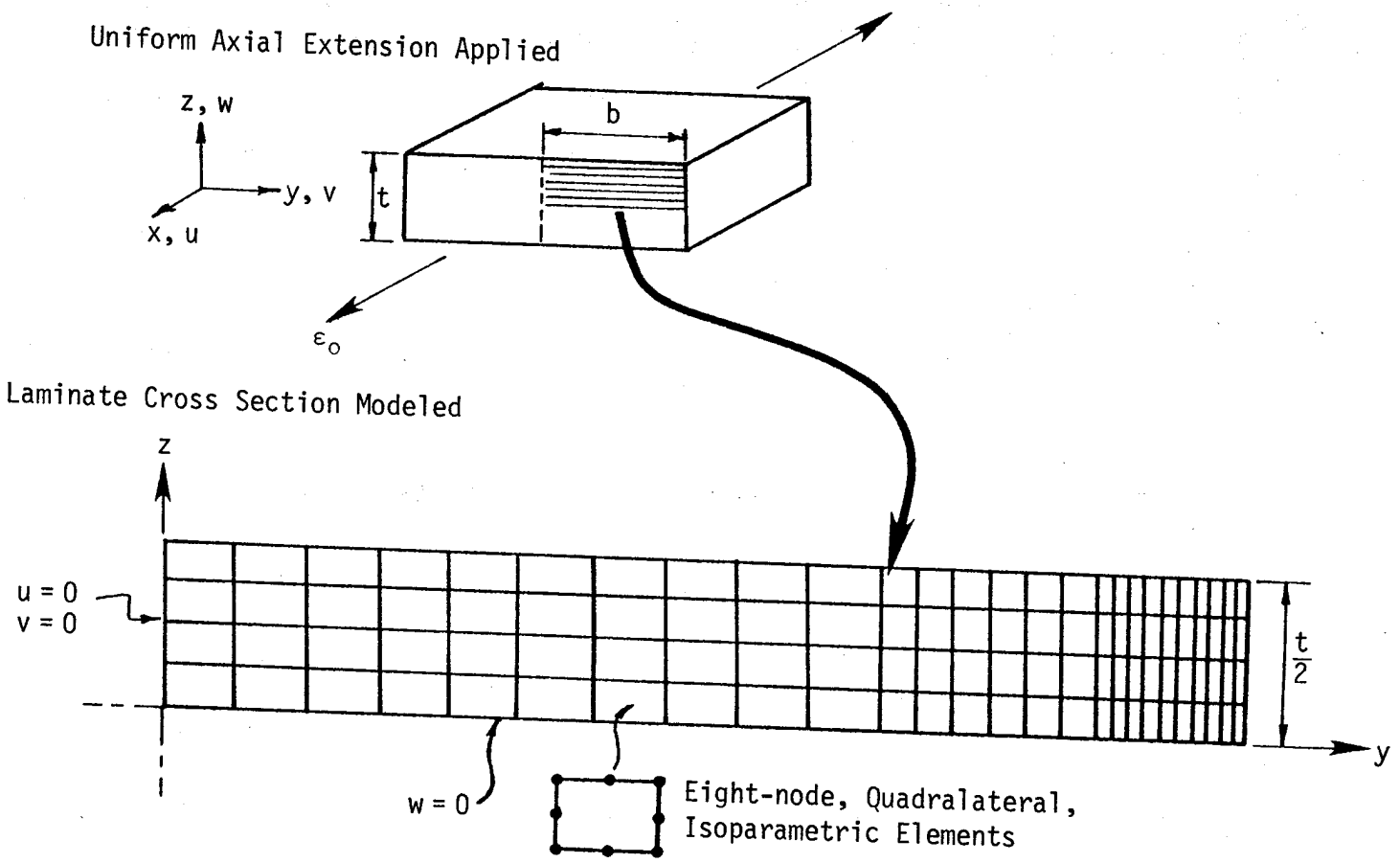


Figure A3. Finite element representation of specimen cross-section.

## Verification of Finite Element Program

Considerable time was spent verifying the finite element program due to conflicting solutions found in the literature.

Stress distributions near a traction free boundary are not the prime concerns of this study, but the solution for stresses near a traction free boundary should provide a good check for the program. Wang and Crossman [12,30,31] have used a similar uniform axial extension element formulation to study edge effects associated with mechanical and thermal loading with transient moisture sorption.

The first problem considered was the stress distributions near a free edge due to a purely mechanical load as in Reference [12]. The following two stacking sequences were considered; $[0/90]_s$ and $[90/0]_s$. The laminate geometry is noted in Figure A4. Due to the symmetrical loading and stacking sequences, only one quarter of the cross-section requires modelling.

The load is input as a unit axial strain $\varepsilon_x = \varepsilon_o = 1$. The thermal load is set to zero. The ply thickness, h, to half width, b, ratio was 1:8, Figure A4(b). The material properties used were:

$$E_1 = 137.8 \text{ GPa}; \quad E_2 = E_3 = 14.5 \text{ GPa}$$

$$G_{12} = G_{13} = G_{23} = 5.86 \text{ GPa}$$

$$\nu_{12} = \nu_{13} = \nu_{23} = 0.21$$

The mesh used consisted of 120 elements with 405 nodes. Each ply contained five elements through the thickness. The element aspect ratio was kept at a maximum of 5:1.

A comparison of the present program and the results obtained from

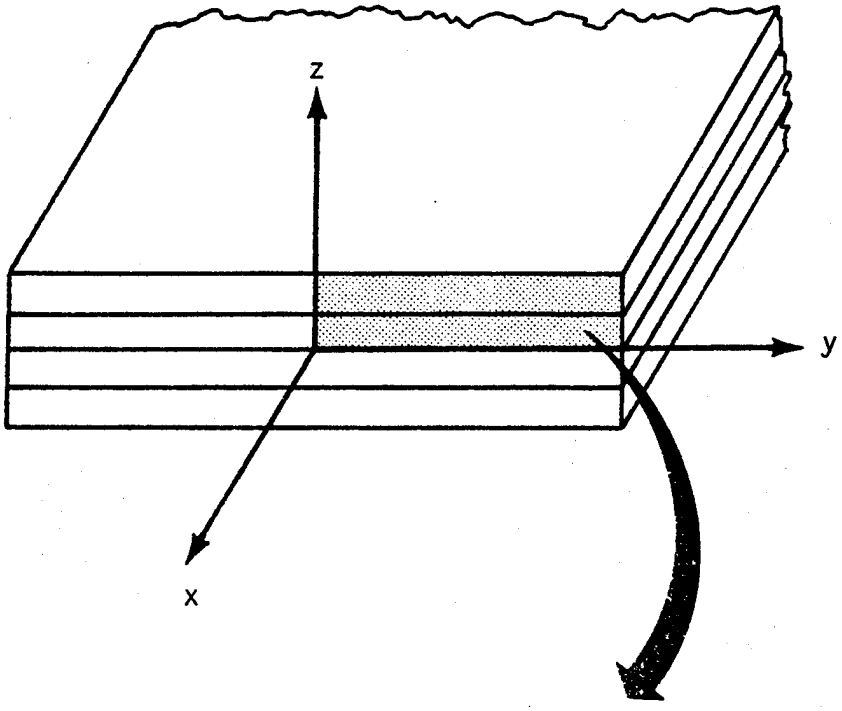


(a) Laminate cross-section.

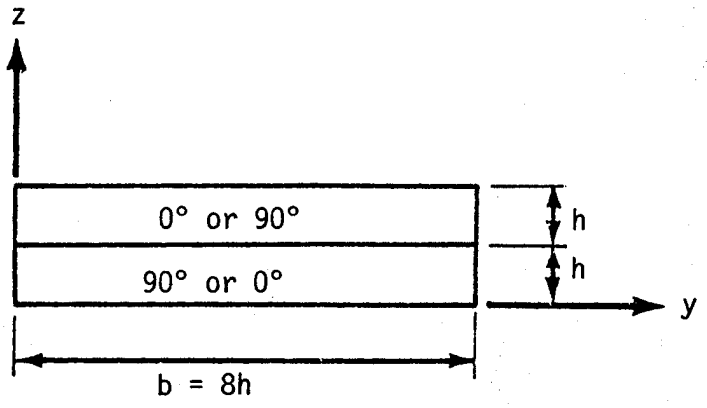


(b) Quarter of cross-section modelled.

Figure A4. Geometry used in analyzing free edge effects.

Reference [12] are shown for a stress distribution at z = h and z = 0 in Figures A5 through A10. The values shown from Reference [12] were digitized directly off of a photo copy of the article. The stress values plotted from the present work were obtained at the nearest Gaussian integration point just below the ply interfaces for stresses at z = h and just above the midplane for stresses at z = 0. All of the figures show good agreement with Reference [12].

As a warning to the reader, caution should be exercised when examining the results of the $[\pm 45]_s$ laminate presented in Reference [12]. Some of the plots shown were drawn with an incorrect sign. The readers are referred to Reference [32] where the correct results for the free edge stresses for the $[\pm 45]_s$ laminate are presented.

The next loading condition was a thermal load. The load consisted of a 1°C temperature change and the average value of $\sigma_{xx}$ transversely across the laminate was zero. The constraint of the zero average value of $\sigma_{xx}$ was to produce a purely thermal load within the confines of the generalized plane strain finite element program. The same material properties and mesh were used for the thermal load as were used for the mechanical load. Only a $[0/90]_s$ stacking sequence was considered for the thermal load case.

A comparison of the present work and the results obtained by Reference [30] for the w and v at the top surface and free edge, respectively, are presented in Figures A11 and A12. Stress distributions at the midplane (z=0) are shown in Figures A13 through A15. The values shown for Reference [30] were obtained in the same manner as stated for the mechanical loading. Good agreement is again shown

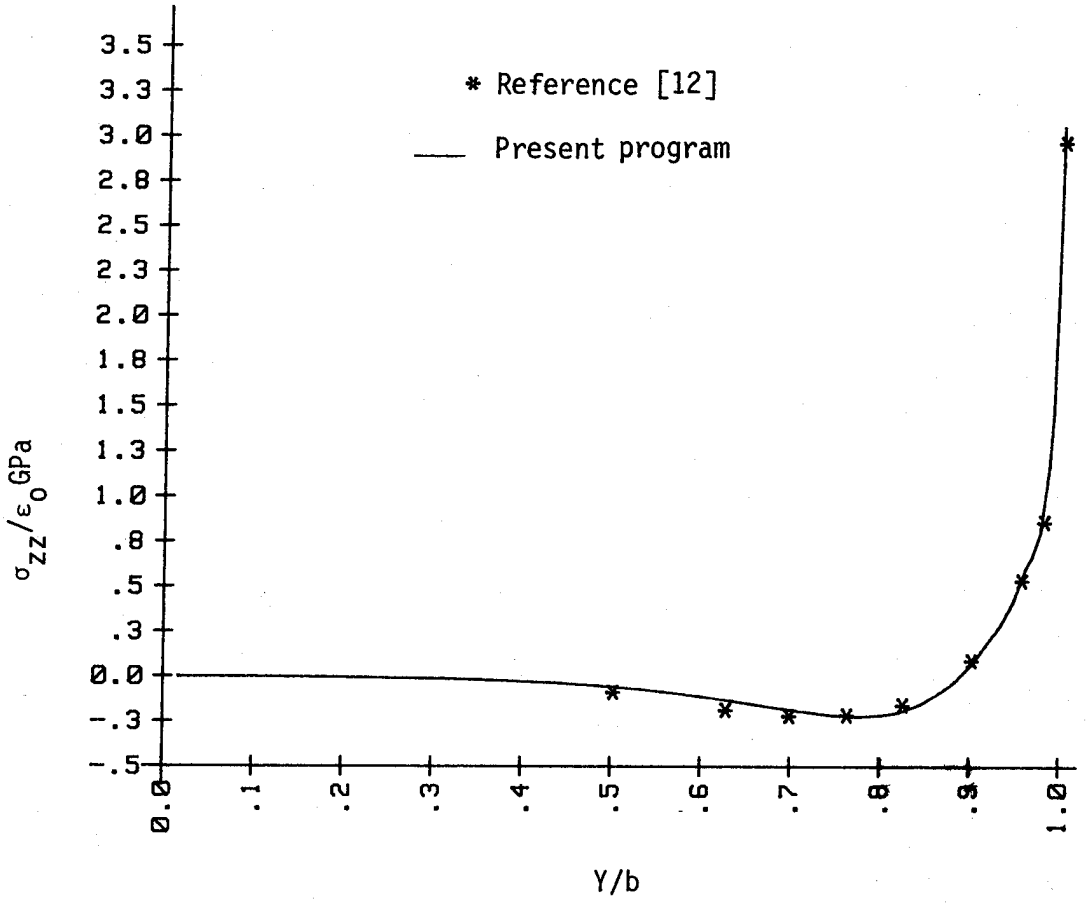


Figure A5. $\sigma_{zz}$ distribution at z = h, for a $[0/90]_s$ laminate under mechanical loading.

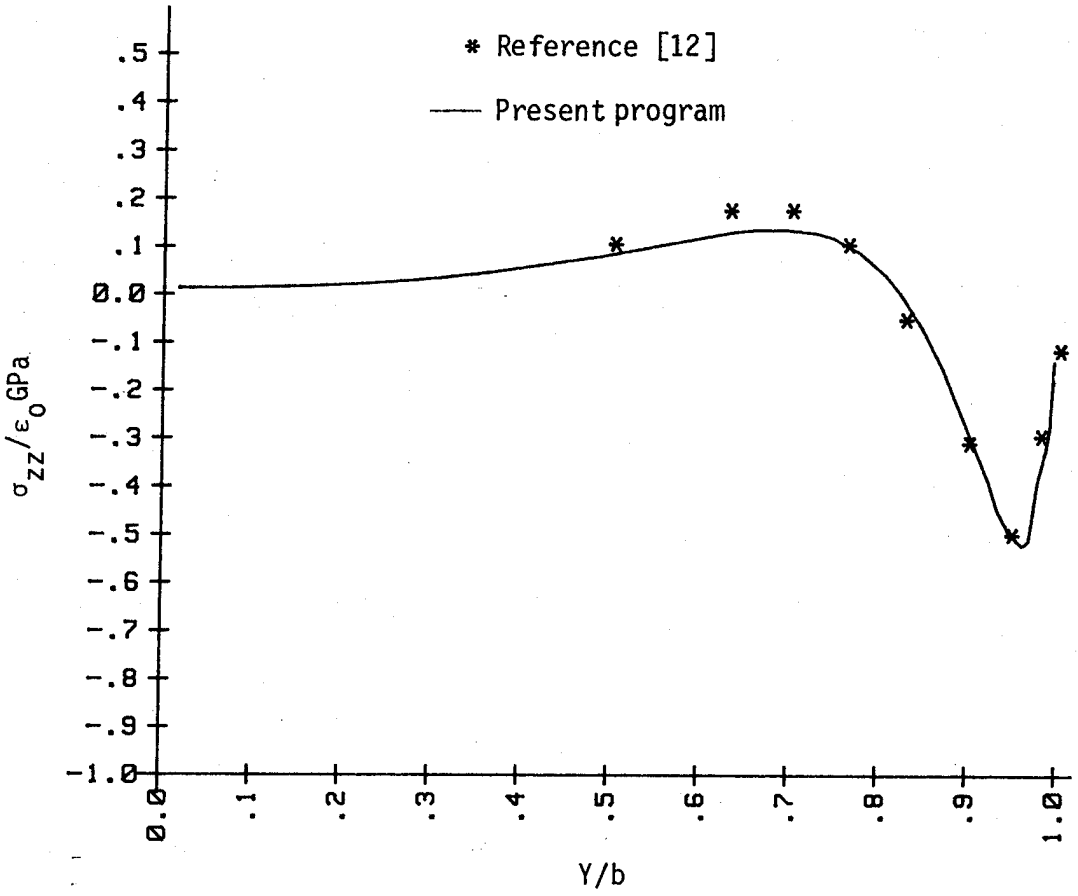


Figure A6. $\sigma_{zz}$ distribution at z = h, for a $[90/0]_s$ laminate under mechanical loading.

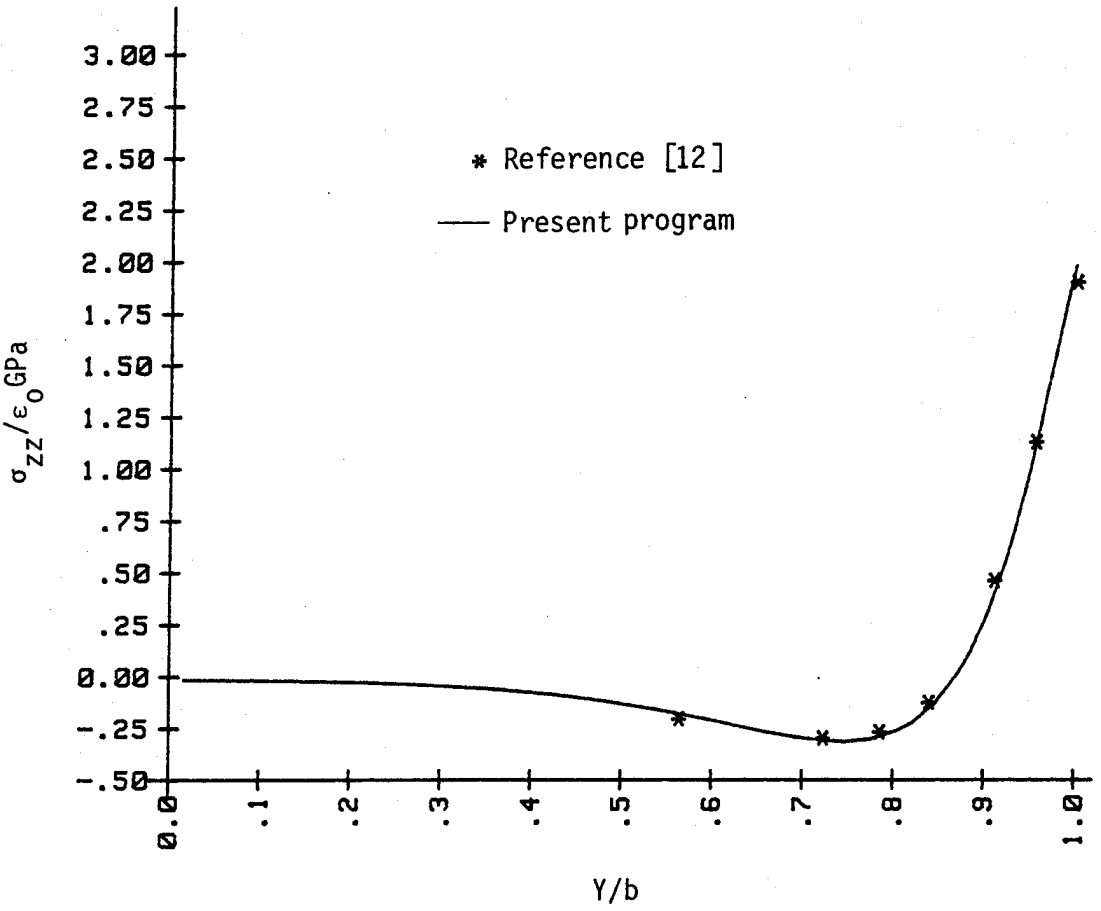


Figure A7. $\sigma_{zz}$ distribution at z = 0, for a $[0/90]_s$ laminate under mechanical loading.

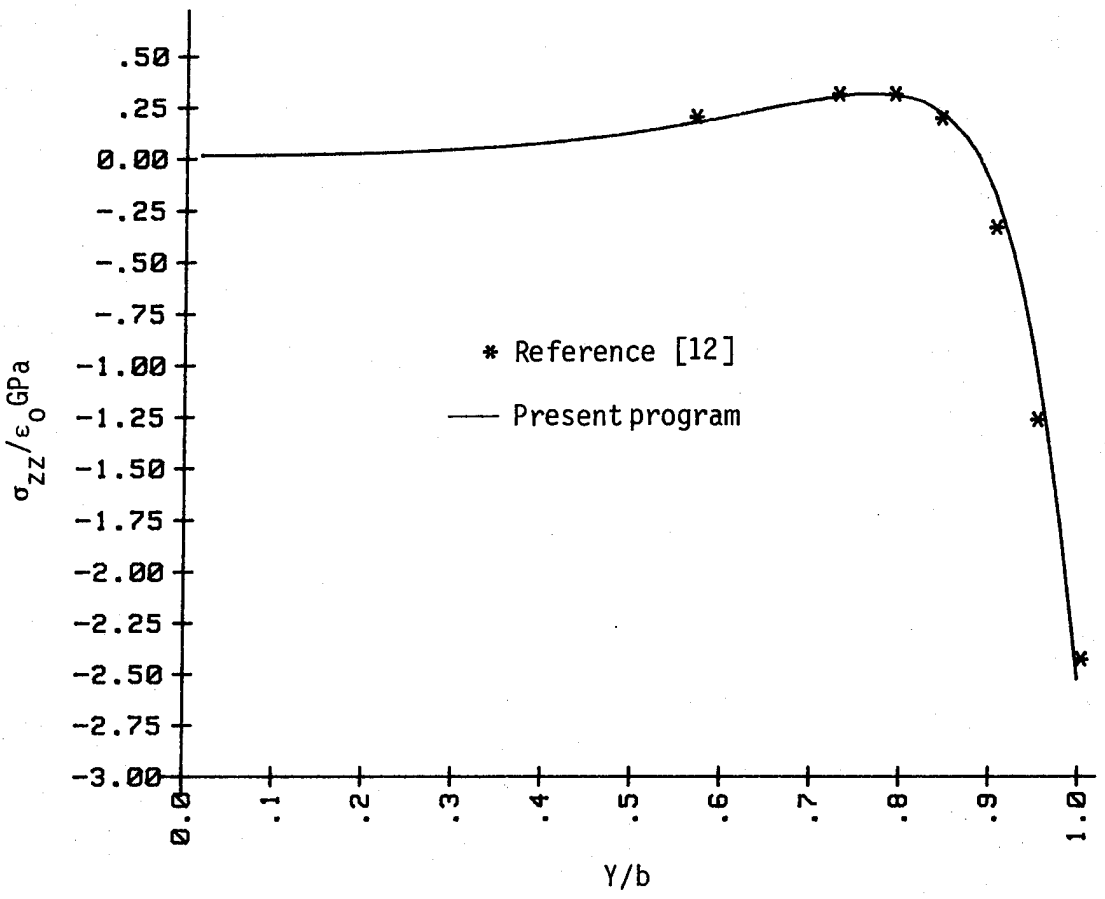


Figure A8. $\sigma_{zz}$ Distribution at z = 0, for a $[90/0]_s$ laminate under mechanical loading.

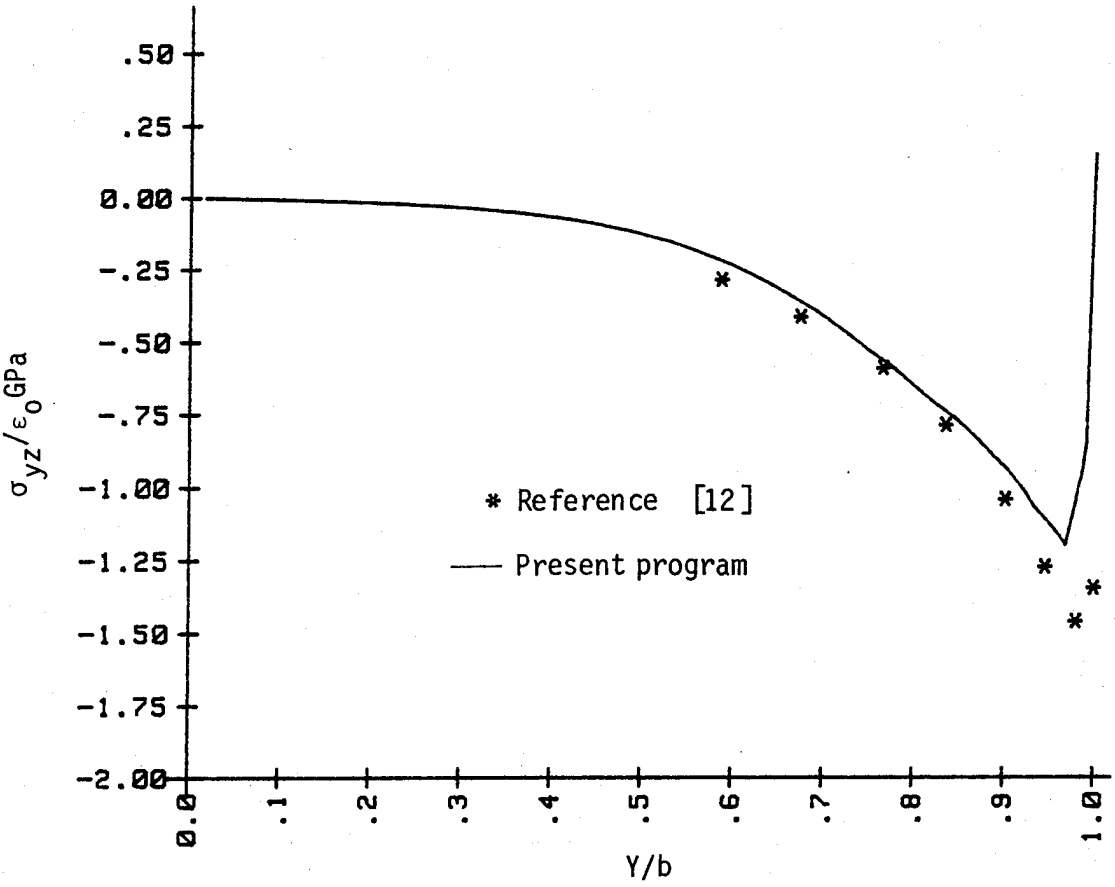


Figure A9. $\sigma_{yz}$ distribution at z = h, for a $[0/90]_s$ laminate under mechanical loading.

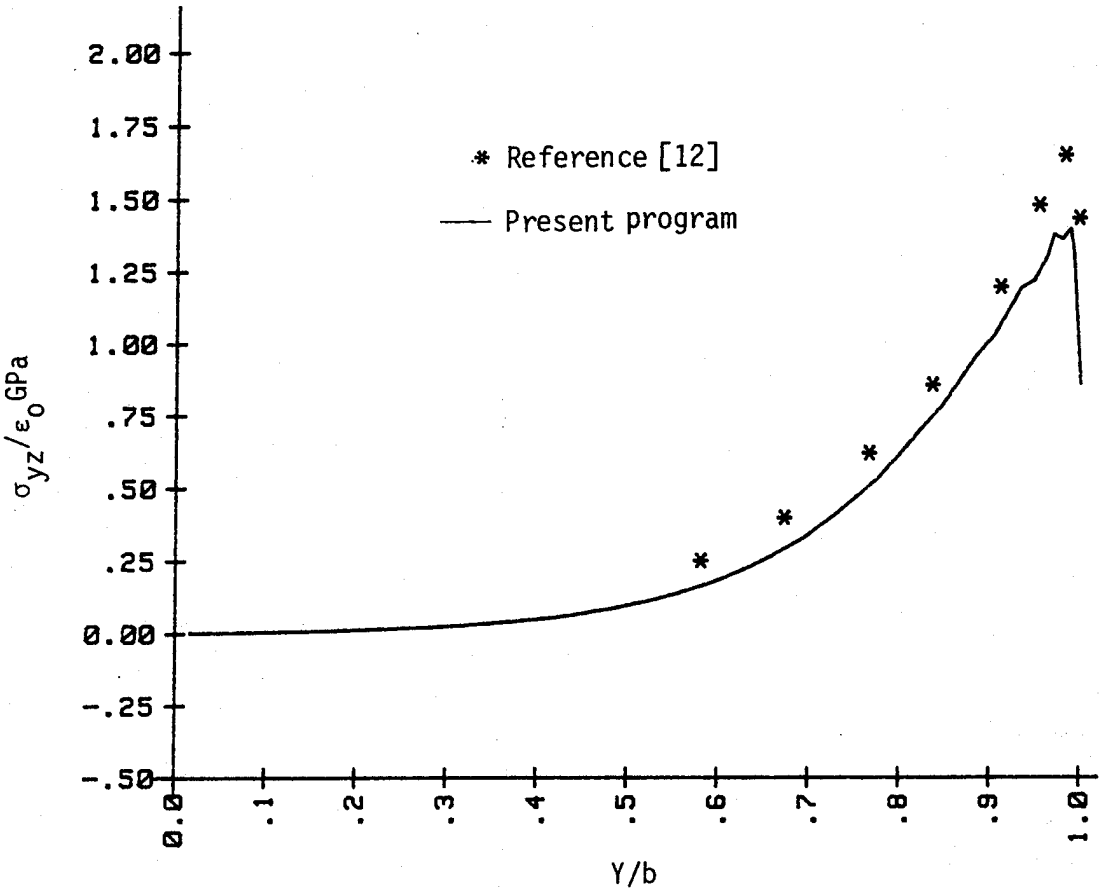


Figure A10. $\sigma_{yz}$ distribution at z = h, for a $[90/0]_s$ laminate under mechanical loading.

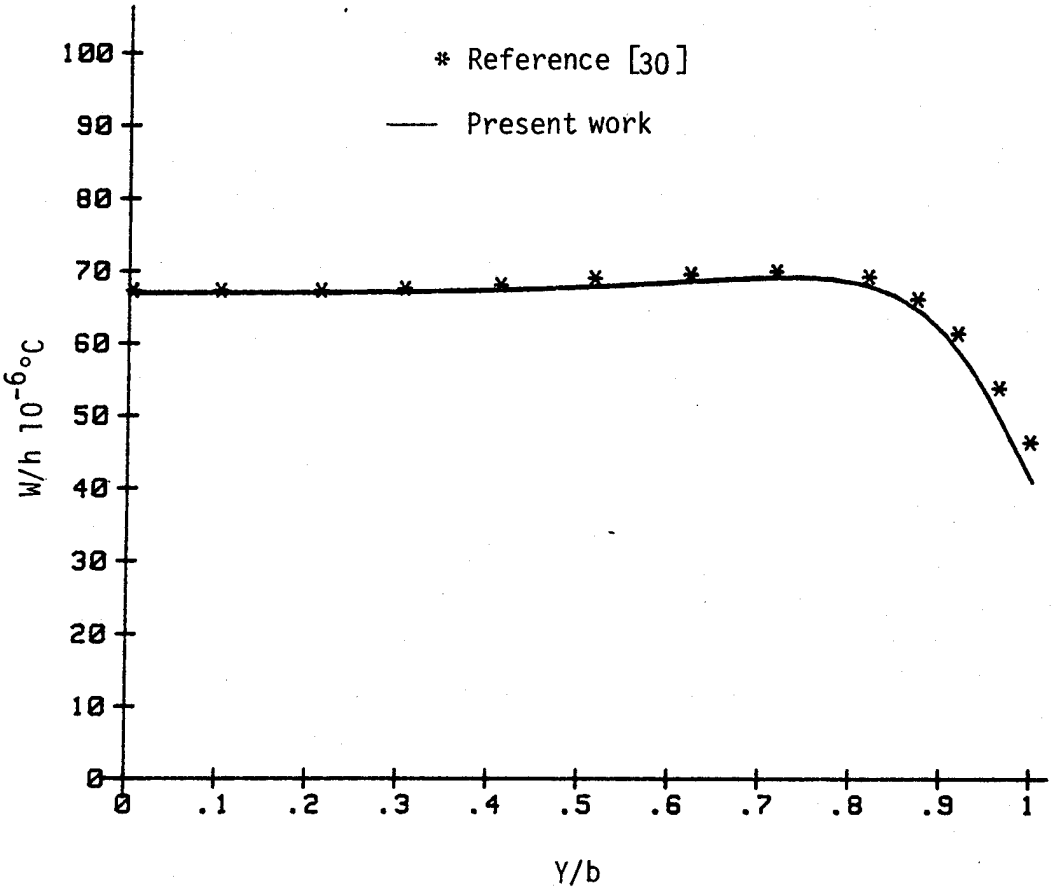


Figure A11. Displacement W at z = 2h, for a $[0/90]_s$ laminate under thermal loading.

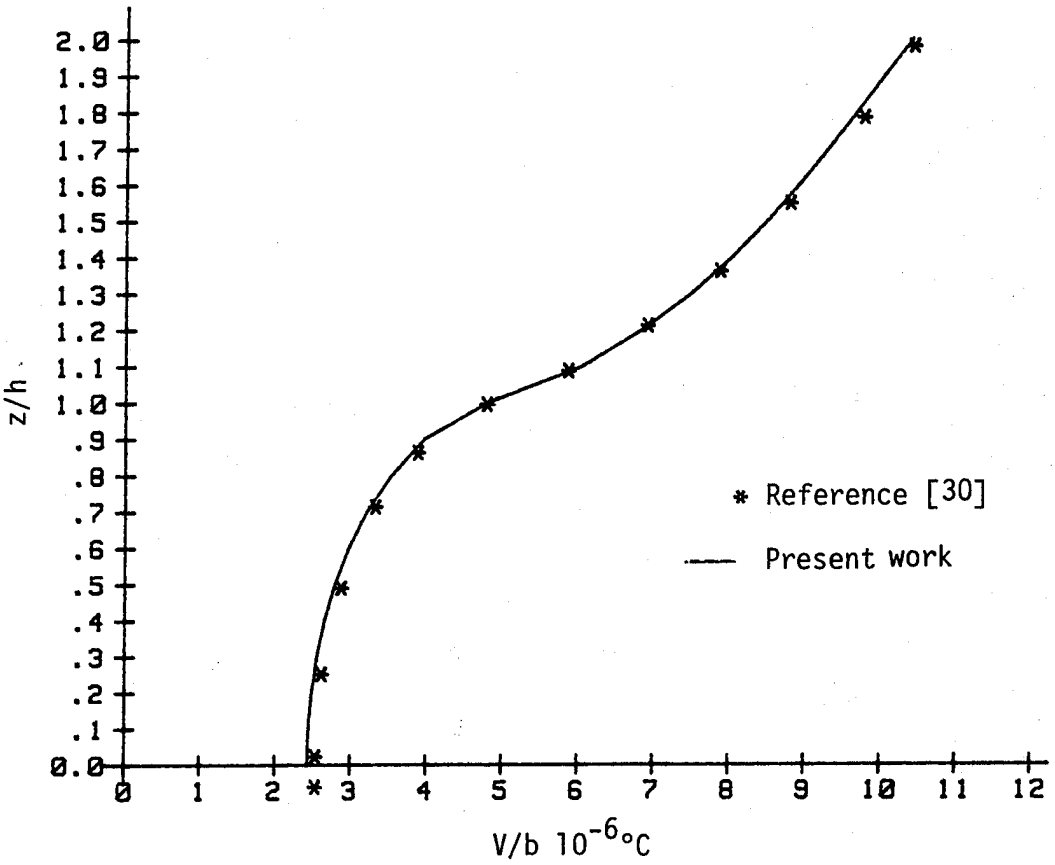


Figure A12. Edge displacement V at Y = b, for a $[0/90]_s$ laminate under thermal loading.

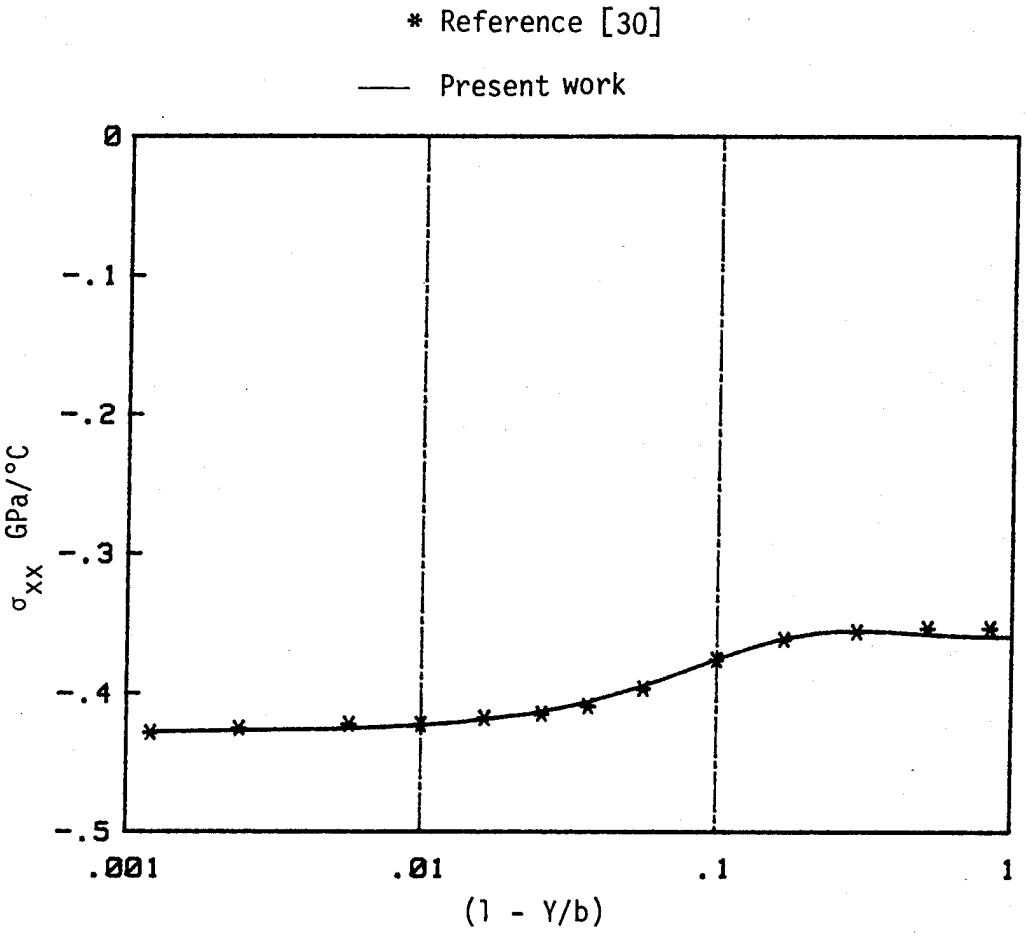


Figure A13. $\sigma_{xx}$ distribution at z = 0, in a $[0/90]_s$ laminate under thermal loading.

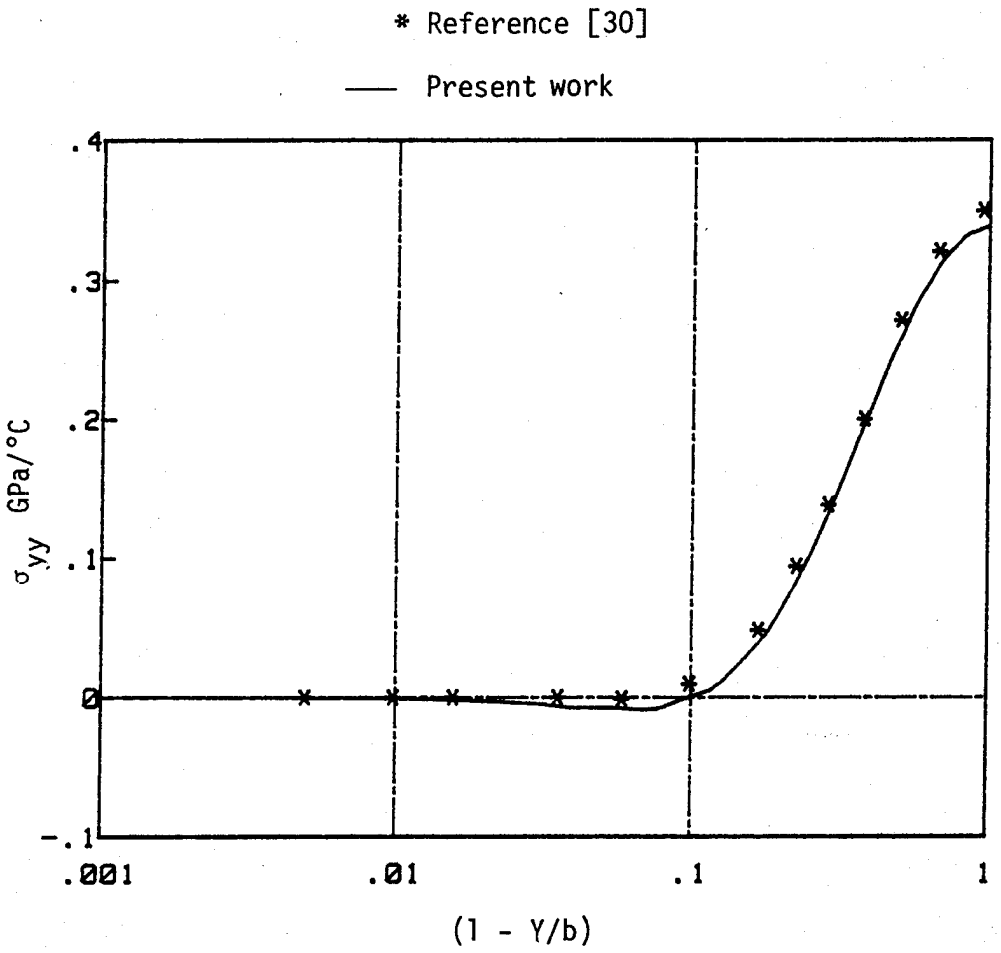


Figure A14. $\sigma_{yy}$ distribution at z = 0, in $[0/90]_s$ laminate under thermal loading.

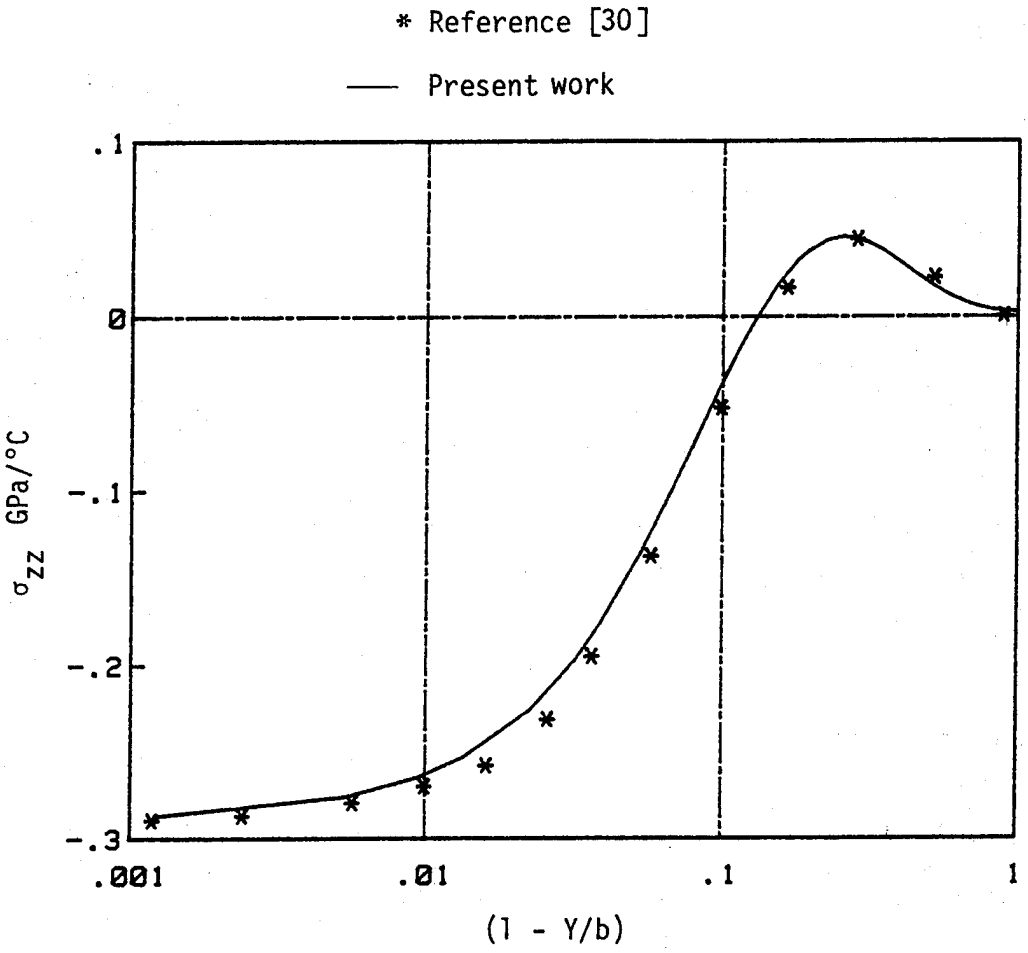


Figure A15. $\sigma_{zz}$ distribution at z = 0, in a $[0/90]_s$ laminate under thermal loading.

for all the figures in the thermal load case.

Thus far, the finite element program has demonstrated its ability to predict diaplacements and stresses for both mechanical and thermal load conditions. The remaining area to be considered will be the fracture analysis capabilities of the program. This area will be addressed next.

The problem considered is a crack in an isotropic plate of finite height and infinite width. The boundary conditions are shown in Figure A16(a). The plane solution given by Rice in Reference [33] is:

$$G_I = \frac{E\, v_o^2}{h}$$

$$G_{II} = G_{III} = 0$$

This problem was modeled by a finite width plate with an aspect ratio of b/h = 5 as shown in Figure A16(b). The mesh consisted of 84 elements with 303 nodes. The crack extension, $\Delta a$ was 0.046b. A total of 15 crack extensions were made. The results are shown in Figure A17. The value of $G_I$ is shown to quickly converge to Rice's solution at a = 0.36b and remains constant for the remainder of the solution.

This concludes the verification of the finite element program.

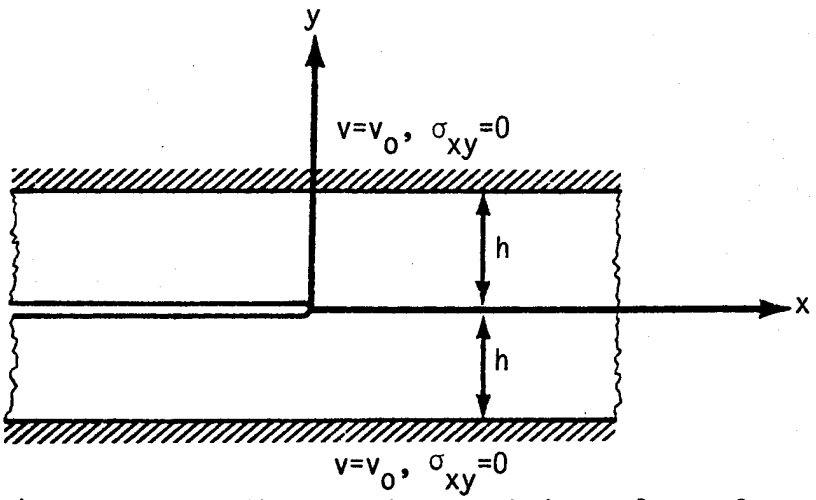


(a) Boundary conditions of a crack in a plate of finite height and infinite width.

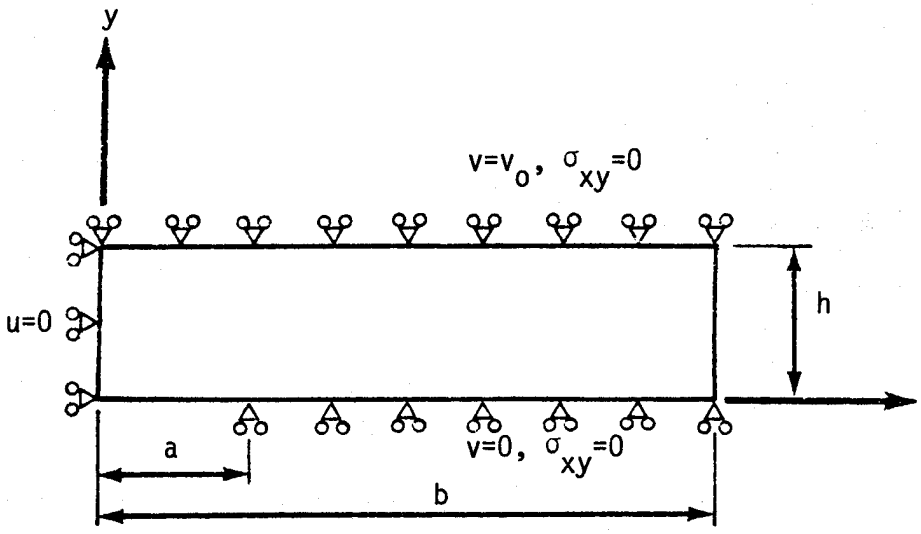


(b) Configuration of finite element model.

Figure A16. Fracture problem of a crack in a plate of finite height and infinite width.

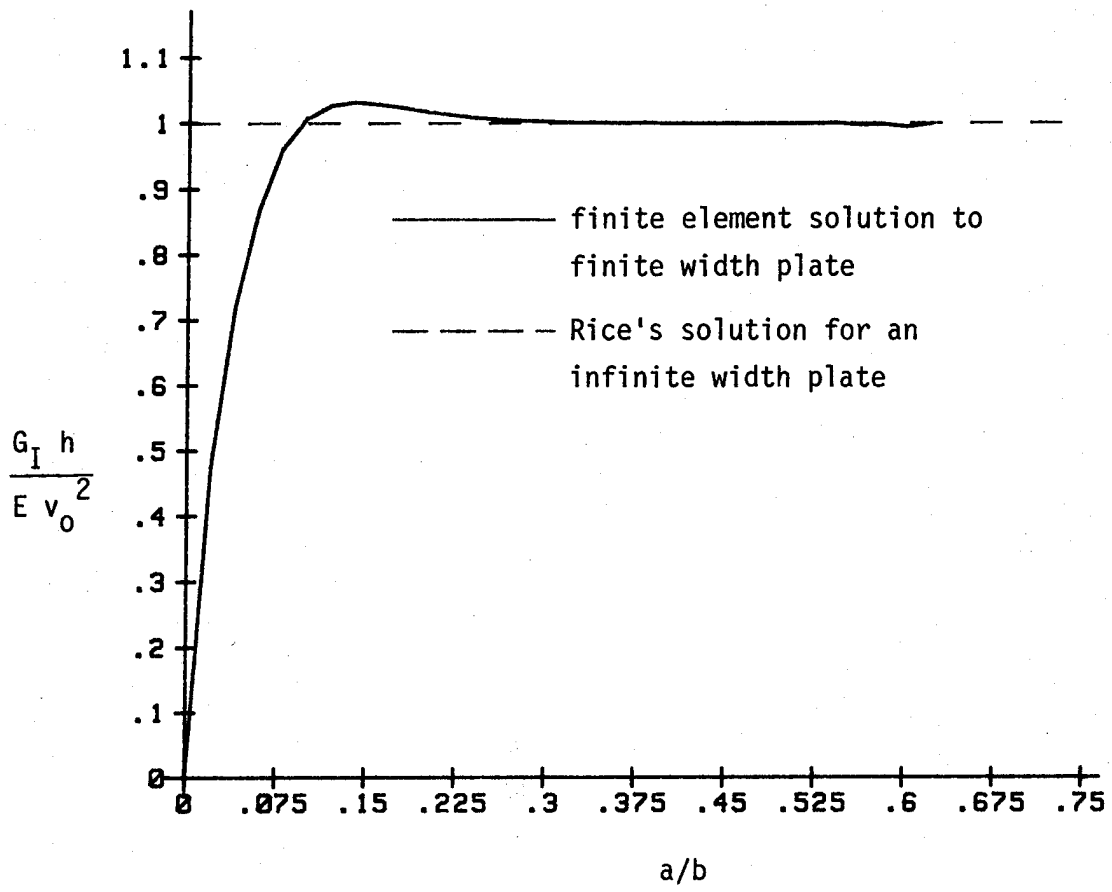


Figure A17. Solution to a crack in an isotropic plate of finite height.

# APPENDIX B

# FATIGUE TEST DATA

Fatigue test data were obtained from Ho and Schapery [10]. The $[\pm 45/90_2]_s$ AS/3501-6 samples were tested at 24°C and 50% RH. The test frequency was 3 Hz with a load ratio of +0.1. Three peak fatigue stress levels, 50%, 55%, and 60% of the ultimate tensile strength, were used. The ultimate tensile stress was reported as 135.6 MPa. In Figures B1, B2, and B3 the mean strain curves are presented. Several data points were obtained from each specimen while the test was in progress. Different test specimens were noted by the different symbols.

The solid line shown is the mean strain function used in the analytical work of this thesis. The function was presented as a piecewise linear curve for simplicity and to avoid any bias associated with an assumed functional form, shown together in Figure B-4.

Other pertinent data relating to the laminate are tabulated in Table B-1.

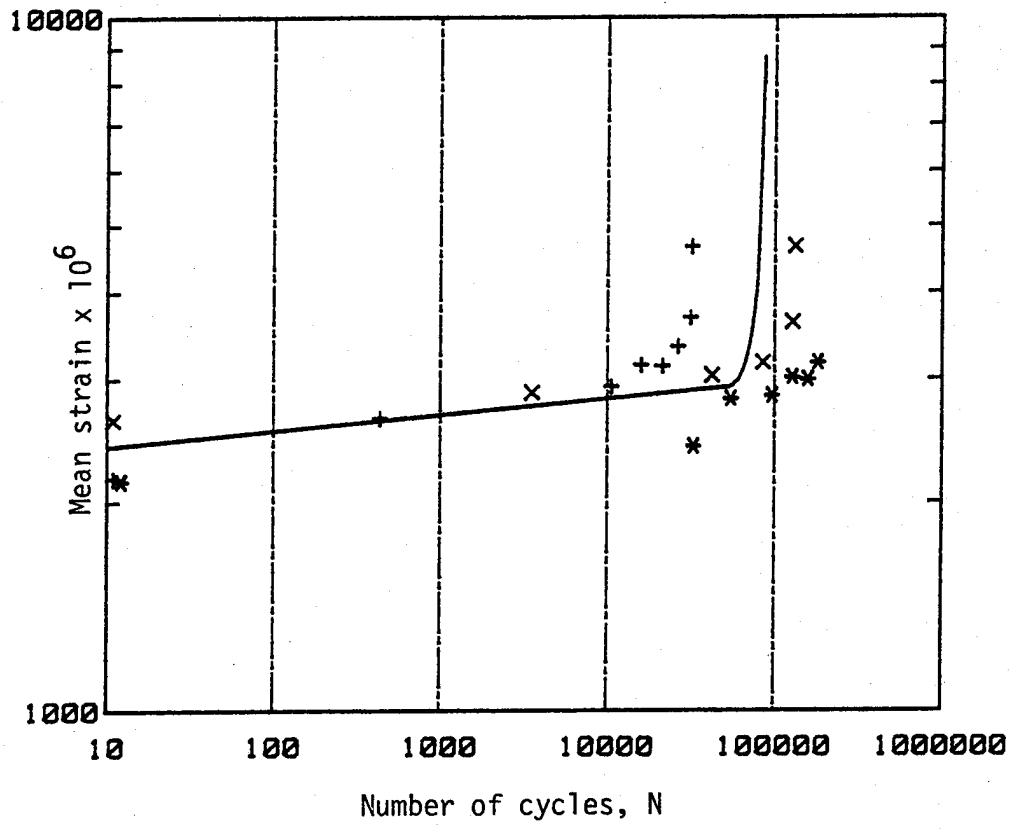


Figure B1. Mean fatigue strain curve for a $[\pm 45/90_2]_s$ laminate at 50% UTS maximum fatigue stress.

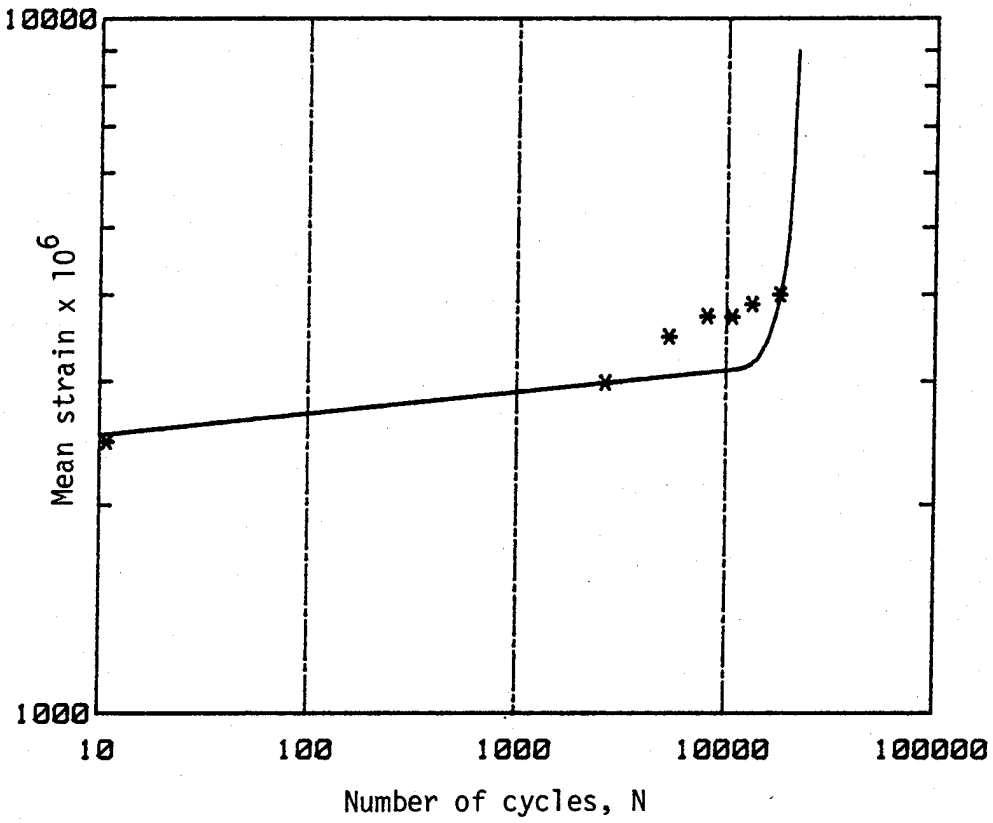


Figure B2. Mean fatigue strain curve for a $[\pm 45/90_2]_s$ laminate at 55% UTS maximum fatigue stress.

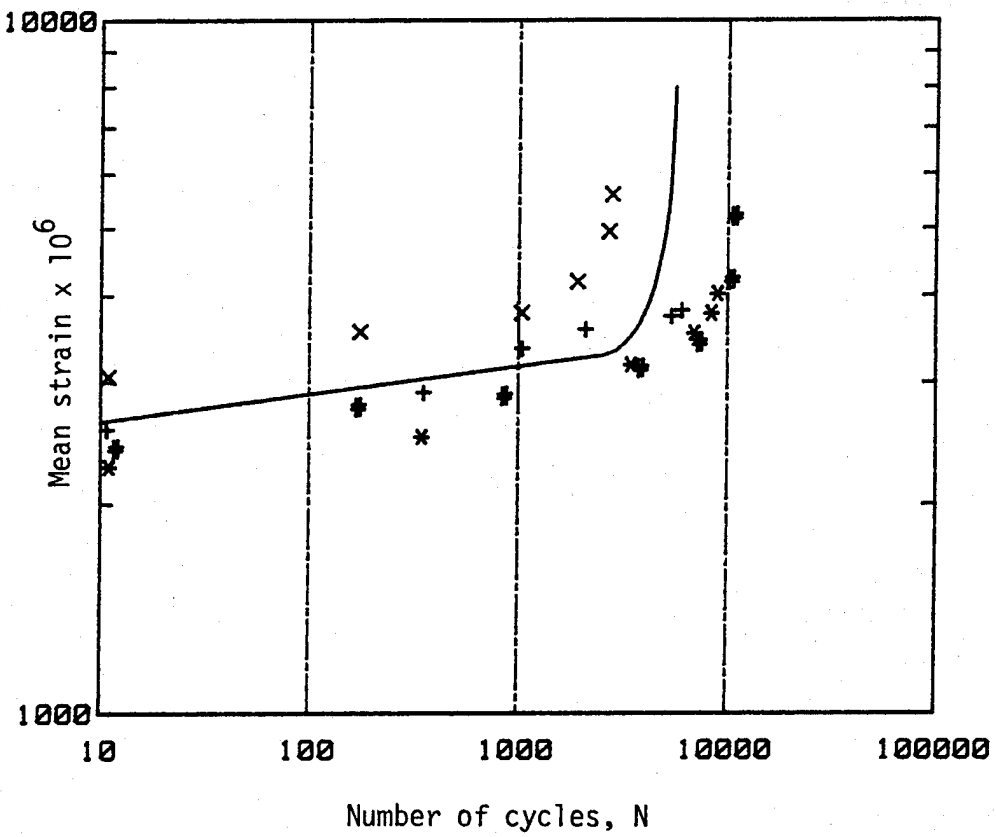


Figure B3. Mean fatigue strain curve for a $[\pm 45/90_2]_s$ laminate at 60% UTS maximum fatigue stress.

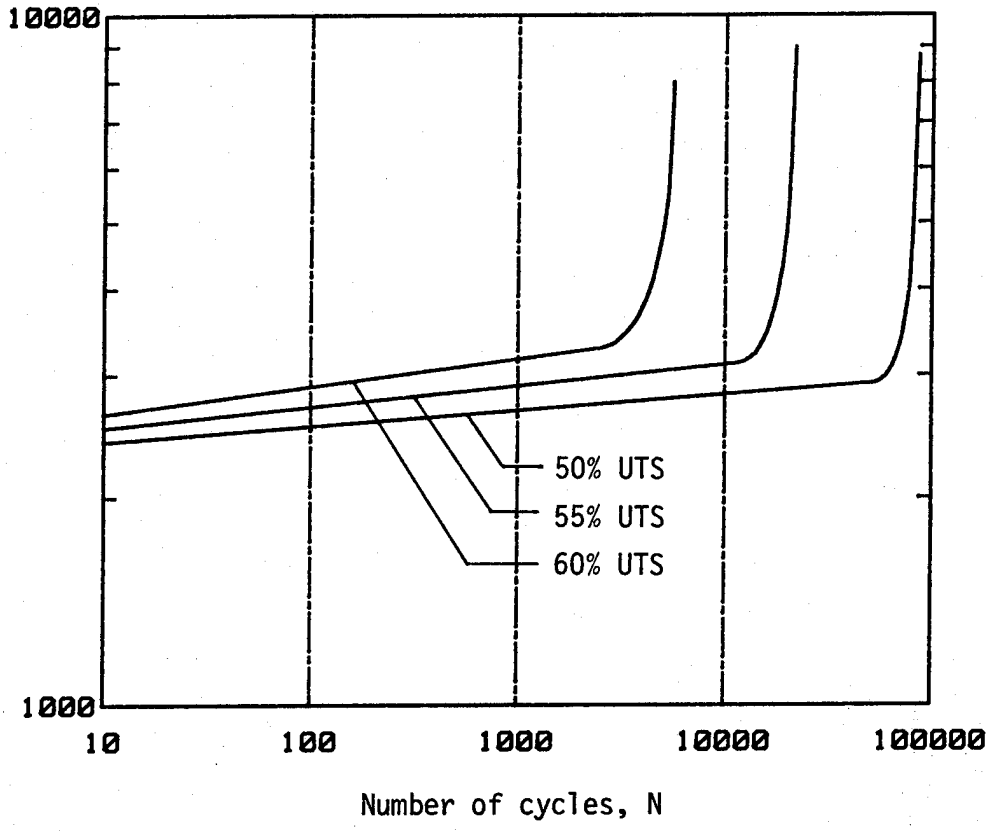


Figure B4. Idealized mean strain curves for a $[\ 45/90_2]_s$ laminate.

Table B1 AS/3501-6, $[\pm 45/90_2]_s$ Laminate Data at 24°C and 50% RH [10]

| | |
|---|---|
| Longitudinal Young's Modulus, $E_1$ | 19.15 GPa |
| Ultimate Tensile Strength, UTS | 135.5 MPa |
| Ultimate Strain | 10540 $\mu\frac{m}{m}$ |
| Fiber Volume (Process Control Panel) | 68.2% |
| Fiber Volume (Vendor Data) | 62% |
| Test Specimen Width | 20.63 mm |
| Ply Thickness | 0.127 mm |

# VITA

Robert Thomas Arenburg was born February 12, 1955 in Longview, Texas. He graduated from Alameda High School, Alameda, California in June of 1973. Robert entered Southern Technical Institute, Marietta, Georgia in September of 1974. He graduated in December 1977. After working a brief period in Atlanta, Georgia, for an engineering firm, he entered the graduate college of Texas A&M University, College Station, Texas in September 1978. Robert is to receive his Master of Science Degree in Civil Engineering in May of 1982, and is currently employed as a stress/fatigue analyst for the Boeing Aerospace Company, Kent, Washington.

Permanent Mailing Address:

500 Hunter Street

Kilgore, Texas 75662